

**IMPERVIOUS SURFACE AREAS AND RUNOFF IN URBAN
WATERSHEDS: A CASE OF MIHANG’O WATERSHED,
NAIROBI-KENYA**

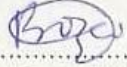
**OMWOYO ONGAGA CYRUS (BSc. Environmental Science)
I56/39188/2016**

**A THESIS SUBMITTED IN PARTIAL FULFILLMENT OF THE
REQUIREMENT FOR THE AWARD OF THE DEGREE OF
MASTERS OF SCIENCE (INTEGRATED WATERSHED
MANAGEMENT) IN THE SCHOOL OF PURE AND APPLIED
SCIENCES OF KENYATTA UNIVERSITY**

NOVEMBER, 2024

DECLARATION

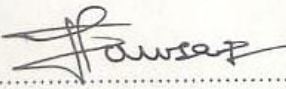
This thesis is my original work and has not been presented for a degree in any other University or any other award.

Signature.....  Date..... November 21st, 2024

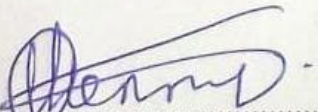
Cyrus Omwoyo Ongaga (BSc. Environmental Science)
I56/39188/2016
Department of Geography

SUPERVISORS

We confirm that the work reported in this thesis was carried out by the candidate under our supervision.

Signature.....  Date..... 25/11/2024

Dr. Mary Makokha
Department of Geography
Kenyatta University

Signature.....  Date..... 22/11/2024

Dr. Kennedy Obiero
Department of Geography
Kenyatta University

DEDICATION

I am grateful to my loving parents, Mr. Charles Ongaga Makori and Mrs. Regina Ongaga whose words of encouragement ring in my ears; your unwavering support throughout my academic journey has been invaluable. To my wife, Fatma Abubakar and kids, Abida Nyanchama Omwoyo, Adil Malik Makori Omwoyo, and Ayman Kamal Basweti Omwoyo, “thank you big” for you have been my support system. My special thanks go to my very large family of brothers and sisters, the Morabu family, and other relatives, who have stuck by my side and are very special.

ACKNOWLEDGEMENTS

I acknowledge and thank the German Academic Exchange Service (DAAD) for funding my master's studies. I acknowledge Kenyatta University and the Department of Geography for allowing me to conduct my research and providing any assistance requested. I wish to thank my supervisors: Dr. Mary Makokha and Dr. Kennedy Obiero, who guided me throughout the process. I acknowledge the substantial input of my mentor and friend, Dr. Isaac Kipkemoi, for dedicating his time to provide guidance throughout my master's program. I acknowledge colleague and friend, Justus Diang'a, for sparing time to brainstorm with me.

TABLE OF CONTENTS

DECLARATION.....	ii
DEDICATION.....	iii
ACKNOWLEDGEMENTS.....	iv
TABLE OF CONTENTS.....	v
LIST OF TABLES	viii
LIST OF FIGURES	ix
ABBREVIATIONS AND ACRONYMS	x
ABSTRACT	xi
CHAPTER ONE: INTRODUCTION	1
1.1 Background of the Study.....	1
1.2 Statement of the Problem	3
1.3 Justification of the Study	4
1.4 Research Hypotheses	5
1.5 Objectives of the Study	6
1.6 Significance of the Study	6
1.7 Scope and Limitations of the Study	7
1.8 Operational Definition of the Key Terms and Concepts.....	7
CHAPTER TWO: LITERATURE REVIEW	9
2.1 Introduction.....	9
2.2 Estimating Impervious Surface Cover	9
2.2.1 Mihang'o Watershed Impervious Surface	13
2.3 Precipitation Trend Analysis.....	14
2.3.1 Rainfall Pattern of Nairobi	16
2.4 Determining Runoff Trend.....	18
2.4.1 The HEC-HMS Model	20
2.4.2 HEC-HMS Modelling Example	21
2.4.3 Runoff Trend over Time	24
2.5 Summary of Literature and Identified Gaps.....	25
2.6 Conceptual Framework	28
CHAPTER THREE: MATERIALS AND METHODS	31
3.1 Introduction.....	31
3.2 Study Area.....	31

3.2.1 Climate	33
3.2.2 Soils and Geology	34
3.2.3 Topography	35
3.2.4 Land Use/Land Cover	35
3.3 Data Collection.....	36
3.3.1 Determining Change of Impervious Surface Area.....	36
3.3.2 Determining Trend of Precipitation Amount	39
3.3.3 Determining Trend of Runoff Amount	40
3.4 Data Collection and Processing Summary	44
CHAPTER FOUR: RESULTS AND DISCUSSIONS.....	47
4.1 Introduction	47
4.2 Impervious Surface Area Trend of Mihang'o Watershed.....	47
4.3 Precipitation Trend of Mihang'o Watershed.....	55
4.4 Runoff Amount Trend of Mihang'o Watershed.....	64
4.4.1 HEC-HMS Calibration Results	65
4.4.3 HEC-HMS Modeling	76
4.4.4 Runoff Amount Trend.....	76
CHAPTER FIVE: SUMMARY, CONCLUSIONS AND RECOMMENDATIONS	81
5.1 Introduction	81
5.2 Objective One.....	81
5.3 Objective Two.....	81
5.4 Objective Three.....	82
5.5 Recommendations	83
REFERENCES.....	84
APPENDICES	93
Appendix A: Research Approval Documents	93
Appendix B: Screenshots Collected During HEC-HMS Procedures.....	95
Appendix C: HEC-HMS Results Windows for the Years of Study	97
Appendix D: Matrix Results from Supervised Classification.....	102
Appendix E: Javascript Code used to Retrieve CHIRPS Data	103
Appendix F: Precipitation on December 29 th , 2022.....	105
Appendix G: Global Hydrologic Soil Groups for Curve Number	106
Appendix H: Linear Regression Analysis for Impervious Surface Area Trend ..	107

Appendix I: Mann-Kendall Trend Test Summary Results	108
Appendix J: Linear Regression Analysis for Runoff Trend.....	109
Appendix K: Correlation Analysis for Impervious Surface Area and Runoff....	110

LIST OF TABLES

Table 2.1: Summary of Literature and the Identified Gaps	26
Table 3.1: Coordinates of Soil Sample Points	41
Table 3.2: Summary Table of HEC-HMS Model Calibration	43
Table 3.3: Summary of Data Collection and Processing	45
Table 4.1: Impervious Surface of Mihang'o Watershed from 2000 - 2022.....	50
Table 4.2: Rainfall for Mihang'o Watershed (2000-2022)	56
Table 4.3: T-test Analysis of CHIRPS and KURS Annual Rainfall.....	59
Table 4.4: Mann-Kendall Trend Test for Mihang'o Watershed Rainfall	61
Table 4.5: USDA-SCS Soil Classification.....	69
Table 4.6: Curve Number for Urban Areas.....	71
Table 4.7: Curve Number for Mihang'o Watershed	72
Table 4.8: Impervious Surface Coefficients from 2000 - 2022	73
Table 4.9: Lag Time for Mihang'o Watershed Sub-basins.....	73
Table 4.10: Measured Rainfall	74
Table 4.11 Summary Table of HEC-HMS Model Calibration Results	75
Table 4.12: Runoff Amount from Mihang'o Watershed	76

LIST OF FIGURES

Figure 2.1: Urbanization in Kenya from 2009 to 2019.....	14
Figure 2.2: Nairobi's Average Climate Seasonality.	17
Figure 2.3: Short Rains Season Statistics for Nairobi.....	18
Figure 2.4: Runoff Flow Changes due to Urbanization	29
Figure 2.5: Modified Runoff Flow Changes due to Urbanization	30
Figure 3.1: Location of Mihang'o Watershed.....	32
Figure 3.2: Process Followed During Supervised Classification.....	37
Figure 3.3: Steps Followed in Completing the HEC-HMS Project	44
Figure 3.4: Summary of the Methodology.....	46
Figure 4.1: Mihang'o Watershed Land Cover Vs. Supervised Classification Image, 2022 .	48
Figure 4.2: Mihang'o Watershed Impervious Surface Cover from 2000 – 2009	44
Figure 4.3: Mihang'o Watershed Impervious Surface Cover from 2012 – 2022.....	49
Figure 4.4: Mass Curve for Impervious Surface.....	50
Figure 4.5: Impervious and Pervious Surface Area (%) of Mihang'o Watershed	52
Figure 4.6: Annual Rainfall.....	57
Figure 4.7: Average Monthly Rainfall	57
Figure 4.8: Seasonal Rains.....	58
Figure 4.9: Mass Curve for Annual Rainfall (2000-2022).....	59
Figure 4.10: Mann-Kendall Test <i>p</i> -values	62
Figure 4.11: Mihang'o Watershed Basin Model.....	66
Figure 4.12: HEC HMS Schematic Network of Mihang'o Watershed.....	67
Figure 4.13: Soil Sample Points.....	68
Figure 4.14: Supplement Matrix for Determining CN.....	72
Figure 4.15: Runoff Trend of Mihang'o Watershed	76
Figure 4.16: Mass Curve for Cumulative Discharge	77

ABBREVIATIONS AND ACRONYMS

APTC	Administration Police Training Center
CHIRPS	Climate Hazards Center InfraRed Precipitation with Station data
DEM	Digital Elevation Map
GIS	Geographic Information System
GSUTS	General Service Unit Training School
HEC-HMS	Hydrological Engineering Center-Hydrological Modelling System
ITCZ	Inter Tropical Convergence Zone
JKIA	Jomo Kenyatta International Airport
KURS	Kenyatta University Rainfall Station
LULC	Land Use Land Cover
MASL	Meters Above Sea Level
NACOSTI	National Commission for Science, Technology and Innovation
NDVI	Normalized Difference Vegetation Index
NLCD	National Land Cover Database
RCMRD	Regional Center for Mapping of Resources for Development
SCS	Soil Conservation Service
USACE	US Army Corps of Engineers
WRA	Water Resources Authority

ABSTRACT

The frequency and severity of flooding in urban watersheds, including the Mihang'o watershed on the outskirts of Nairobi, has been on the rise. Over the years, Mihang'o has witnessed continuous urban expansion. This urbanization disrupts natural landscapes by replacing vegetated areas with impervious surfaces, which limit water infiltration and significantly increase surface runoff within the watershed. The overall objective of this study was to evaluate the relationship between change in impervious surface area and runoff amount of Mihang'o watershed from 2000 - 2022. The specific objectives of this study were: To determine change in impervious surface area of Mihang'o watershed, trend of precipitation amount in the watershed and the trend in runoff amount from the watershed from 2000 - 2022. Supervised classification was done on Landsat images using ArcGIS (10.4) to determine percentages of impervious surface cover for the study period and linear regression analysis was done to establish the trend. CHIRPS rainfall data was retrieved from Google Earth Engine then processed in MS Excel to produce monthly and annual rainfall totals then Mann-Kendall trend tests were used to establish the rainfall trend for the watershed. The HEC-HMS model was used to simulate runoff from the watershed with the rainfall data and impervious surface area percentages as inputs then linear regression analysis was done to establish the runoff trend. Impervious surface area increased by 87.03% from 2.78% (0.49 km^2) of the total surface area of the watershed in 2000 to 22.21% (3.91 km^2) in 2022. Rainfall analysis showed two rainfall seasons: short rains November to December and long rains March-April-March, with the highest annual rainfall being 1172.8 mm and the least annual rainfall being 491.7 mm, which is consistent with the Nairobi region's climate data that shows no significant linear trend in rainfall. The Mann-Kendall trend tests results (Sen's slope results ($\beta = .832$), Kendall's tau results ($\tau b = .146$), and p -value (.625)) confirmed that there is no trend in rainfall time series of Mihang'o watershed. Runoff increased by 84.75% from 0.18 mm in 2000 to 1.18 mm in 2022. The regression analysis results ($p < .001$) supported the alternative hypothesis (H_1) that there is a positive trend in the impervious surface area time series; the Mann-Kendall trend test ($p > .05$) supported the null hypothesis (H_0) that there is no trend in the rainfall data time series; the linear regression results ($p < .000$) supported the alternative hypothesis (H_1) that there is a positive trend in the runoff time series. Overall, correlation analysis found a significant positive relationship between impervious surface area and runoff $r (6) = .99$, $p < .000$. As the study has demonstrated a significant positive relationship between impervious surface area and runoff in the urban watershed, urban planners can leverage these findings and embrace development practices that reduce runoff, including expanding green spaces such as green roofs, permeable pavements, and urban forestry, increasing storage capacity of excess rainfall and runoff water, and constructing retention basins and infiltration trenches on the streams.

CHAPTER ONE: INTRODUCTION

1.1 Background of the Study

Impervious surfaces are defined as surfaces that prevent water penetration (Stanuikynas et al., 2000). In watershed management, naturally occurring conditions such as dense soil layers, hardpans, and bedrock, despite limiting water movement, are not categorized as impervious surfaces (Stanuikynas et al., 2000). Impervious surfaces are created by man, including buildings, tarmac roads or highways, rooftops, sidewalks, parking lots, lawns, patios, and paved surfaces, such as asphalt and concrete (Ebrahimian et al., 2016a; Tang et al., 2018). O'Driscoll et al. (2010) note that urbanization leads to an increase in the total impervious area within a watershed.

Shuster et al. (2005) describe urbanization as the disruption of natural landscapes, ultimately replacing vegetated areas with impermeable surfaces. Urbanization is driven by population growth, which increases the demand for residential and commercial spaces, often encroaching on previously green areas (Miller et al., 2014). The United Nations (2018) projected that approximately 68% of the world's population will reside in urban areas by 2050. Consequently, impervious surface areas in watersheds are expected to expand in parallel with urban development.

The primary concern associated with urbanization and the resultant impervious surface increase is the disruption of the normal hydrological cycle in a watershed. Total impervious area decreases precipitation infiltration and surface storage while increasing runoff (Ebrahimian et al., 2016a). In undeveloped settings, trees, depressions, natural lands, bushes, and soil delay overland flow and enhance the infiltration of rain (O'Driscoll et al., 2010; Xu & Zhao, 2016). According to

Ligtenberg (2017), approximately 10% of precipitation is transformed to runoff in a forested watershed, but approximately 55% of precipitation becomes runoff in a 75% impervious watershed. According to Ebrahimian et al. (2016b), impervious surfaces in urban watersheds make water flow faster, resulting in a shorter concentration time and lag time. This reduces the ability to infiltrate precipitation but increases runoff or outflow from the catchment (Ebrahimian et al., 2016b). Nonetheless, other factors influencing runoff amount include the amount of precipitation, type of imperviousness, watershed's soil type, slope of watershed, size of the watershed and sub-basins, length of the reaches, longest flow path, initial abstraction, catchment's centroid positioning and elevation, and whether impervious surfaces are connected or not connected to a drainage channel (US Army Corps of Engineers [ACE], 2009; Chathuranika et al., 2018; Guo et al., 2019; Rezaei et al., 2019; Xu & Zhao, 2016).

Kenya is a developing country that is characterized by rapid urbanization (Bosco et al., 2011). In recent years, there has been a surge in development activities, particularly road and building construction, throughout major towns and their surrounding areas (Gachanja et al., 2023; Mbuthia et al., 2022). In Nairobi, the land use/land cover (LULC) has changed from forest, shrubs, plantations, bare land, and grassland to roads and built-up areas (Bosco et al., 2011). There has also been an increasing trend of flooding during rainy seasons in the City and its environs. However, research conducted on the problem of runoff and flooding in the city have focused on unplanned urbanization, poor maintenance of drainage systems, and poor disposal of garbage as the cause of floods (Muli, 2008; Owuor & Mwiturubani, 2022; Tom et al., 2022). Little evidence is available about the relationship between urbanization's impervious surface increase with runoff. Based on global findings, the

resultant increase in impervious surface area in Nairobi should be among the main reasons for floods downstream (Ebrahimian et al., 2016a; Ligtenberg, 2017; Miller et al., 2014; O'Driscoll et al., 2010; Shuster et al., 2005; Xu & Zhao, 2016). As a result, this study was conceptualized with the aim of quantifying the impervious surface area and runoff amount over time in Mihang'o, a developing urban watershed in the outskirts of Nairobi city. The findings of this study are critical in understanding runoff in developing urban watersheds.

1.2 Statement of the Problem

Kenya has had significant development activities in the recent past, including road and building construction (Gachanja et al., 2023; Mbuthia et al., 2022). Nairobi is one of the fastest growing cities in Africa with annual growth rate of 4% (Nairobi City County [NCC], 2023). This is attributed to high immigrants that come to the city in search of job opportunities. The proximity of Mihang'o to Nairobi City and Jomo Kenyatta International Airport (JKIA) has influenced rapid urbanization in the watershed (Gachanja et al., 2023; NCC, 2023). According to Gachanja et al. (2023), the majority of the Nairobi city working population are from Embakasi region, which includes Mihang'o watershed and accounts for 23 percent.

Consistent with the expanding population of the city particularly in Mihang'o watershed, the problem of rapid urbanization and impervious surface area increase, and consequently, increase in runoff and flooding (Ligtenberg, 2017; Xu & Zhao, 2016) is evident in Mihang'o. More tarmacked roads, residential and commercial buildings have been developed in Mihang'o since 2010. These areas were originally natural lands (Bosco et al., 2011). During the rainy season, flooding frequency and intensity downstream of River Mihang'o and at the Kangundo Road-Eastern Bypass

Highway junction have become increasingly concerning in recent years (Okwiri, 2021).

While poor urban planning and management could be a contributing factor to the problem of runoff in Mihang'o (Muli, 2008; Owuor & Mwiturubani, 2022; Tom et al., 2022), this study focused on establishing the relationship between impervious surface area increase and the runoff amount. By the time this study was conducted, there was inadequate knowledge about the relationship between the impervious surface area increase and runoff amount from Mihang'o watershed. Nairobi's population, which was approximately 4,672,000 in 2022, is projected to raise to 5,050,000 in 2027 (NCC, 2023). Given the ongoing urbanization in the Mihang'o watershed and greater Nairobi, it is crucial to examine the relationship between impervious surface areas and runoff in urban watersheds to develop effective solutions.

1.3 Justification of the Study

Increase in impervious surface area in a watershed results in increase in runoff from the watershed (Ebrahimian et al., 2016a). Runoff is a problem for several key reasons including water pollution, flooding, loss of biodiversity, soil erosion, ground water depletion, climate change vulnerability, and public health risk (Gachanja et al., 2023; Mbuthia et al., 2022; NCC, 2023; Okwiri, 2021). Mihang'o watershed has had increased urbanization and impervious surface area since the year 2000 (Gachanja et al., 2023; NCC, 2023). Similarly, there has been a consistent trend of high volume of runoff and flooding from the watershed. The runoff and floods downstream of River Mihang'o cut transport at the intersection of Kangudo Road - Eastern Bypass

Highway. The floods in Mihang'o also destroy property and take lives (Okwiri, 2021).

By the time this study was conducted, little evidence was available quantifying the relationship between increase in impervious surface area and runoff in a watershed. The studies that were reviewed associated poor urban planning, poor maintenance of drainage systems, and poor disposal of garbage as the cause of floods (Muli, 2008; Owuor & Mwitubani, 2022; Tom et al., 2022). It is essential to determine the direct contribution of impervious surface area to runoff from a watershed in order to develop practical solutions. Therefore, this study aimed to quantify the relationship between increase in impervious surface area and runoff in Mihang'o watershed was necessary. Findings from this study are critical for urban planners as there is need growing need to uphold environmental sustainability practices in cities including reduced runoff.

1.4 Research Hypotheses

The hypotheses of this study included:

- i. **H₀** There is no trend in impervious surface area time series of Mihang'o watershed.
- H₁** There is a positive trend in impervious surface area time series of Mihang'o watershed.
- ii. **H₀** No trend in the rainfall data time series of Mihang'o watershed.
- H₁** There is a trend in the rainfall data time series of Mihang'o watershed.
- iii. **H₀** There is no trend in runoff time series of Mihang'o watershed.
- H₁** There is a positive trend in runoff time series of Mihang'o watershed.

1.5 Objectives of the Study

The study's overall objective was to evaluate the relationship between change in impervious surface area and runoff amount in Mihang'o watershed from 2000 - 2022. The specific objectives of this study were to:

- i. Evaluate change in impervious surface area of Mihang'o watershed from 2000 to 2022.
- ii. Assess precipitation trend, amount in Mihang'o watershed from 2000 to 2022.
- iii. Determine trend in runoff amount from Mihang'o watershed from 2000 to 2022.

1.6 Significance of the Study

The significance of this study lies in its exploration of increase of runoff from urban watersheds, which has been largely overlooked in existing literature. By examining the quantitative relationship between increase in runoff and impervious surface area due to urbanization, this research addresses a critical gap that hinders our understanding of how much runoff is produced from a watershed that is undergoing urban development and impervious surface increase. Previously, no study had been conducted on impervious surface area and runoff in Mihang'o watershed. Existing studies attributed poor disposal of waste, poor urban planning, and poor management of drainage systems as a cause of runoff and flooding in Nairobi and the environs (Muli, 2008; Owuor & Mwiturubani, 2022; Tom et al., 2022). The findings have practical implications for urban planners, as they provide insights that can inform environmental sustainability practices. Additionally, this study lays the groundwork for future research in effectiveness of different mitigation strategies, the role of vegetation in reducing runoff, and the socio-economic impacts of urban runoff

management, thereby contributing to a more comprehensive understanding of runoff in urban watersheds.

1.7 Scope and Limitations of the Study

The research focused on the Mihang'o watershed, a smaller watershed within the larger Athi Catchment Area. While this choice provided valuable insights into the impacts of urbanization on runoff, a more comprehensive study involving a larger watershed with multiple sub-basins would enhance the generalizability and applicability of the findings for urban planning. The selection of the Mihang'o watershed was informed by its development history, reflecting the typical characteristics of a rapidly urbanizing watershed on the outskirts of Nairobi over the past 20 years (Gachanja et al., 2023; NCC, 2023; Onyango et al., 2021). Mihang'o watershed, located near the airport and Nairobi's urban center, has experienced significant urban sprawl in recent years, accommodating expansion from the densely populated districts surrounding the city. This characteristic made Mihang'o an ideal model study area. The Hydrological Engineering Center Hydrological Modelling System (HEC-HMS) model employed to simulate runoff was chosen for its accuracy in representing hydrological processes within a watershed, and the modeling process was meticulously conducted to ensure credible and reliable results. Although some input data for the HEC-HMS model, such as routing parameters and curve numbers, were approximated, these estimations were guided by the Technical Reference Manual for HEC-HMS (USACE, 2009).

1.8 Operational Definition of the Key Terms and Concepts

- i. **Impervious surface.** Impervious surface in normal usage refers to any impermeable surface, but in this study, it refers to manmade impermeable

surfaces (Stanuikynas et al., 2000). In this study, the following were considered impervious surfaces: buildings (rooftops) and roads, including gravel and dirt roads; tarmacked roads and streets; and paved curbs, open ditches, storm sewers, parking lots, and driveways (Ebrahimian et al., 2016a; Tang et al., 2018). Pervious surfaces in this study included vegetation, bare land, water bodies, and agriculture (Stanuikynas et al., 2000). Impervious surface area can either be total impervious area or effective impervious area. Total impervious area refers to all impervious areas in the catchment, while effective impervious area is a fraction of total impervious area that is hydraulically connected to stream channels (Ebrahimian et al., 2016a). The impervious surface area of a watershed can be converted to a percentage.

- ii. **Precipitation/Rainfall.** Precipitation and rainfall are used interchangeably in this thesis. They both refer to condensed water in the atmosphere falling on the Earth's surface (Cambridge Dictionary, 2023).
- iii. **Runoff.** The words floods, outflow, and discharge have been used interchangeably a few times in this study; they simply hold the same meaning as runoff, which refers to accumulated overland flow from a watershed after a rainfall event (ACE, 2009).
- iv. **Urban watershed.** A watershed dominated by development activities indicated by LULC features including many buildings and road networks (Ebrahimian et al., 2016b). Contrastingly, a rural watershed may be dominated by agriculture and large tracts of open land (Bosco et al., 2011).

CHAPTER TWO: LITERATURE REVIEW

2.1 Introduction

In this chapter relevant literature was reviewed based on the study's objectives namely impervious surface area, precipitation trend, and runoff. Runoff and flooding are prevalent in Mihang'o during rainy seasons, therefore, this review was necessitated by the need to develop an understanding of the relationship between runoff and impervious surface area due to urbanization over time. The main thematic areas reviewed are estimating impervious surface area, Mihang'o watershed impervious surface, analysis of precipitation trend, Nairobi's rainfall pattern, and modelling runoff using the HEC-HMS model. The chapter also involves a discussion of the conceptual framework adopted for this study.

2.2 Estimating Impervious Surface Cover

There are a variety of methods for calculating impervious surface area. According to Brabec et al. (2002), in the past, imperviousness was typically evaluated using grid overlay and planimetric techniques. Then, over the years, impervious surface estimation methods evolved including a field investigation approach, stereophotogrammetric, and inference methods. However, these traditional methods for estimating imperviousness have diminished with the invention of the Geographic Information System (GIS).

The grid overlay sampling method was most common in the 1970s for assessing larger areas. According to Bird et al. (2002), grid overlay follows these steps: a grid is overlaid on maps or aerial images of the region of research, several grid intersections are selected, the proportion of overlapping impervious areas is calculated, the process is repeated, and then the findings are averaged. The

disadvantage of the grid overlay method is that it is not very accurate, primarily because it mostly depends on the judgment of the user to distinguish pervious and impervious surfaces (Bird et al., 2002).

Using the planimetric technique, an analyst uses aerial pictures or topographic maps of the study region to define and measure apparent impervious areas and then estimates the impervious surface area percentage (Chabaeva et al., 2007). This method is still used and regarded as trustworthy, but the time and effort necessary to create fresh planimetric datasets for research regions bigger than a neighborhood makes it unfeasible. Nonetheless, in recent years, several communities with active GIS initiatives have generated planimetric datasets on impervious areas (Civco et al., 2006; Dougherty et al., 2004; Exum et al., 2005).

The field investigation approach has been utilized in the past for small study areas (Lee & Heaney, 2003). Field investigation method is beneficial because it allows for calculating both the total impervious area and effective impervious area. However, this technique is uncommon outside of site-scale initiatives because it takes much longer than the planimetric approach.

Stereophotogrammetric methods are used to obtain more precise measurements from large-scale aerial photographs. Stereophotogrammetric methods are preferred and regarded as the most precise because of the ability to eliminate many aberrations that impair accuracy. In Stereophotogrammetric methods, a rectified photo may give much information, but the photo's resolution, determined by the height at which the image was shot, is a limiting factor (Chiari et al., 2005).

The inference method involves the researcher using a table containing each LULC cover classification together with respective impervious surface coefficients to convert LULC data of the area being studied into an imperviousness estimate (Dougherty et al., 2004). Through rigorous hydrological studies, imperviousness coefficients for various regions have been created. Additionally, these hydrological studies have investigated and reported on different techniques for producing the imperviousness coefficients (Bird et al., 2002). Nonetheless, the accuracy is influenced by the researcher's competence, the resolution of the data, and the categorization system employed (Dougherty et al., 2004).

Advances in remote sensing have come to enhance direct methods. For instance, while the planimetric technique depends on humans visually identifying particular impervious regions on aerial pictures or maps, modern technologies for creating imperviousness datasets using images from the satellite allow analysts to include in computer algorithms the criteria for identifying impervious areas. Brabec et al. (2002) described this method for image classification as supervised classification. Alternatively, in unsupervised classification, the software's analysis of an image uses techniques that determine which pixels are related and group them into classes (Tang et al., 2018). Some GIS applications used to determine impervious surface area cover include MassGIS Imperviousness, ArcGIS, National Land Cover Database (NLCD) Imperviousness, and NLCD Land Cover (Granato, 2010). The ArcGIS is widely available to student researchers.

Scholars who have evaluated the precision of the various techniques and datasets used to determine impervious surface area support aerial picture interpretation over most satellite data-driven approaches (Chabaeva et al., 2007; Dougherty et al., 2004;

Draper & Rao, 1986). For instance, Draper and Rao (1986) found satellite data-driven approaches were less feasible for small study areas, such as a town than aerial photography. According to Chabaeva et al. (2007), the multiple data source strategy produces the most accurate estimations, compared to coefficients of land cover produced by impervious surface analysis tool or the imperviousness dataset of the US National Land Cover Database. According to Ebrahimian et al. (2015), multiple data source strategy may integrate analysis of rainfall-runoff data using empirical equations; using satellite-derived spatial data, for example, elevation and land cover with GIS techniques; and using field surveys of study sites such as inspection of downspout connectivity and street connectivity to the drainage system. The approach is especially suitable for determining effective impervious area because effective impervious area is a fraction of total impervious area (Ebrahimian et al., 2016b).

The disadvantage of remote sensing techniques in estimating impervious surface area is that the image's spatial resolution, cloud cover, and tree canopy affect its accuracy, especially on a micro-scale (Ebrahimian et al., 2015). Also, effective impervious area cannot be distinguished from total impervious area properly by using remote sensing techniques only. Even with this, the disadvantage of most other methods of estimating impervious surface area is that they are expensive and time-consuming to collect particular data, require expertise, and may produce unreliable results. With the accessibility of GIS-based tools and techniques for estimating impervious surface area, the GIS method has become attractive to most researchers. GIS-based tools and techniques are also attractive because of their applicability to ungauged watersheds and because spatial data is continuously increasing in availability and quality (Ebrahimian et al., 2015).

2.2.1 Mihang'o Watershed Impervious Surface

By the time this study was conducted, no research had focused on impervious surface trend in Mihang'o. However, several studies have investigated land use changes in Nairobi, of which Mihang'o watershed is part. The general finding is that Nairobi has demonstrated an increasing trend of urbanization. For instance, Mundia and James (2014) examined the spatial-temporal impacts of land use changes on land surface temperature (LST) through analysis of the NDVI, LULC, and LST for 24 years using Landsat satellite images. Mundia and James (2014) found that urbanization increased with shrubs, forests, grassland, plantations, and bare land being replaced by built-up areas, which was substantiated by a negative correlation found between LST and NDVI thus indicating increase in LST resulted from a shrinkage of vegetation cover and expansion of built-up areas or bare lands. Though the Mundia and James' (2014) study focused on surface temperature, it also revealed that Nairobi has significantly transformed from forests, shrubland, bare land, and grassland to built-up area.

Also, Bosco et al. (2011) investigated land cover types and pattern within Nairobi region using Landsat satellite data over a 30-year period to understand the dynamics in the spatial configuration of land uses in definitive ecosystem-level processes. Bosco et al. (2011) found that between 1976 and year 2000, urban areas and barren surfaces increased by more than 98% and 100%, respectively, and the coverage of forests and riverine vegetation decreased significantly by up to 60% and 67%, respectively.

According to Gachanja et al. (2023), population growth is a major indicator of the level of urbanization. While Kenya's population has grown from about 8 million in 1969 to 50 million in 2019, the urban population accounts for about 25% of the total population (Figure 2.1), and Nairobi's population of about 4,397,073 people

constitutes more than 30% of Kenya's urban residents (Gachanja et al., 2023). Nairobi's expanding population has led to a rising demand for residential and commercial space. In turn, green spaces have shrunk, and impervious surfaces due to construction activities and industrialization have substantially increased (Bosco et al., 2011; Mundia & James, 2014).

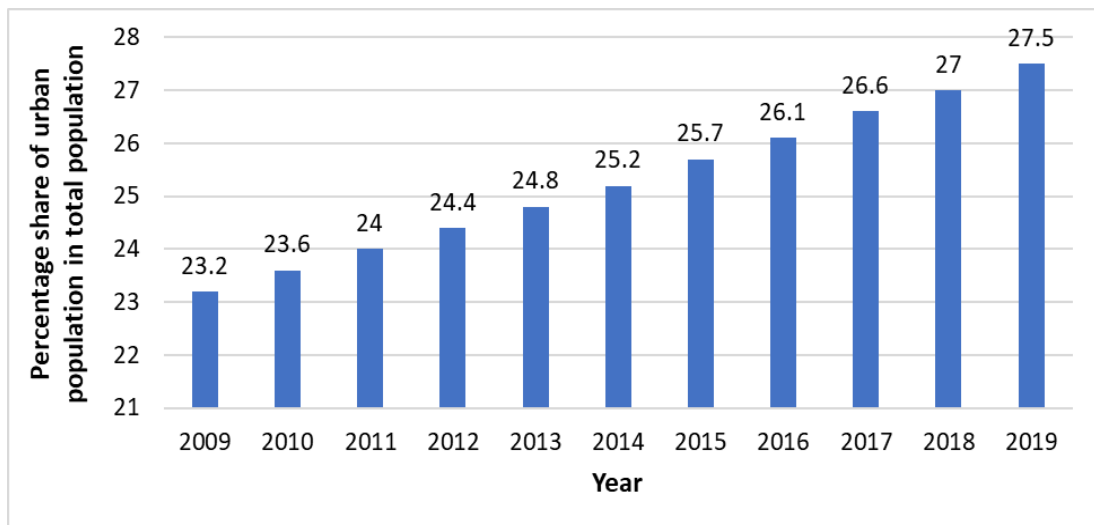


Figure 2.1: Urbanization in Kenya from 2009 to 2019 (Gachanja et al. 2023).

2.3 Precipitation Trend Analysis

Rainfall trend, often known as a precipitation trend, refers to marked variation in the temporal and spatial patterns of rainfall. In other words, rainfall trend is the general tendency, movement, or direction and pattern in which rainfall occurs. Scholars have suggested several approaches for determining rainfall trend. Generally, precipitation trend tests are either parametric or nonparametric (Bhat et al., 2019). A parametric test relies on the data's statistical distributions while a nonparametric test does not. Linear regression is one of the examples of parametric methods to test and model trends. Examples of nonparametric models include the Spearman's rho (SR), Mann-Kendall (MK) test, and Sen's slope. The nonparametric tests are often preferred because of their robustness and flexibility as they do not depend on normal

distribution of the data; they can handle data that is skewed, have outliers, or have different scales or units (Kandane-Rathnayake et al., 2013; Willems, 2012). The tests can be directly applied to the data if the data meets assumptions of constancy of distribution and independence. Rainfall data is often not normally distributed, thus making nonparametric tests most suitable for use (Alam et al., 2021). Nonetheless, because they analyze non-normally distributed data, nonparametric tests' power is often fairly weak; thus, the tests, in most cases, fail to reject a hypothesis even though the hypothesis could be true (Kandane-Rathnayake et al., 2013; Willems, 2012).

Alam et al. (2021) stated that Sen's slope method estimates the trend extent in time series data. The method provides the actual slope of a trend, for instance, the quantity of change every year. According to Serinaldi et al. (2020), who analyzed Sen's method, which is regarded as an innovative trend analysis model, cast doubts on the Sen's slope methodology and concluded that like every other parametric technique developed for trend analysis, it is influenced by serial correlation, distribution shape, and sample size.

The Spearman's rank correlation coefficient is used in analyzing monotonic patterns. Ahmad et al. (2015) analyzed precipitation trends using Spearman's rho and Mann-Kendall tests and concluded that the performance of the Spearman's rho and Mann-Kendall tests were consistent at the verified significance level. Nonetheless, scholars in the field of hydrology concur that the Mann-Kendall test has typically been utilized in rainfall trend analysis for the longest time (Alam et al., 2021; Jenifer & Jha, 2021; Sen, 2017; Treppiedi, 2021). Alam et al. (2021) describe the Mann-Kendall test as the test used to determine a monotonic increasing or decreasing trend

in a time series; it does not need normal distribution of the data; and does require that there is no autocorrelation. Therefore, this study utilized the Mann-Kendall test in determining rainfall trend in Mihang'o watershed because it is the most common method recommended by hydrologists.

2.3.1 Rainfall Pattern of Nairobi

The study area is a small part of Nairobi, Kenya; therefore, Nairobi's rainfall pattern is adopted. Nairobi is located along the Inter Tropical Convergence Zone (ITCZ), which influences the rainfall patterns of the region (University of Cape Town [UCT], 2017). The ITCZ crosses over Nairobi twice a year, following the movement of the overhead sun, causing bimodal distribution of rainfall (Figure 2.2). Nairobi's short rains occurring between November – December (ND) when the ITCZ migrates south over the region amount to about 200 mm (UCT, 2017). According to Kilavi et al. (2018), November rains are usually light showers of short duration; however, December rains are influenced by the inflow of Congo air mass and outbreaks of cold air from the middle latitudes. While the ITCZ is still south of the region between January and February, Nairobi receives little rainfall amounting to 80 mm (Kilavi et al., 2018). The long rains are received between March and May (MAM) when the ITCZ migrates northwards over the region, amounting to approximately 310 mm (UCT, 2017). The end of long rains matches with the ITCZ's northward shift in May, however moisture advection from the Indian Ocean linked with Indian Monsoons might cause considerable orographically related rainfall between May and June. The ITCZ is at the north between June and October thus little rainfall is experienced in Nairobi (UCT, 2017).

Interannual rainfall variability in Nairobi is large because while the long-term average is 615 mm, some years may record below 370 mm and some years above

750 mm (UCT, 2017). The MAM and ND rainfall amounts vary independently of each other. For instance, while the long-term average for the long rains is 310 mm, it may fluctuate by up to +/- 260 mm. Also, while the long-term average for the short rains is 200 mm, it may fluctuate by up to +/- 250 mm (Figure 2.3). The rain days and daily mean rainfall amount, also show interannual variability that is closely related to rainfall totals (UCT, 2017).

Nairobi's rainfall also displays variability on the multi-year timescale. The El Nino and La Nina conditions usually cause above-average and below-average rainfall, respectively. Also, decadal rainfall variability is experienced in Nairobi; however, the 35-year length data is insufficient to display variability (UCT, 2017).

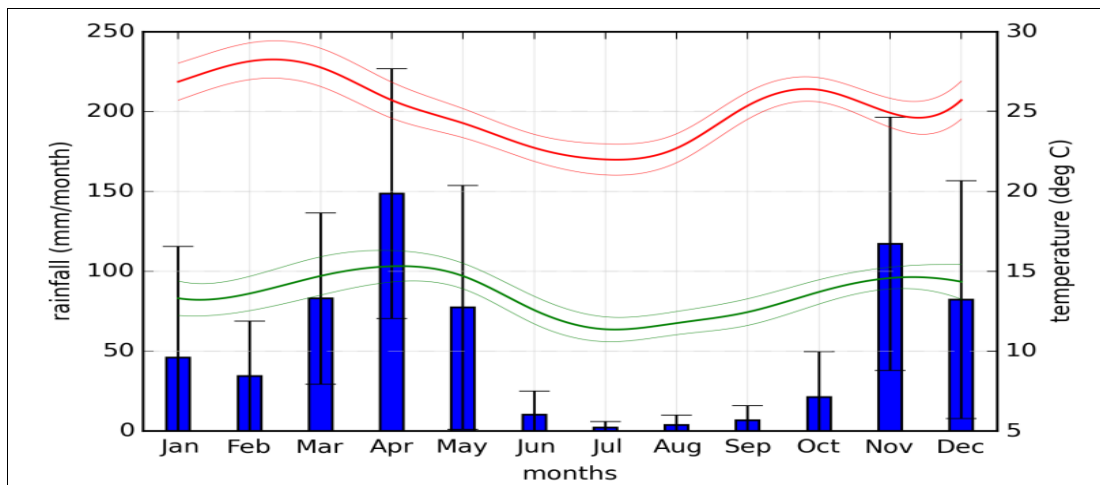


Figure 2.2: Nairobi's Average Climate Seasonality.¹ (UCT, 2017)

¹ The blue bars depict the mean monthly total rainfall (mm/month) with whiskers showing +/- 2 standard deviations. The red and green lines represent the monthly mean daily maximum and minimum temperature, respectively.

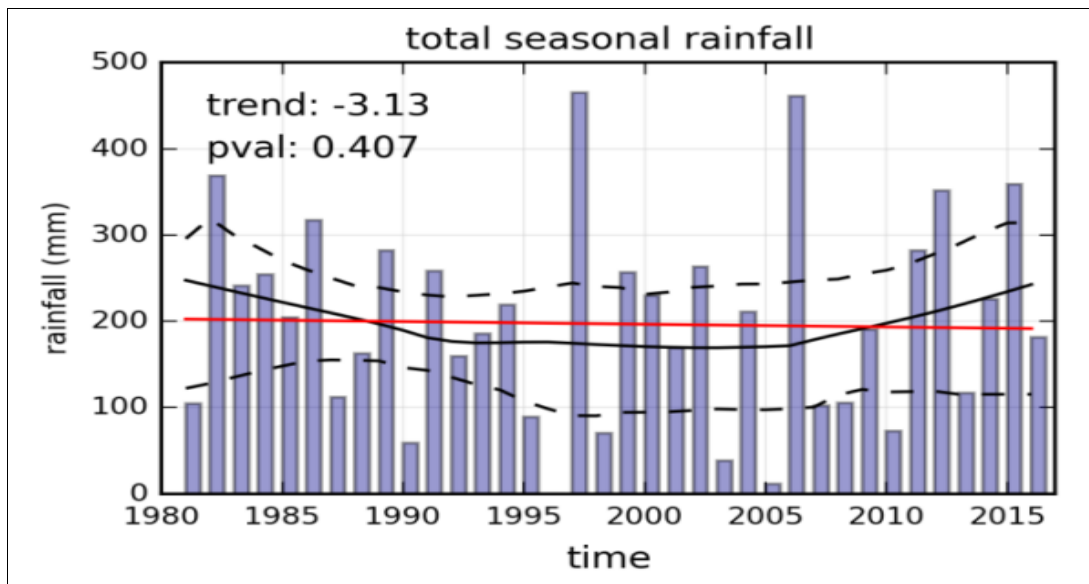


Figure 2.3: Short Rains Season Statistics for Nairobi.² (UCT, 2017)

2.4 Determining Runoff Trend

Runoff is the amount of overland flow after a rainfall event. Runoff is the remainder of water after the rest has infiltrated and can be exacerbated by an impervious surface (Rahajeng, 2010). Several models can simulate runoff, which requires precipitation and impervious surface coefficient as the essential data inputs (Kalra, 2022). According to Xu and Zhao (2016), there are a variety of models and procedures to use to simulate runoff, which depends on the researcher's expertise, the problem's complexity, the availability of data, and the expected output results. The models include the HEC-HMS, the European Hydrological System Model, the Topography Based Hydrological Model, the Water Erosion Prediction Project (WEPP), the Storm Water Management Model (SWMM), the Soil and Water Assessment Tool (SWAT), and the Modular Modeling System (Xu & Zhao, 2016). Besides using model applications to simulate runoff, the other methods include the curve number, runoff plot, and isotopic tracer (Guo et al., 2019).

² Short rains season data between 1981-2016 with the blue bars representing annual statistic. The red line represents the Theil-Sen linear trend line. The median is represented by the solid black line. The dashed represents the 95th confidence interval.

This study used the HEC-HMS model. Several high-quality studies have used the HEC-HMS and have established its efficacy and reliability. For instance, Verma et al. (2010) evaluated WEPP and HEC-HMS in simulating runoff. Verma et al. (2010) found WEPP model's deviation of total runoff volume ranged between -13.96% and 13.05% while HEC-HMS' ranged between -2.55% and 31%, suggesting that the WEPP model is more accurate. However, Verma et al. (2010) found higher values of Nash-Sutcliffe error (NSE) and lower values of root mean square error (RMSE) when using HEC-HMS to calibrate, which indicates HEC-HMS's streamflow simulation is more reliable than compared to WEPP. Verma et al. (2010) concluded that HEC-HMS is more robust compared to WEPP in modeling streamflow.

Most studies that were reviewed compared HEC-HMS with SWAT and had varied results. Ferreira et al. (2021) evaluated SWAT and HEC-HMS performance in fluvial flow simulation and found that their obtained indices indicated that both software systems satisfactorily simulated the flow but SWAT was more robust and statistically superior for future predictions. Also, in a study conducted by Chathuranika et al. (2022), the results inferred that the HEC-HMS model adequately simulated medium flows, the SWAT model adequately simulated high flows, and both models accurately simulated low flows. Nonetheless, Chathuranika et al. (2022) recommended SWAT.

However, in the study conducted by Aliye et al. (2020), SWAT's NSE was found to be greater than 0.67 and Coefficient of Determination (R^2) greater than 0.78, while the HEC-HMS' NSE was found to be greater than 0.73 and R^2 greater than 0.87. Based on the results of their study, Aliye et al. (2020) concluded that the streamflow simulated by HEC-HMS model was more satisfactory compared to the SWAT

model. These results supporting the efficiency of HEC-HMS are consistent with those of Belay et al.'s (2022) study that compared loss models within HEC-HMS and those of Yu and Zhang's (2023) study that analyzed the efficacy of the HEC-HMS in modeling floods in urbanized basins.

2.4.1 The HEC-HMS Model

Despite the mixed results about the HEC-HMS's efficacy, I chose to use it in this study because of having expertise in it. The HEC-HMS model, created by the Hydrologic Engineering Center (HEC) - a department of the US Army Corps of Engineers - integrates all hydrologic processes in dendritic watershed systems (Hydrologic Engineering Center-US Army Corps of Engineers [USACE], 2009). The model simulates rainfall-runoff processes across a wide variety of areas, including runoff and flood hydrology simulation of a large river basin water, natural watershed runoff, and small urban. The model operates various big tasks related to hydrological studies, for instance, open channel routing, runoff transform, losses, parameter estimation, meteorological data analysis, and simulation of rainfall-runoff. The model's ability to simulate runoff in both long-term and short-term events, its use of common methods, and its simplicity of operation have contributed to its popularity in hydrological studies (USACE, 2009).

The required data for building an HEC-HMS model include impervious area percentage, LULC cover, elevation, hydrograph information, and soil. The basic information about the catchment's physiographic characteristics, including routing reaches, junctions, sub-basins features, such as centroid elevation, basin centroid, basin slopes, longest flow path, and centroidal longest flow lengths, are extracted

from a digital elevation map (DEM) of a place, after processing using ArcGIS or HEC-GeoHMS (USACE, 2009).

The HEC-HMS has the loss models for calculating runoff volume, the transform models for computing the runoff of excess precipitation, the baseflow models for computing baseflow, and the routing models for computing attenuation (USACE, 2009). HEC-HMS interface has a title bar, toolbar, menu system, and four panes. The panes include the Watershed Explorer, showing where files and folders in which operations are contained; the Desktop, where the work is done; Component Editor, showing the operations; and the Message Logs, showing a transcript of the operations made. HEC-HMS presents the results of simulations in tables and graphs.

2.4.2 HEC-HMS Modelling Example

The HEC-HMS model configuration includes a basin model, a meteorological model, input data (time series data), and control parameters (Gebre, 2015). Additionally, several supporting data, as dictated by the predetermined loss, transform, and routing specifications, should be determined before starting an HEC-HMS project (Tassew et al., 2019). The following sections contain a description of how these prerequisites are determined ahead of starting an HEC-HMS project.

Basin Model. Basin information is the fundamental step in the HEC-HMS project. The basin model carries watershed physical parameters information (Sahu et al., 2020). The watershed physical parameters required in an HEC-HMS project include sub-basins, river reaches, junction, sink, size of sub-basins, and slope of the sub-basins. The ArcGIS can be used to process the watershed physical parameters a shapefile. While preparing the basin model, the loss, transform, and routing specifications have to be entered (USACE, 2009).

The Loss Model. In HEC-HMS' loss models, the runoff volume is generally calculated by subtracting the volume of water intercepted, infiltrated, stored, transpired or evaporated from the precipitation. HEC-HMS has nine loss methods; the Soil Conservation Service Curve Number (SCS-CN) loss method is commonly used. According to Tassew et al. (2019), the advantage of the SCS-CN loss method is that it is a simple conceptual method for estimating the runoff amount from a rainfall event and it is well supported by primary data. Furthermore, the SCS-CN loss approach is solely based on the curve number, which is a function of the key runoff-producing watershed parameters of soil type, LULC, and previous moisture content (USACE, 2009). Gebre (2015) stated that the curve number method assumes that runoff is directly proportional to the precipitation after an initial abstraction of 20% of the potential maximum storage. The other advantage of the SCS-CN method is that it is used in diverse environments and yields credible results as complex models despite its simplicity (Lastra et al., 2008). However, the disadvantage of the SCS-CN technique is that it does not take into account temporal change of rainfall, rainfall intensity, or average ground slope. The CN values range from approximately 30 for permeable soils with high infiltration rates to 100 for water bodies (Tassew et al., 2019). The loss model also requires impervious surface coefficients as an input. In each simulation run, the CN value is a constant variable while the impervious surface coefficient is the changing variable.

The Transform Model. The HEC-HMS transform models simulate transformation of excess precipitation to runoff on the watershed. There are seven transform models in HEC-HMS; the Soil Conservation Service Unit Hydrograph (SCS-UH) model is one of them. The only input for this method is the lag time (T_{lag}) (Tassew et al., 2019; USACE, 2009), thus making SCS-UH suitable for use in this small-scale

study. Lag time is the amount of time between the peak amount of rainfall and the peak discharge in the river (Sultan et al., 2022) and is calculated based on the time of concentration T_c , as shown in Equation (2.1) (Sultan et al., 2022; Tassew et al., 2019).

$$T_{lag} = 0.6T_c \quad (2.1)$$

where T_{lag} and T_c are in minute.

The concentration time is estimated based on the basin's characteristics including length of the reach and topography using Kirpich's formula as shown in Equation (2.2) (Sultan et al., 2022; Tassew et al., 2019).

$$T_c = 0.0078 \times \left(\frac{L^{0.77}}{S^{0.385}} \right) \quad (2.2)$$

where S is the slope in (ft/ft) and L is the reach length in feet.

The Routing Model. Flood runoff attenuates while passing along the channel reach because of channel storage effects. This attenuation is taken into account by the routing models offered in HEC-HMS. The Muskingum routing method was developed by Gerald McCarthy of the US Army Corps of Engineers in 1938. The Muskingum method is a popular lumped flow routing technique that has been widely employed in river engineering since its creation (Tassew et al., 2019; USACE, 2009).

The Muskingum routing approach approximates the downstream outflow hydrograph from the upstream input hydrograph of a channel reach (Tassew et al., 2019). Two parameters are required for this model calibration: the flood wave's travel duration (K) through the routing reach and dimensionless weight (X), which corresponds to the flood wave's attenuation as it goes through the reach (USACE, 2009). According to Tassew et al. (2019), $X = 0.5$ indicates a full wedge, $X = 0$ indicates no wedge,

such as a level pool reservoir, and X values for natural streams are between 0 and 0.3, with a mean of 0.2.

Precipitation Data. The precipitation data for the rainfall event are put in the time-series file. The specified hyetograph method enables specifying the precise time-series for the hyetograph at sub-basins. The method is beneficial when precipitation data is processed outside of the program and then imported without change. This method is also beneficial when the whole sub-basin is represented by a single precipitation data (USACE, 2009).

The meteorologic models is used to set meteorologic boundary conditions for the sub-basins' (USACE, 2009). Results computed by a meteorologic model are matched with the sub-basins in the basin models using the name of the sub-basin. The control specifications file is a significant component in the HEC-HMS project, even though it does not contain much parameter data. The control specifications file controls when the start and stop time and time interval of a simulation (USACE, 2009).

2.4.3 Runoff Trend over Time

Generally, runoff increases in a watershed with increase in impervious surface as a result of developmental activities. According to Bajracharya et al. (2015), as more landscapes become covered with impervious surfaces, the amount of water that infiltrates decreases, while run-off amount increases. Nonetheless, besides impervious surface area, the amount of runoff is determined by several other factors, including whether impervious surfaces are connected or not connected to a drainage channel, the soil type in the watershed, slope of the watershed, amount of precipitation, length of the reaches, and size of the watershed (Chathuranika et al., 2018; Guo et al., 2019; Rezaei et al., 2019; USACE, 2009; Xu & Zhao, 2016).

2.5 Summary of Literature and Identified Gaps

Table 2.1 provides a summary of some of the pertinent sources reviewed and the identified gaps filled by this study.

Table 2.1: Summary of Literature and the Identified Gaps

Author (s)	Objective	Methods	Summary of Findings	Identified Gaps
Bajracharya, A. R., Rai, R. R., & Rana, S. (2015).	To study run-off conditions in urban areas, focusing on Kathmandu Metropolitan City (KMC).	The curve number method.	Results showed runoff is significantly high, demonstrated by the run-off totals pre- and post-development.	Other intervening variables for runoff not accounted for including hydrologically connected impervious surfaces to a drainage channel, slope of the watershed, and length of the reaches. The HEC-HMS model used in this study accounted for several intervening variables that comprehensively influence runoff.
Bosco, N. J., Geoffrey, M. M., & Kariuki, N. (2011)	To understand spatial configuration changes of land uses in ecosystem using Nairobi City and its environs between 1976 and year 2000.	Landsat satellite data analysis; supervised classification.	Between 1976 and year 2000, urban areas and barren surfaces increased by more than 98% and 100%, respectively, and the coverage of forests and riverine vegetation decreased significantly by up to 60% and 67%, respectively.	The study involved Nairobi's data between 1976 and 2000, which is outdated in 2020s. Nonetheless, the article stands out as a major reference. This study built and extended on Bosco et al.'s (2011) by providing up to date findings on impervious surface cover in Mihang'o watershed.
Gachanja et al. (2023)	To describe urbanization and population growth in Nairobi.	Non-experimental time series design, using both qualitative and quantitative data & expert opinion.	Nairobi's population constitutes at least 30% of Kenya's urban residents. Nairobi's expanding population has led to a rising demand for residential and commercial space turning green spaces to impervious surfaces.	Did not describe quantitative increase of impervious cover in Nairobi. This study quantified impervious surface cover over the years.

Mundia & James (2014)	To examine the spatial-temporal impacts of changes in land on LST in Nairobi between 1986 and 2010	Analysis of the LST, LULC, and NDVI using Landsat satellite images	Urbanization increased; built up areas replaced shrubs, forests, grassland, plantations, and bare land	The study's limitation is that it may not provide a clearer picture of the current situation considering that significant urbanization has occurred in Nairobi since 2010. Nonetheless, the article stands out as a major reference. This study built and extended on Mundia & James' (2014) by providing up to date findings on impervious surface cover in Mihang'o watershed.
Kilavi et al. (2018)	To examine the nature, causes, impacts, and predictability of the rainfall events in central Kenya, including Nairobi City	Archival analysis/computation	Nairobi has bimodal distribution of rainfall consistent with movement of the ITCZ over the region	Data analyzed was of between 1971 and 2018 and is for a wider area including Central Kenya and Nairobi City. This is foundational for this study. However, this study produces an updated findings of rainfall trend in Nairobi, particularly Mihang'o watershed.
University of Cape Town (2017)	To describe Nairobi's climate	Expert opinion	Nairobi has two rainfall seasons: short rains (ND), and long rains (MAM). Annual total rainfall varies between approximately 300 and 900mm/year	Analyzed data between 1980 and 2014. There was a need for an updated research findings on rainfall, which this study filled.

2.6 Conceptual Framework

This study adopted and modified the *Runoff Flow Changes resulting from Urbanization's Impervious Surface Area* conceptual framework that describes the quantitative relationship between urbanization, or rather the level of impervious surface, and runoff (Figure 2.4). According to the *Runoff Flow Changes resulting from Urbanization's Impervious Surface Area* conceptual framework, as urbanization increases, thus increasing impervious surface area, runoff increases too. Notably, in natural ground cover, runoff is approximately 10%; when the impervious surface is between 10% and 20% of the watershed, runoff increases to about 20%; when the impervious surface is between 35% and 50%, runoff is approximately 30%; and when the impervious surface is between 75% and 100%, runoff is approximately 55% (Ligtenberg, 2017). According to the framework, infiltration and evapotranspiration reduce proportionately with increased runoff. Overall, according to the conceptual framework, precipitation is a constant, the independent variable is impervious surface area due to urbanization, and the dependent variables are runoff, evapotranspiration, and infiltration (Ligtenberg, 2017). Nonetheless, on the model, only the relationship between impervious surface and runoff, evapotranspiration, and infiltration are displayed (Paul & Meyer, 2001).

Based on the findings from the reviewed literature, the *Runoff Flow Changes resulting from Urbanization's Impervious Surface Area* conceptual framework is an abstract guide because more factors in a watershed influence the amount of runoff (USACE, 2009). Therefore, in the modified conceptual framework (Figure 2.5), as the researcher, I have only introduced the intervening variables, watershed factors, that determine the amount of runoff. The intervening variables include the amount of precipitation received, watershed's soil type, type of imperviousness, size of the

watershed and sub-basins, slope of watershed, length of the reaches, positioning of sub-basin centroid and elevation, initial abstraction, longest flow path, and whether impervious surfaces are connected or not connected to a drainage channel (Chathuranika et al., 2018; Guo et al., 2019; Rezaei et al., 2019; USACE, 2009; Xu & Zhao, 2016). Most of these intervening variables are factored into a simulation model to determine a more accurate amount of runoff from a watershed.

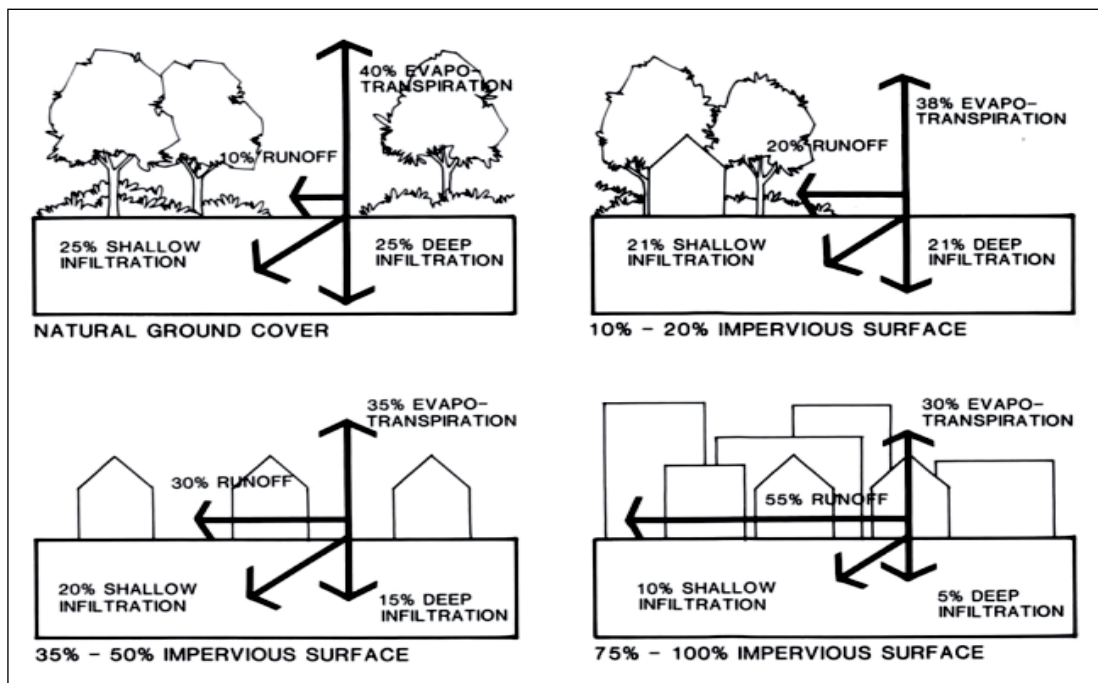


Figure 2.4: Runoff Flow Changes due to Urbanization (Paul and Meyer, 2001)

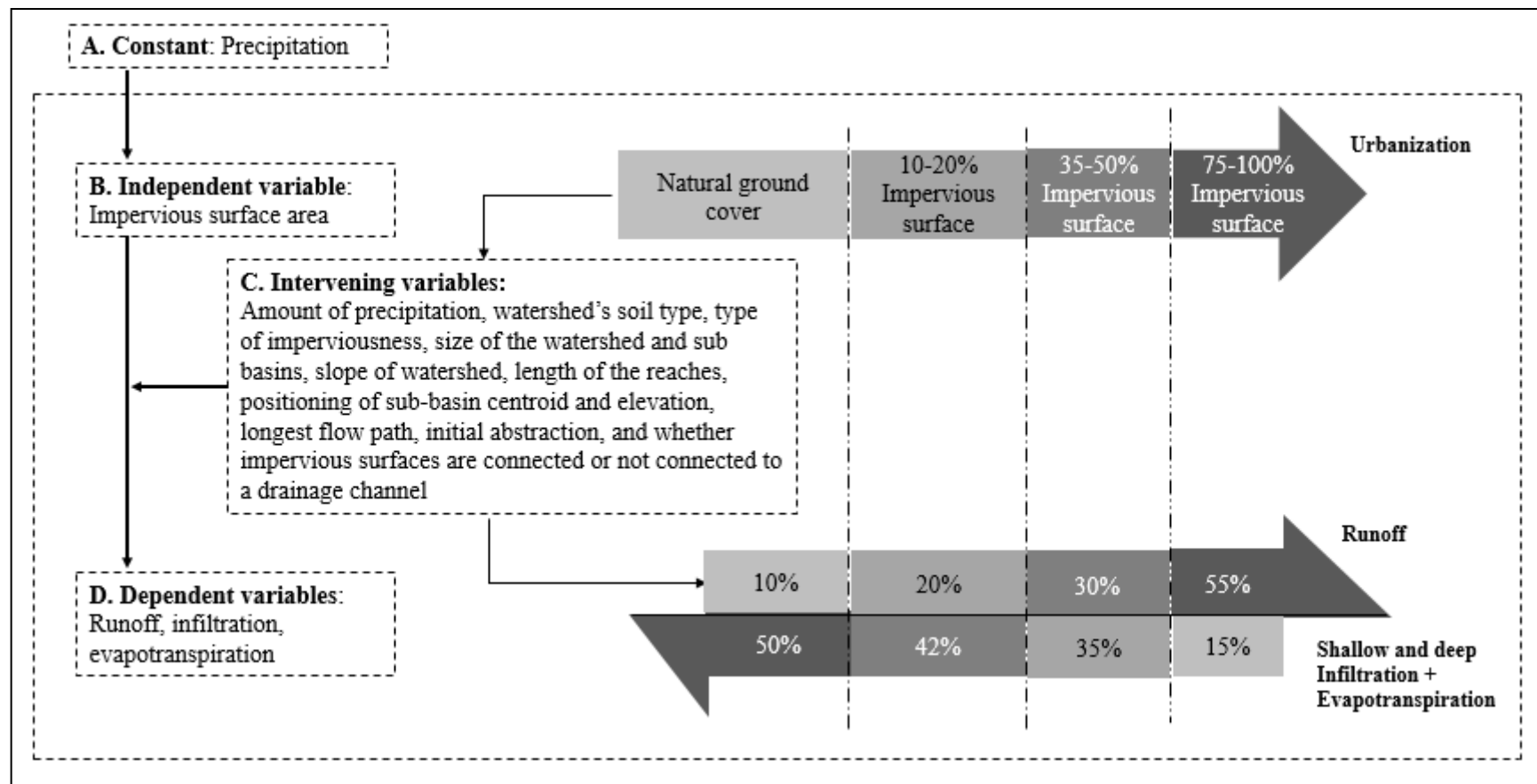


Figure 2.5: Modified Runoff Flow Changes due to Urbanization (Adopted and modified from Paul and Meyer, 2001)

CHAPTER THREE: MATERIALS AND METHODS

3.1 Introduction

This chapter explains the research design adopted for this study. It also gives a detailed description of the study area as well as outlining the research instruments, methods of collecting data on impervious surface area, rainfall, and runoff in Mihang'o watershed. Additionally, the chapter explains the analysis procedures of the data collected to achieve the study's objectives.

3.2 Study Area

Mihang'o watershed is located on the outskirts of Nairobi City and south of the equator, lying between longitudes $36^{\circ} 55'$ and $36^{\circ} 60'$ east and latitudes $1^{\circ} 15'$ and $1^{\circ} 20'$. The watershed covers an approximate area of 17.6 km² traversing Nairobi and Machakos counties, as shown in Figure 3.1, with Ruai – Embakasi – Mihang'o sub-locations in Nairobi County and Katani in Machakos county. Its altitude ranges from 1,499 meters above sea level (MASL) northeast of River Mihang'o's outlet to 1,624 MASL at JKIA. The river pours its water into the Nairobi River, a drainage system in the upper Athi drainage basin (Water Resources Authority [WRA], 2014). The watershed has notable features such as an international airport, the General Service Unit Training School (GSUTS), the eastern bypass highway, and the Administration Police Training Center (APTC). Being on the periphery of Nairobi City, Mihang'o has a high settlement density influenced by the closeness to the city.

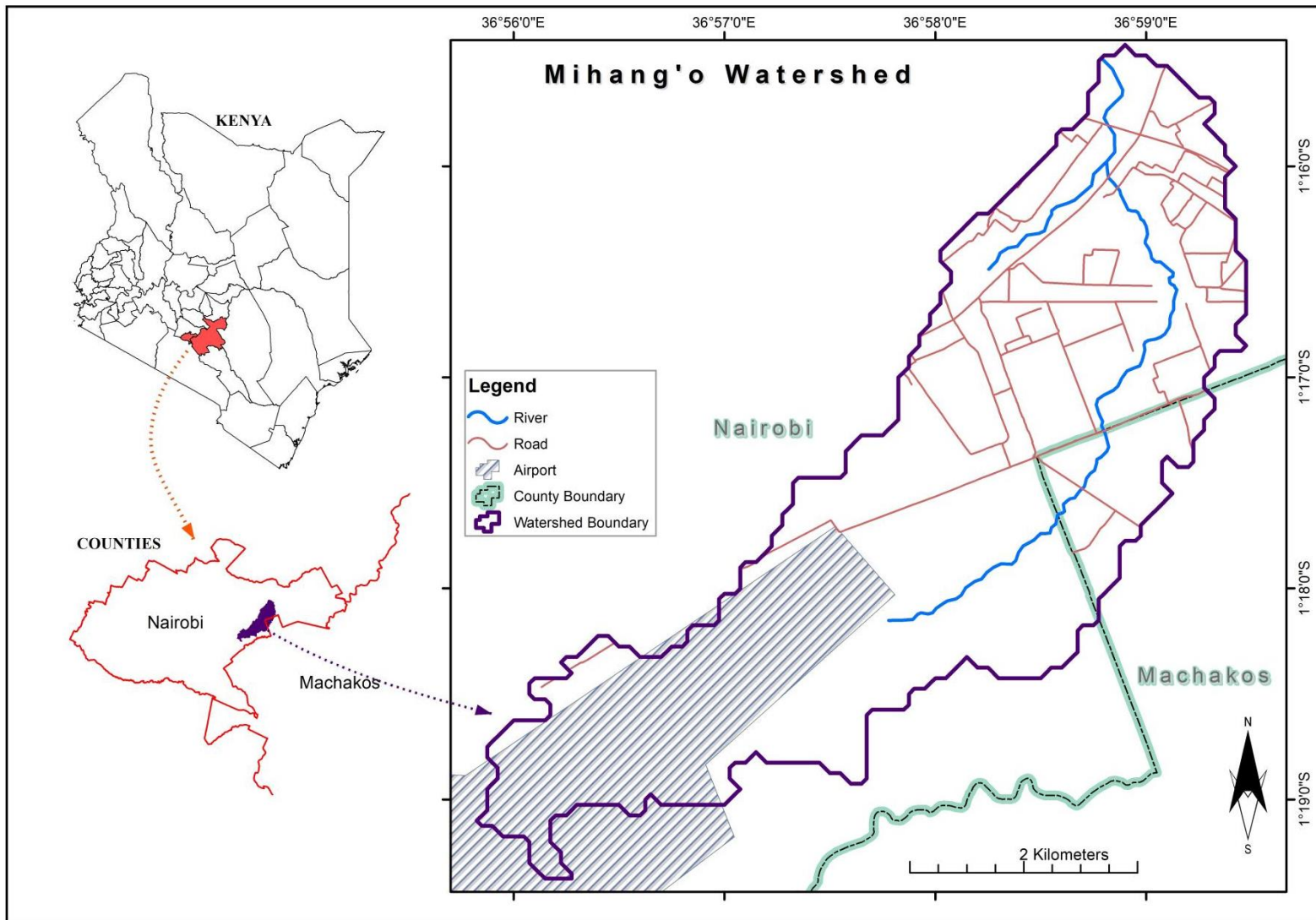


Figure 3.1: Location of Mihang'o Watershed

3.2.1 Climate

Mihang'o watershed is part of the Nairobi region, located in ecological zone five and classified as a sub-humid region with a subtropical highlands climate (Muli, 2008). Nairobi is averagely 1663 (Mwathi, 2016; NCC, 2023), located at the eastern edge of the East African Rift Valley, which significantly impacts its climate (Distances, 2023). Rainfall varies strongly from year to year (Kotikot et al., 2024; UCT, 2017). Typically, Nairobi's annual total rainfall varies between approximately 300 and 900mm/year, though it can be much higher during extreme years. There are primarily two rainfall seasons in Nairobi (Muli, 2008). The long rains (MAM) averagely record 310 mm, and the short rains (ND) record approximately 200 mm. Though some rains totalling 80 mm are recorded between January and February, they are little compared to the main seasons. June to October is a relatively dry period (Kotikot et al., 2024; UCT, 2017).

Nairobi's temperature data displays variability at several time scales. Diurnal temperature variability is approximately 12 °C. Though the temperature changes throughout the year, the seasonal cycle is relatively small because of Nairobi's position immediately south of the equator. This results in a daily minimum temperature fluctuating by approximately 5 °C and daily maximum temperature fluctuating by approximately 6 °C (UCT, 2017). As shown in Figure 2.2, the long-term data shows that January – March are the warmest months, with an average daily maximum temperature of 27.5 °C and a secondary peak of 26 °C experienced between September – November. These warm months correspond with the onset of the rainy seasons. Also, the daily maximum temperature is lowest (22.5 °C), usually between June and August. The warmest night-time temperatures are averagely 15 °C during March – May and coldest night-time temperatures are averagely 11.4 °C in

July (UCT, 2017). The average annual temperature year-to-year differences are small, only around 1°C (UCT, 2017). According to Muli (2008), the long-term mean annual temperature for Nairobi is approximately 23°C.

3.2.2 Soils and Geology

Mihang'o watershed is part of the Eastern and lower parts of Nairobi's physiographic landforms. While Nairobi is roughly 1663 MASL (NCC, 2023), Mihang'o watershed's elevation is lower, averaging 1562 MASL. The watershed's landscape is generally gently undulating, sloping northwards. The watershed has two tributaries that converge and drain into the Nairobi River (Muli, 2008).

As part of the larger Nairobi sub-catchment area, Mihang'o watershed constitutes the area where volcanic activities dominated the geological history and controlled the geomorphological evolution (Onyancha et al., 2011). The area has layers of tuff and lava subjected to varying degrees of weathering. As a result, the Nairobi trachytes cover the watershed. They are formed of superimposed trachytic lava flows, occasionally porphyritic, with phenocrysts of feldspar in affine-grained matrix (Akech et al., 2013).

The soil survey reveals the complex relationship between landforms and geology in many parts of Kenya (Muli, 2008). Soils in Mihang'o watershed take the characteristics of soils of Athi River town as it is on the eastern side of Nairobi city. In this area are patches of vertisols soils, a complex of well-drained to imperfectly drained shallow to moderately very dark, greyish brown, firm, slightly to moderately calcareous, rock stony or gravelly clay. These soils combined have a permeability coefficient between 0.013 cm/hr and 0.38 cm/hr (Muli, 2008).

3.2.3 Topography

Mihang'o watershed is generally a gently undulating landscape (Mwathi, 2016). The watershed gently slopes from south to north, with its highest point at JKIA, which stands at 1624 MASL, and its lowest point at the outlet near the Eastern Bypass-Kangundo Road junction, at 1499 MASL (NCC, 2023). The watershed is relatively long and narrow, stretching 8.8 km from southwest to northeast, with a maximum width of 2.5 km. The watershed has an outcrop of rocks at a quarry site in the northern part. There are no significant water bodies in the watershed because the streams are tributaries of the Nairobi River and are seasonal. Over the years, human encroachment has caused the streams to dry up, leaving behind channels that now serve as conduits for waste and runoff water (Mwathi, 2016).

3.2.4 Land Use/Land Cover

Mihang'o watershed was originally a shrubland, grassland, and bare land where wildlife roamed. However, over the years, man occupied the area and caused urbanization (Mwathi, 2016). As a suburb of Nairobi, Mihang'o is primarily characterized by multi-story residential buildings. Also, the watershed is connected with tarmacked roads in most areas. The infrastructure, including the buildings and tarmac roads, emerged and increased since 2000 after the prospect of upgrading the Eastern Bypass Highway that connects the Mombasa Highway and Thika Super Highway. As a result, the empty spaces in the watershed have shrunk over the years and are now characterized by a mixture of nucleated, linear, and dispersed settlement patterns (Mundia & Aniya, 2005).

The southern part of the watershed is predominantly empty because it is occupied by JKIA, GSUTS, and the APTC, which have few scattered structures (Mwathi, 2016;

NCC, 2023). The other few empty spaces are undeveloped plots and recreational areas such as hotels, churches, schools, playgrounds, administrative centers, and an abandoned quarry near Ruai (Gachanja et al., 2023; NCC, 2023). Though the area hosts people working in the city and other suburbs, a significant proportion of the population are small-scale business people; therefore, most buildings have shops on the ground floor. The area also has bus stations, kiosks, pubs, workshops, gas stations, and garages (NCC, 2023).

3.3 Data Collection

Data collection and processing is described in detail in this section based on the sequence of the three objectives of this study. Data collection was done upon approval of the research proposal by Kenyatta University's Graduate School and reception of the National Commission for Science, Technology and Innovation (NACOSTI)'s approval letter.

3.3.1 Determining Change of Impervious Surface Area

Satellite images were used to determine changes in land cover in Mihang'o watershed over the years. Landsat 7 satellite images (15-meter spatial resolution) over Nairobi were obtained from Regional Center for Mapping for Resource Development (RCMRD) with acquisition dates from July to September, when the atmosphere is clear and cloud and haze-free. A clear sky enables the satellite to capture clearer images of land use features (Mikelsons & Wang, 2021).

I singled out Landsat images for 2000, 2003, 2006, 2009, 2012, 2015, 2018, and 2022 for the study to determine LULC change, or rather impervious surface area trend. Studies recommend a 5 to 10-year time periods as optimal for capturing land use changes (Güneralp et al., 2020; Seto & Shepherd, 2009). According to Seto and

Shepherd (2009), shorter periods cannot capture all changes occurring, and longer periods may not demonstrate a traceable trend. Güneralp et al. (2020) studied urban land use change over a long-time frame of 44 years, between 1970 and 2014. This study's time frame of 22 years, between 2000 and 2022, is short; therefore, as the researcher, I used a 3-year gap to increase the number of units included to show a clear trend.

With the Mihang'o watershed shapefile and tools in the Multivariate toolset of the ArcGIS (10.4) Spatial Analyst extension, the I completed the supervised classification of the satellite images for each year of study. Figure 3.2 shows the procedure followed in supervised classification.

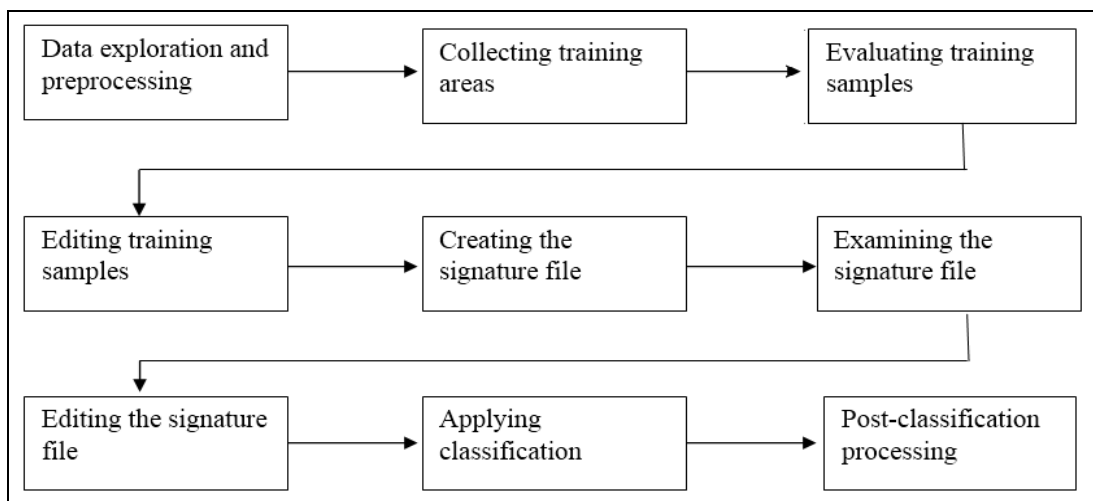


Figure 3.2: Process Followed During Supervised Classification

The supervised classification was used to process land cover. Though supervised classification is tedious and time-consuming, it is an accurate approach (Alves & Sanches, 2023). Classes are defined by the researcher in supervised classification, unlike unsupervised classification, in which classes are automated (Campbell, 2002). Therefore, supervised classification is detailed and requires the researcher to be knowledgeable about the watershed. Supervised classification also allows the

detection of mistakes or issues and customized correction (Alves & Sanches, 2023).

For instance, since the researcher controls the process, sections of known identity can be linked. Additionally, supervised classification is suitable for a smaller study area (Campbell, 2002), such as Mihang'o watershed, which is 17.6 km².

Mihang'o watershed is a developing urban area - the notable LULCs include building structures for residential units, commercial businesses, small industries, churches, schools, and administrative centers; there are bare lands or rather open fields; there are patches of vegetation and agriculture; and there are networks of tarmac roads, paved parking lots, driveways, and gravel and dirt roads.

I selected the following classes based on the existing land LULC of Mihang'o watershed: water, buildings, vegetation, agriculture, bare land, and tarmac. Therefore, impervious surfaces in the watershed included rooftops (buildings), paved parking lots, driveways, tarmacked streets and roads, gravel and dirt roads, paved curbs and storm sewers, and paved open ditches. These impervious surfaces were dissolved into a single entity.

3.2.1.1 Data Quality Control for Impervious Surface

The essence of data quality control is to ensure the study's quality and to maintain proper data analysis, meaning, and interpretation. The Google map of Mihang'o watershed in conjunction with ground truthing were employed to counter check results of supervised classification. Additionally, mass curve technique was used to check the consistency of the resultant impervious surface percentages of the years of study.

3.3.2 Determining Trend of Precipitation Amount

The Climate Hazards Group InfraRed Rainfall with Station (CHIRPS) v2.0 dataset was used in this study (Kotikot et al., 2024). It is a quasi-global dataset available at a relatively high spatial resolution of 0.05° and multiple time steps (daily, 5-day) beginning 1981 to present. It is developed based on high-resolution infrared satellite measurements and blended with ground observation station data (Kotikot et al., 2024). The rainfall data was downloaded from Google Earth, a geobrowser that renders a three-dimensional representation of the Earth, based primarily on satellite imagery (Science Education Resource Center [SERC], 2020). Google Earth is free, though users need to create a user account (SERC, 2020).

A customized JavaScript code was used to download CHIRPS rainfall data from Google Earth. The script estimated daily rainfall data in Mihang'o watershed from 2000 to 2022. Google Earth allows data to be exported as Excel files. To be consistent with the first objective, daily rainfall data for 2000, 2003, 2006, 2009, 2012, 2015, 2018, and 2022 were picked for processing from the downloaded file. The rainfall data for the selected years were computed into monthly and annual totals.

A disadvantage of CHIRPS is that its agreement with ground observations tends to vary across space and time, depending on the density of gauge stations (Kotikot et al., 2024). Therefore, in areas with sparse gauge stations, CHIRPS is prone to errors, particularly underestimating rainfall in high-elevation zones and overestimating it in lowland areas. In addition, CHIRPS is suggested to have a slight dry bias and was found to struggle in capturing extreme rainfall in some parts of the world (Kotikot et al., 2024).

Nonetheless, CHIRPS was chosen as the primary rainfall dataset in this study due to both its performance in validation studies, and due to its wide-ranging use in both Kenya drought research and operations (Kotikot et al., 2024). CHIRPS data is developed based on high-resolution infrared satellite measurements and blended with ground observation station data, therefore, it closely matches data that is interpolated from gauge observations in areas with a dense network of stations, making it credible and reliable. According to Kotikot et al. (2024), over ten research papers have validated CHIRPS across Kenya, with a majority finding excellent correlation against reference gauges. Additionally, the Kenya's National Drought Management Authority (NDMA) uses CHIPRS as a benchmark dataset in drought early warning and meteorological research across Kenya. Kotikot et al. (2024) stated that CHIRPS has also been employed as an input dataset for several trend analyses in the East African region and was found to perform well.

3.2.2.1 Data Quality Control for Impervious Surface

Considering the strengths and limitations of CHIPRS dataset, rainfall data from Kenyatta University Rainfall Station (KURS) (Station Number: 9136248) was also collected and analyzed alongside Mihang'o watershed's CHIRPS data to confirm accuracy of the CHIRPS data. Additionally, mass curve technique was employed to assess the consistency of the rainfall data.

3.3.3 Determining Trend of Runoff Amount

The HEC-HMS model simulated the runoff amount from the watershed. The HEC-HMS simulates rainfall-runoff in a variety of geographic locations. (Tassew et al., 2019). HEC-HMS model efficiently completes simulations projects in hydrological

studies, such as rainfall-runoff simulation, meteorological data analysis, and parameter estimation, among many more (Sahu et al., 2020).

3.3.3.1 HEC-HMS Model Calibration

The basin model was first prepared. The ArcGIS was used to process the watershed physical parameters from the Mihang'o shapefile. The physical parameters produced included: sub-basins, river reaches, junction, sink, size of sub-basins, and slope of the sub-basins.

The SCS-CN loss method was selected as the loss model in this study. Therefore, I computed the CN of Mihang'o watershed based on the soil group and land use. The CN Tables in the HEC-HMS Technical Reference Manual, particularly the Curve Number for Urban Areas table, was used (Civil GEO, 2023; USACE, 2023). To validate the data from the literature, soil samples from five points in the watershed were collected for soil analysis to classify soil texture. Table 3.1 shows the coordinates of the soil sample points. The soil analysis to classify soil texture was conducted at the field and in the lab.

Table 3.1: Coordinates of Soil Sample Points

Sample point	X	Y
1	36.9842	-1.2587
2	36.9795	-1.2627
3	36.9880	-1.2727
4	36.9694	-1.2912
5	36.9576	-1.3120

Regarding LU/LC of Mihang'o watershed, literature evidence showed that the watershed has a mixture of land uses having transformed from an originally shrub

land to a developing urban area. Further, Google map and ground truthing were used to confirm Mihang'o watershed's LU/LC. The data showed that watershed is now made up of residential units, commercial businesses, small industries, hotels, churches, schools, playgrounds, administrative centers, bus stations, kiosks, pubs, workshops, gas stations, and garages.

The Soil Conservation Service Unit Hydrograph (SCS-UH) model was chosen in this study as the transform model. I deduced the following from the ArcGIS basin processed results: the basin's physical parameters including the slope length (ft/ft) and reach length (ft) of each sub-basin. The slope length (ft/ft) and reach length (ft) were used to calculate time of concentration (T_c) then the lag time (T_{lag}) (Equation 2.1 and Equation 2.2) (Tassew et al., 2019; USACE, 2009).

The Muskingum routing approach was selected for this study. The approximation of inputs including the flood wave's travel duration (K) through the routing reach and dimensionless weight (X) were based on previous studies. As for precipitation data input, the rainfall data for the 29th December 2022 between 12 noon and 6 pm in Mihang'o watershed was used in this study.

Data Quality Control for the HEC-HMS Model was conducted. The CN value put in the HEC-HMS model is a product of soil type and LU/LC of the watershed. Soil type of Mihang'o watershed was validated through soil analysis of soil samples collected from the watershed. LU/LC of Mihang'o watershed was validated through Google map and ground truthing. Additionally, mass curve technique was used to check for consistency of resultant runoff values of the years of study.

Table 3.2 contains the summary of HEC-HMS calibration to simulate runoff from Mihang'o watershed. The table highlights the required input parameters and selected models and their respective input data.

Table 3.2: Summary Table of HEC-HMS Model Calibration

Input parameters	Model	Specific Model Selected	Data Input
Basin model (watershed physical parameters information)	Loss model Transform model	Soil Conservation Service Curve Number (SCS-CN) Soil Conservation Service Unit Hydrograph (SCS-UH)	CN T_{lag} (Lag time)
	Routing model	Muskingum routing method	(i) Flood wave's travel duration (K) through the routing reach (ii) Dimensionless weight (X)
Precipitation data	Time-series data (precipitation model)	Specified hyetograph	Mihang'o watershed's rainfall data for 29 th December 2022 between 12 noon and 6 pm.
	Meteorologic models	-	Met 1
	Control specifications	-	Start time: 29 Dec 2022, 12:00 End time: 29 Dec 2022, 23:00

3.3.3.2 Modeling Procedure

The HEC-HMS project was launched after putting together the supporting data discussed in the preceding subtopics. A HEC-HMS project was completed procedurally. Figure 3.3 is a flowchart showing the steps followed in completing the HEC-HMS project.

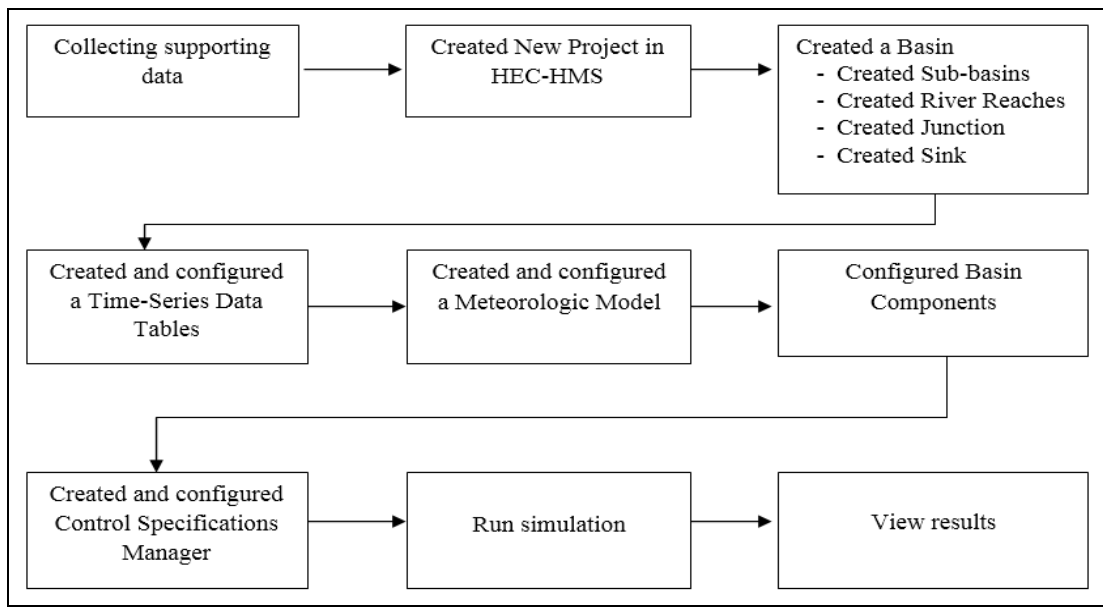


Figure 3.3: Steps Followed in Completing the HEC-HMS Project

3.4 Data Collection and Processing Summary

Table 3.3 shows the summary of data collection and processing for the research project's objectives. Figure 3.4 shows the summary this study's methodology. The consistency of this study's methodology with other high-quality studies (Hamilton et al., 2021; Li & Wang, 2009; Rahajeng, 2010; Tassew et al., 2019) support the validity and reliability of this study and its results.

Table 3.3: Summary of Data Collection and Processing

Objective	Data Source and Collection Procedure	Data Processing Procedure	Outcomes (Chapter 4)
(i) Determining change in impervious surface area	<ul style="list-style-type: none"> • Source is Landsat Images for the years 2000, 2003, 2006, 2009, 2012, 2015, 2018, and 2022 • Mihang'o watershed shapefile used to extract watershed's data from the satellite images 	Supervised classification using the Multivariate toolset of the ArcGIS (10.4) Spatial Analyst extension	Impervious surface percentages for the years of study
(ii) Determining trend in rainfall amount	<ul style="list-style-type: none"> • CHIRPS rainfall data in Google Earth for the years 2000, 2003, 2006, 2009, 2012, 2015, 2018, and 2022. • Mihang'o watershed shapefile and JavaScript code customized for Mihang'o watershed used to extract watershed's rainfall data from Google Earth. • Further, data triangulation for rainfall data was attained through collection of rainfall data from Kenyatta University Rainfall Station. 	<ul style="list-style-type: none"> • Excel files containing daily rainfall. Rainfall computed to monthly totals. • Hourly rainfall between 12 noon and 6 pm for Mihang'o watershed on 29th December, 2022 (single rainfall event) 	Hydrographs
(iii) Determining trend in runoff	<ul style="list-style-type: none"> • Impervious surface percentages (outcomes from objective 1) • Hourly rainfall between 12 noon and 6 pm for Mihang'o watershed on 29th December, 2022 (single rainfall event) • Physical characteristics acquired from Mihang'o watershed shapefile • Soil properties acquired from literature. • Further, soil analysis was done on samples collected from the field. • Land-use land cover data was acquired from literature. Data triangulation on LU/LC attained through Google Earth satellite image analysis and ground truthing. 	Data processing using HEC-HMS (Figure 3.3)	Peak discharge values and corresponding graphs

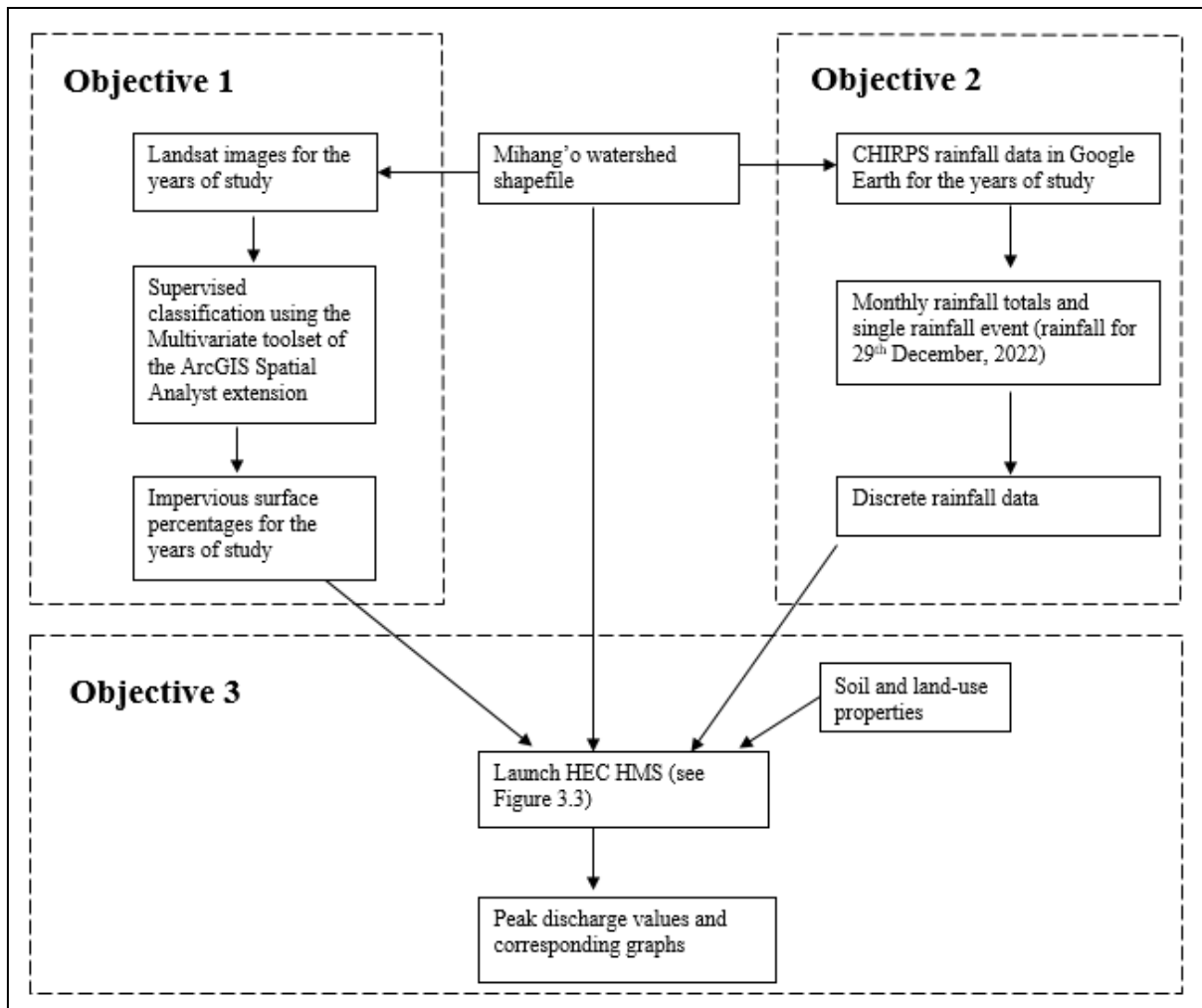


Figure 3.4: Summary of the Methodology

CHAPTER FOUR: RESULTS AND DISCUSSIONS

4.1 Introduction

This chapter presents the study results and discussions. The chapter is divided in three main parts. The first section involves the results and discussion of the impervious surface area trend, the second section entails the results and discussion of precipitation trend while the third section gives the analysis and discussion of the runoff trend in the study area. The third section also involves a detailed discussion of the HEC-HMS calibration and modeling.

4.2 Impervious Surface Area Trend of Mihang'o Watershed

Each of the Landsat images of Mihang'o watershed for the years of the study underwent supervised classification. Impervious surfaces were bundled into a single entity; pervious surfaces, too, were bundled into a single entity. Figure 4.1 displays the results of data quality control that entailed counterchecking the resultant image of 2022's supervised classification of the Mihang'o watershed against 2022's Google Earth satellite image and ground truthing. The figure shows the significant features in the Mihang'o watershed, including those that influence urban growth, such as the roads, trading centres, learning institutions, and healthcare facilities, among others. Figure 4.2 and Figure 4.3 display the distribution of impervious surfaces in Mihang'o watershed from 2000 - 2022. Figures 4.2 and 4.3 show an increasing trend of urbanization, otherwise the expansion of impervious surfaces around the roads, trading centres, learning institutions, and health care facilities in Mihang'o watershed.

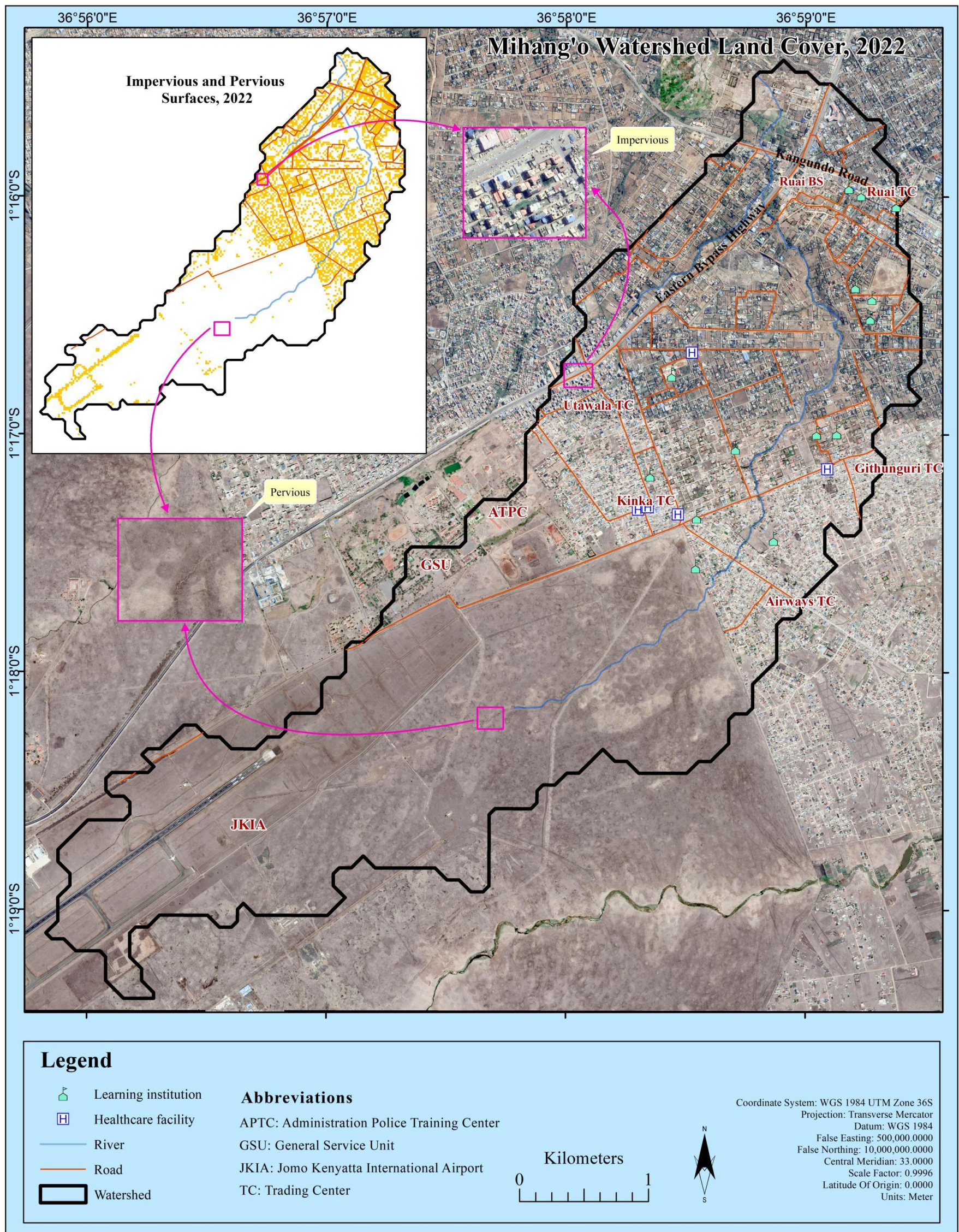


Figure 4.1: Mihang'o Watershed Land Cover Vs. Supervised Classification Image, 2022

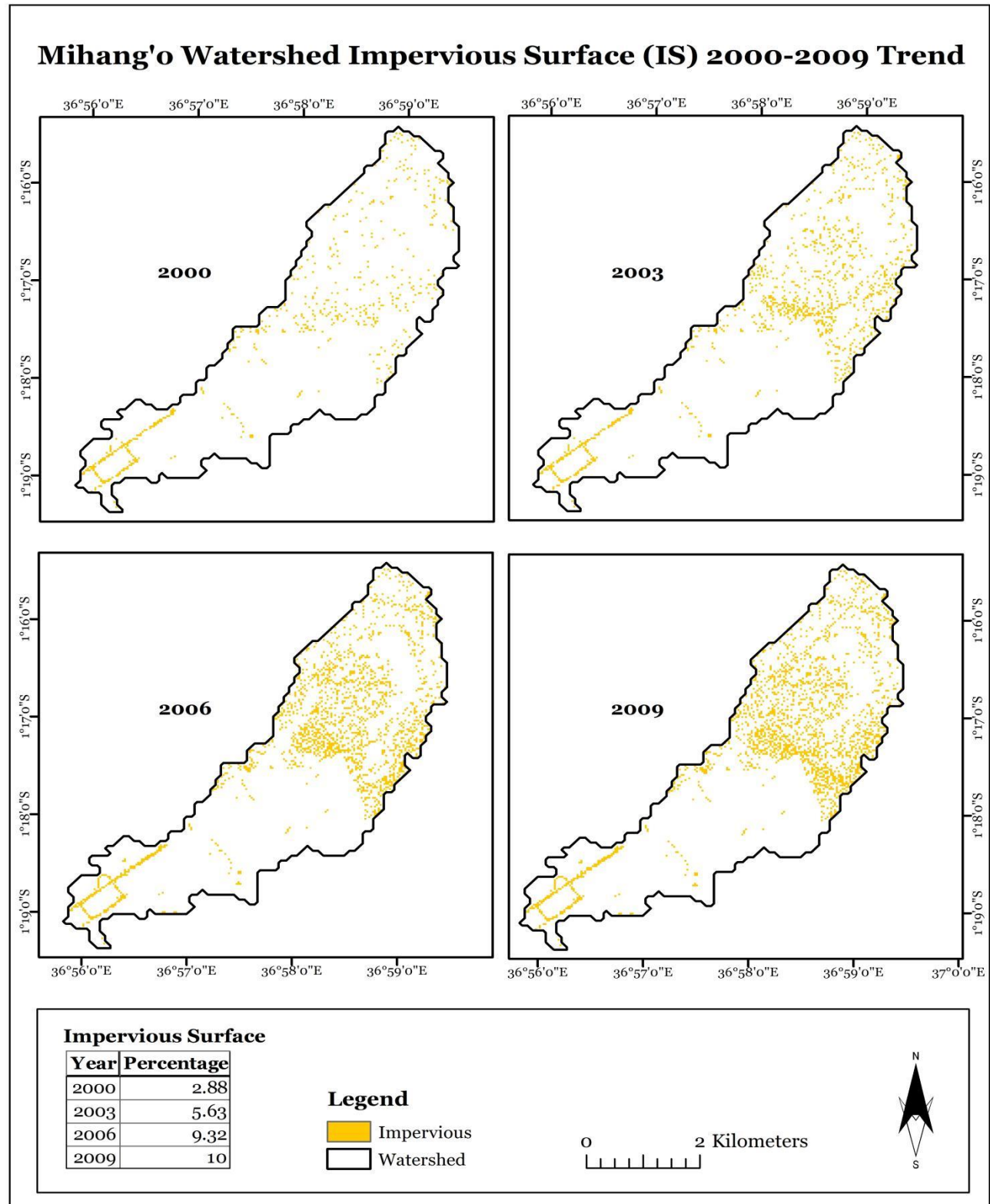


Figure 4.2: Mihang'o Watershed Impervious Surface Cover from 2000 – 2009

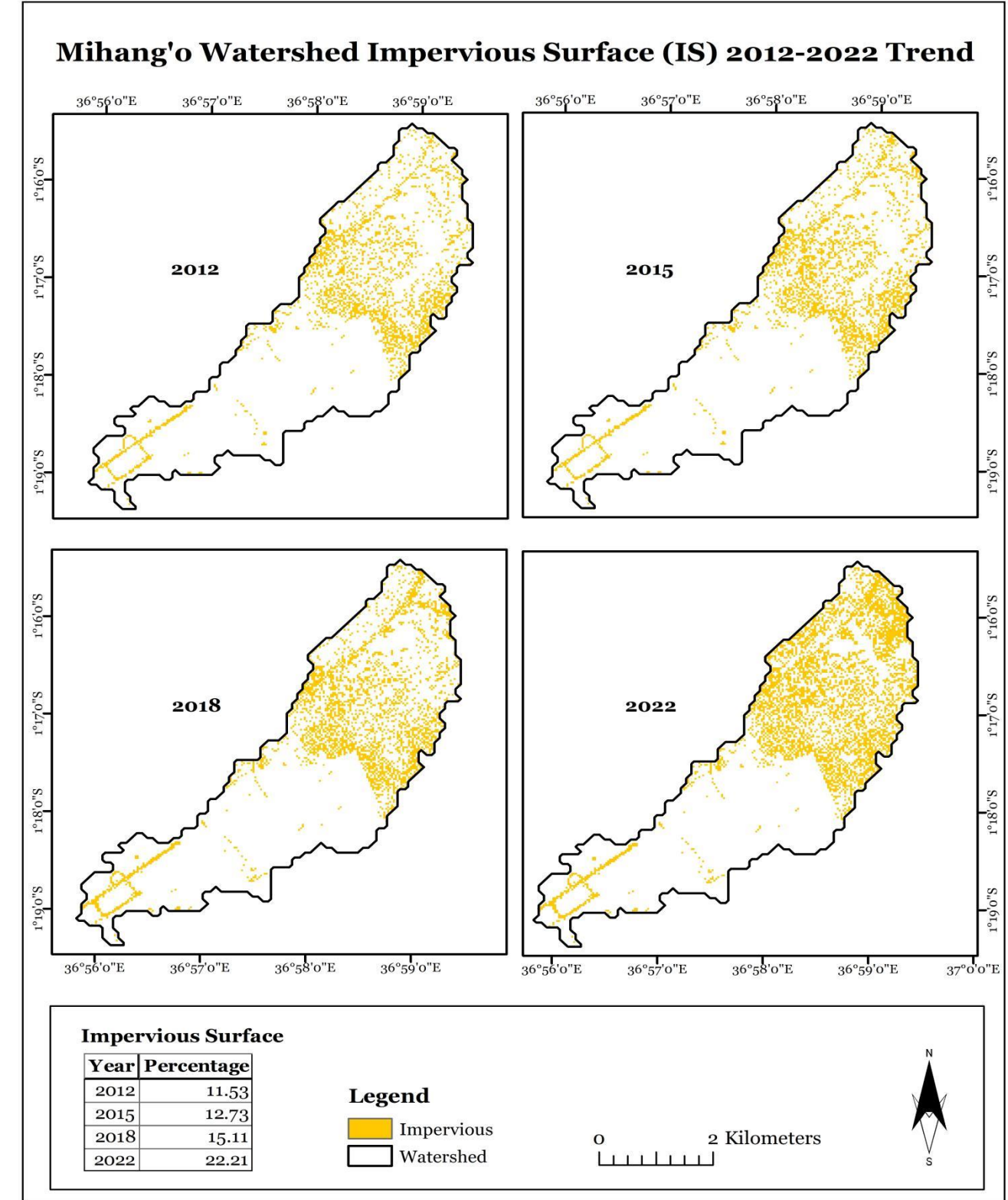


Figure 4.3: Mihang'o Watershed Impervious Surface Cover from 2012 – 2022

Besides displaying maps, supervised classification using ArcGIS also quantifies the area covered by impervious surface in a watershed. Table 4.1 shows the area (km^2) of impervious surface in Mihang'o watershed across the years of study. Using the data of area of impervious surface, the percentage for area of impervious surface for each year of study was calculated as in Equation (4.1). Table 4.1 also displays the corresponding impervious surface percentages for each year of study.

$$\% \text{ Impervious Surface Area} = \left\{ \frac{\text{Total Impervious Surface Area}}{\text{Total Area of Watershed}} \right\} \times 100 \quad (4.1)$$

Table 4.1: Impervious Surface of Mihang'o Watershed from 2000 - 2022

Year	2000	2003	2006	2009	2012	2015	2018	2022
Impervious surface	(km^2)	0.49	0.99	1.64	1.76	2.03	2.24	2.66
	(%)	2.78	5.63	9.32	10	11.53	12.73	22.21

Further, the impervious surface percentage data was subjected to quality control using single mass curve technique. Figure 4.4 displays the graph of mass curve of the impervious surface percentage data for Mihang'o watershed from 2000 and 2022.

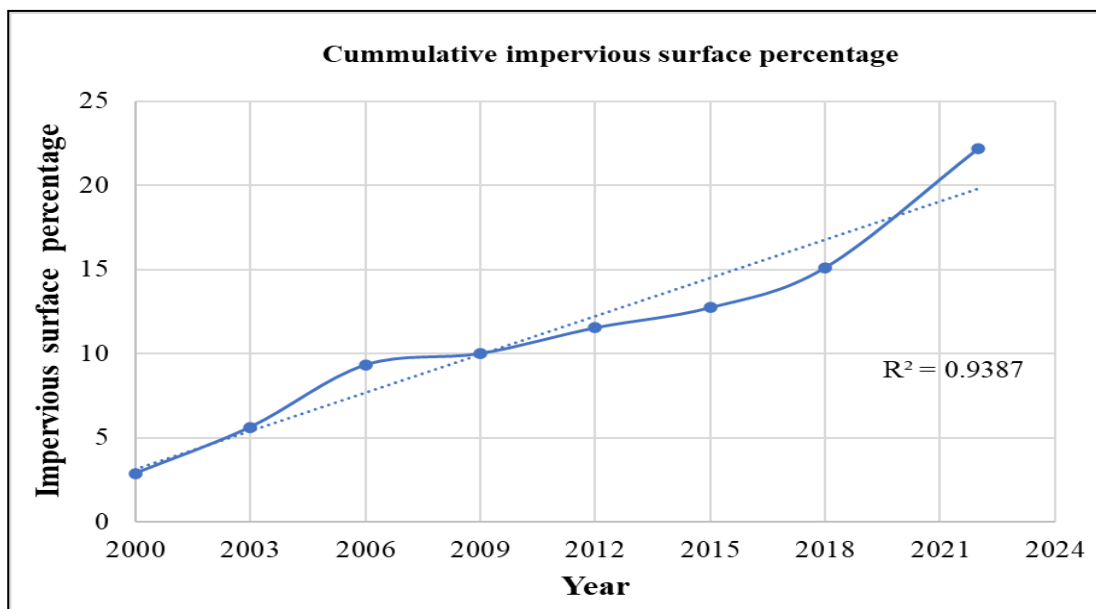


Figure 4.4: Mass Curve for Impervious Surface of Mihang'o Watershed from 2000-2022

The graph shows all impervious surface percentage points across the years of study are almost on a straight line. The coefficient of determination test results ($0.9 < R^2 < 1$) is a strong positive, which confirmed a positive trend in impervious surface percentage time series of Mihang'o watershed. The mass curve quality control results determined that the data was homogenous and reliable for use in this study for analysis and interpretation.

Consistent with the images in Figure 4.2 and Figure 4.3 displaying the increase in the size of impervious surface in Mihang'o watershed, the data in Table 4.1 presents the quantitative increase of impervious surface coverage in the watershed over the years. Mihang'o watershed's total area is 17.6 km^2 . The results show that in the year 2000, the impervious surface area was 0.49 km^2 , representing 2.78% of the total surface area of the watershed. The impervious surface area of the watershed increased over the years to 3.91 km^2 in 2022, representing 22.21% of the total surface area.

Figure 4.5 is a line graph created from data in Table 4.1, representing the percentage increase in impervious surface area of the watershed over the years. The line graph shows a slow, gradual increase in impervious surface between 2000 and 2015 and a drastic increase in impervious surface between 2015 and 2022. The graph also shows a proportionate decrease in pervious surface of the watershed over the years.

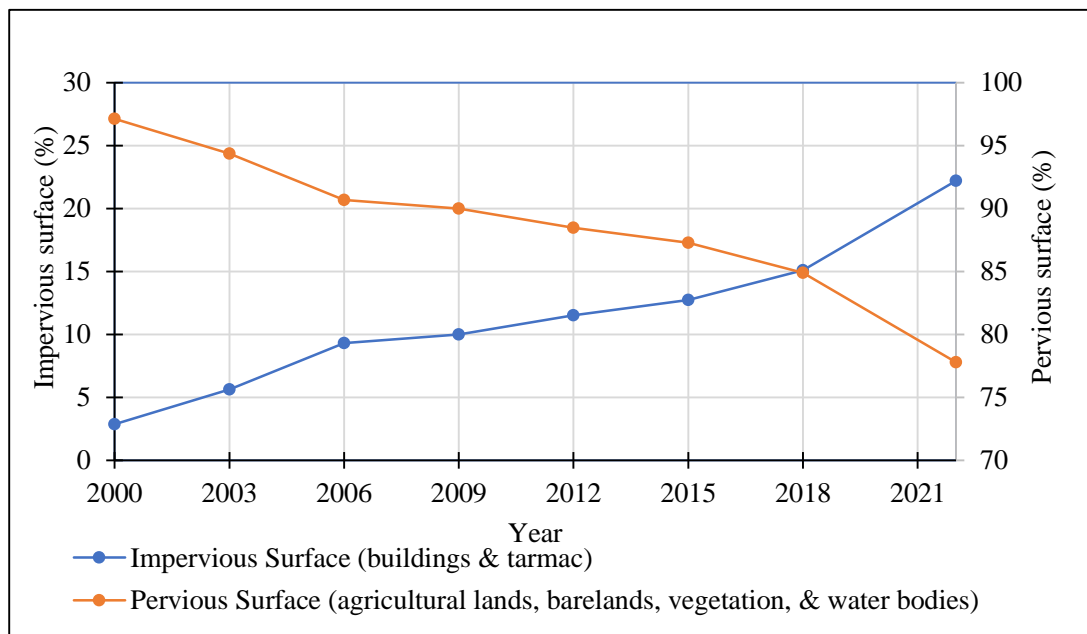


Figure 4.5: Impervious and Pervious Surface Area (%) of Mihang'o Watershed

The hypotheses for the first objective were:

- H_0 There is no trend in impervious surface area time series of Mihang'o watershed.
- H_1 There is a positive trend in impervious surface area time series of Mihang'o watershed.

Using a simple linear regression to predict impervious surface area over the years, a significant regression equation was found ($F(1,6) = 91.822, p < .001$) with an R^2 of .939. The statistical results confirm that the trend in impervious surface increment is significant, with an approximate increment of 3.96% (0.88 km^2) each year. Therefore, based on the alternative hypothesis (H_1) of this study, there is a positive trend in the impervious surface area time series of Mihang'o watershed.

Originally, Mihang'o watershed had large tracts of unoccupied land because a significant part was Githunguri Ranch and government reserves for JKIA, APTC, and GSU. In the early 2000s, the area attracted settlement as the population of Nairobi expanded. Land property companies sold and distributed the land in plots.

Mihang'o as a settlement area was attractive due to its affordability and closeness to Nairobi city. The prospect of Eastern Bypass cutting through Mihang'o made the area more attractive to people.

Over the years, urbanization has gradually increased in the watershed. According to Gachanja et al. (2023), industrialization, employment opportunities, commercialization, modernization, social benefits, and rural-urban transformation are the main causes of urbanization. All these factors have been evident in Mihang'o post the year 2000. For instance, established businesses have branches, including banks, schools, hospitals, and hotels in Mihang'o. Mihang'o has also contributed to the city's increasing population, which strongly indicates urbanization in the area (Gachanja et al., 2023). Since 2015, the gradual expansion of the Eastern Bypass Highway led to a drastic increase in urbanization in the Mihang'o watershed. More residential units have been developed, more businesses have been established, and more road networks have been created and tarmacked, resulting in the rapid increase in impervious surface area in the watershed. Contrastingly, pervious surfaces, including the patches of agricultural lands, barelands, vegetation, and water bodies in the watershed, have declined to give room to development. As of 2023, the Eastern Bypass Highway has been expanded to a 4-lane major highway in Kenya.

This study demonstrated an increase in the impervious surface area in the Mihang'o watershed over the years. Similar studies on LULC changes in Nairobi and its surrounding areas, using GIS, have shown a comparable upward trend in impervious surfaces, thus reinforcing the findings of this study, which focused on just a portion of Nairobi (Bosco et al., 2011; Mundia & Aniya, 2005; Mundia & James, 2014; Munyoki et al., 2024; Mwathi, 2016). For instance, Bosco et al. (2011) found that

between 1976 and year 2000, while urban areas and barren surfaces increased by more than 98% and 100%, respectively, the coverage of forests and riverine vegetation decreased significantly by up to 60% and 67%, respectively. According to Mundia and Aniya (2005), the Landsat images for 1976, 1988 and 2000 revealed that built-up area expanded by about 47 km². Although the Mundia and James' (2014) study focused on LST, their finding of a negative correlation between LST and NDVI revealed that Nairobi has undergone significant transformation, shifting from forests, shrubland, bare land, and grassland to built-up areas and bare lands. According to Munyoki et al. (2024), their study on LULC changes in the Mbagathi River catchment for the period 1990-2020 established that forest cover reduced from 32% to 14% and grassland reduced from 53% to 30%, but bare ground increased from 10% to 38% and urban land cover increased from 4% to 17%. Also, Mwathi (2016) found that between 1988 and 2010, Nairobi city experienced an increase of 280.15% in urban built-up areas and open lands, a decrease by 38% in forest cover, and a decrease by 98% in agricultural and riparian vegetation.

Urban and bare ground land covers have increased at the expense of forest and grassland covers (Munyoki et al., 2024). According to Mwathi (2016), agricultural and riparian vegetation, rangelands, shrubs, and forests have been replaced by the expansion of built-up areas and open lands. Factors influencing the land cover and land use (LCLU) dynamics of the city included population growth, economic activities, urban development policies, and a weak enforcement framework (Mwathi, 2016). Mundia and Aniya (2005) noted that the road network influenced the spatial patterns and structure of urban development, leading to the expansion of built-up areas in both a gradual and linear manner along major roads. Mundia and Aniya (2005) integrated demographic and socio-economic data with LULC change and

found that economic growth and proximity to transportation routes were the major factors promoting urban expansion. Similarly, in the case of the Mihang'o watershed, the gazettlement and expansion of the Eastern Bypass Highway were significant drivers of urbanization in the area. Consistent with the finding in Mihang'o watershed, Mundia and Aniya (2005), Munyoki et al. (2024) and Mwathi (2016) observed that the urban expansion was accompanied by loss of natural land and urban sprawl.

4.3 Precipitation Trend of Mihang'o Watershed

Rainfall data was collected from the CHIRPS rainfall dataset. The CHIRPS data was accessed through Google's Earth Engine Data Catalog. A JavaScript code was used to single out daily rainfall data for Mihang'o watershed from 2000 to 2022. The data included 3277 counts; the rainfall was processed into monthly and annual rainfall for the years of study. In the effort to conduct data quality control, KURS data was also collected and analysed alongside the CHIRPS data. KURS provided rainfall data for only post 2005, when the university owned an automatic weather station (AWS) therefore, prior years were left blank in the analysis (Table 4.2). Despite lack of daily rainfall data for years prior to 2005, data from KURS was suitable for use in analyzing CHIRPS rainfall data for Mihang'o watershed because KURS is the neighboring weather station to the watershed. Additionally, data for only two years of study, 2000 and 2003, were missing from the KURS data, therefore, sufficient data was available for comparing with CHIRPS data to determine consistency.

Table 4.2: Rainfall for Mihang'o Watershed (2000-2022)

CHIRPS	Year	Jan	Feb	Mar	Apr	May	Jun	Jul	Aug	Sep	Oct	Nov	Dec	ANNUAL		MAM	ND
		2000	9.6	6.6	30.5	86.7	63.7	12.2	0.0	0.0	13.0	28.2	171.2	69.9	491.7		180.9
	2003	27.1	17.3	43.6	152.8	211.4	9.7	0.0	13.6	22.1	46.6	137.0	33.7	714.8		407.7	170.6
	2006	10.4	28.5	111.3	177.9	96.2	6.4	0.0	8.8	15.6	28.5	305.2	188.4	976.9		385.4	493.5
	2009	47.2	23.9	29.7	76.1	77.9	16.2	0.0	0.0	5.6	60.0	87.9	106.8	531.3		183.7	194.7
	2012	9.8	15.5	24.1	298.2	169.4	23.1	0.0	10.2	13.4	60.1	184.3	182.8	990.8		491.6	367.1
	2015	8.3	32.4	49.5	218.1	82.5	17.3	0.0	5.1	6.2	56.1	253.8	126.8	856.0		350.1	380.5
	2018	30.3	30.2	239.2	282.4	196.8	32.5	10.8	18.7	15.4	34.1	120.1	162.3	1172.8		718.5	282.3
	2022	40.4	39.6	53.3	103.3	40.5	6.1	0.0	0.0	11.4	23.2	167.9	36.3	521.9		197.2	204.1
		22.9	24.2	72.7	174.4	117.3	15.4	1.3	7.0	12.8	42.1	178.4	113.4				
KU Rainfall Station	Year	Jan	Feb	Mar	Apr	May	Jun	Jul	Aug	Sep	Oct	Nov	Dec	ANNUAL		MAM	ND
	2000																
	2003																
	2006	9.6	33.9	96.9	323.6	68.3	11.7	3.1	22.1	34.1	24	404.6	114.6	1146.5		488.8	519.2
	2009	63.9	38	84.6	63.1	96	7.1	6.2	3.9	1.2	97.7	49.7	93.7	605.1		243.7	143.4
	2012	0	4.5	4.2	250.7	186.7	59.3	5.3	31.2	38.5	135.6	126.5	220.5	1063		441.6	347.0
	2015	8	40.8	22.8	234.4	143.6	77.1	0	8.3	8.2	125.9	129.2	231.7	1030		400.8	360.9
	2018	2.5	0	204.2	228.6	219.6	24.9	56.9	4.7	0	17.2	49.5	173.8	981.9		652.4	223.3
	2022	54.1	25.2	15.3	120.5	53.1	2.9	14.1	15.8	2.5	4.8	163.1	33.3	504.7		188.9	196.4
		23.0	23.7	71.3	203.5	127.9	30.5	14.2	14.3	14.1	67.5	153.8	144.6				

Figure 4.6 is a graph displaying annual rainfall data for Mihang'o watershed derived from CHIRPS and KU Weather Station. Figure 4.7 displays the average rainfall, and Figure 4.8 displays the seasonal rainfall.

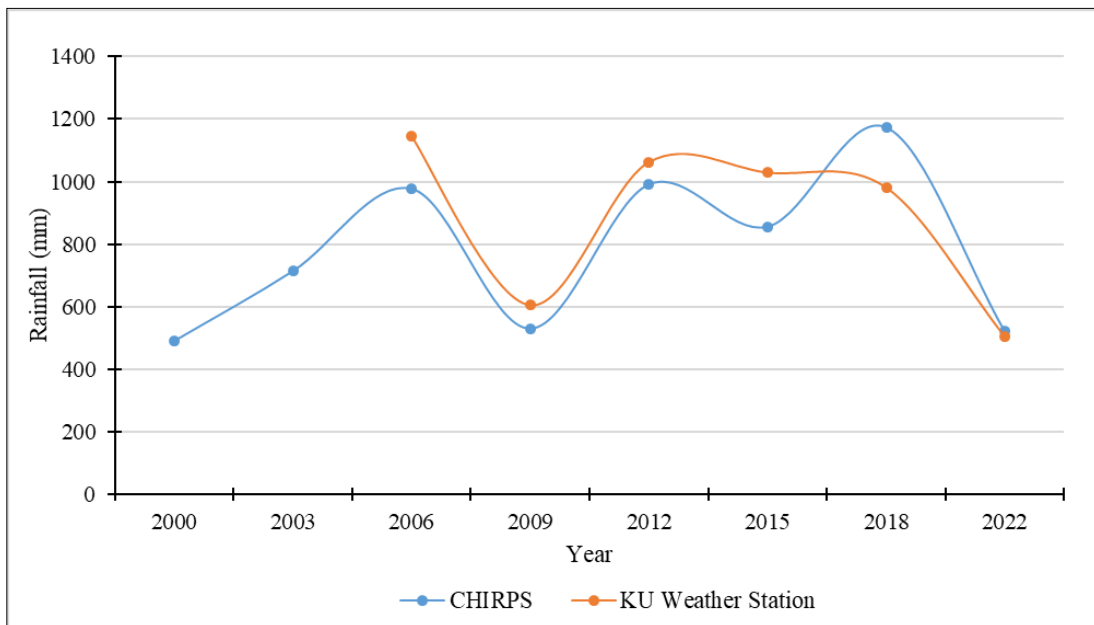


Figure 4.6: Annual Rainfall

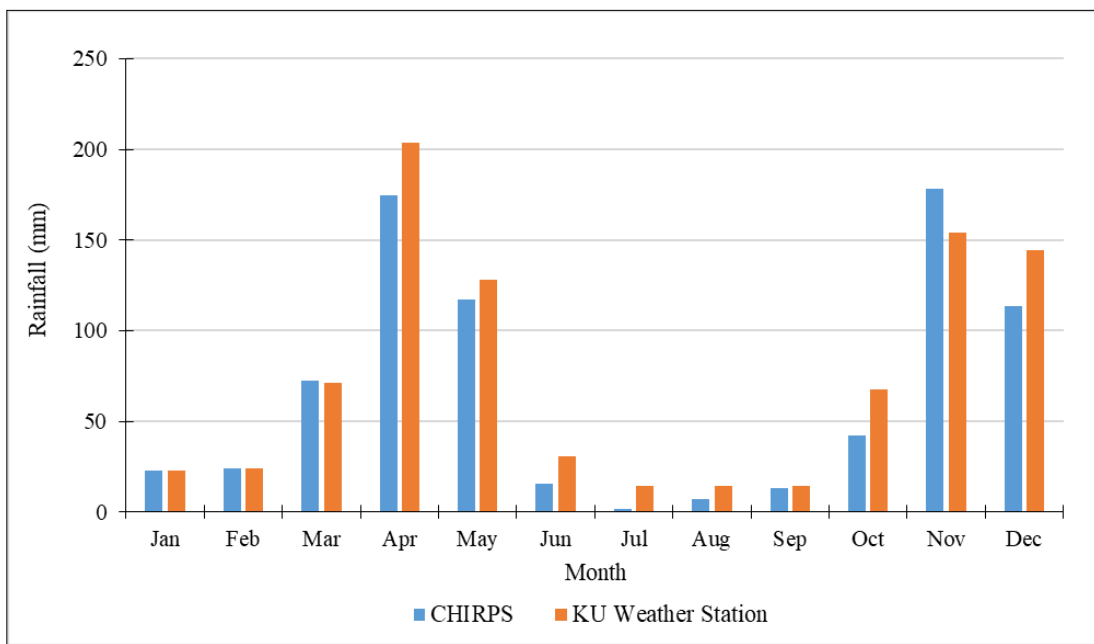


Figure 4.7: Average Monthly Rainfall

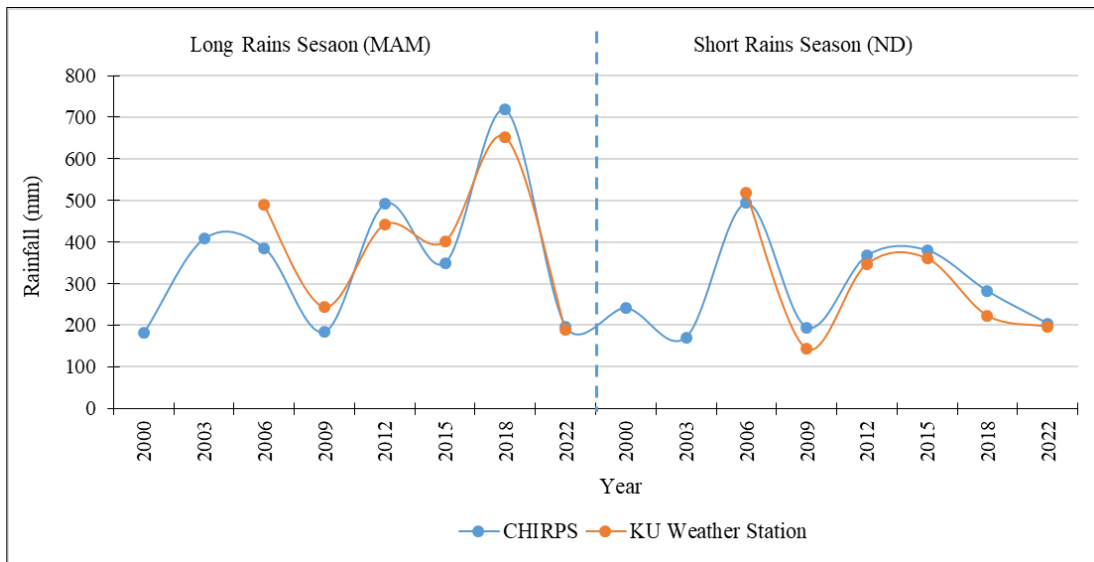


Figure 4.8: Seasonal Rains

The rainfall analysis shows that data points for annual rainfall (Figure 4.6) and seasonal rains (Figure 4.8) from CHIRPS and KURS are flowing consistently and close to each other. The bar graph in Figure 4.7 also shows the average monthly rainfall from CHIRPS and KURS are close. CHIRPS data is associated with underestimation or overestimation or rainfall amount, or rather low correlation with observation data, especially in rural regions where there are less rain-gauge stations (Kotikot et al., 2024). Nonetheless, independent t-test was conducted on CHIRPS and KURS annual rainfall for 2006, 2009, 2012, 2015, 2018, and 2022 (Table 4.3) to assess accuracy of the dataset. The independent t-test results indicated a p -value of 0.765, strongly confirming no significant difference between the two datasets. Therefore, the CHIRPS data collected and used as primary rainfall dataset is accurate and reliable for use in data analysis and interpretation. Further, the mass curve for annual rainfall for Mihang'o watershed (Figure 4.9) shows that all data points are almost on a straight line and a strong positive coefficient of determination ($0.9 < R^2 < 1$), which reinforce the reliability of that data.

Table 4.3: T-test Analysis of CHIRPS and KURS Annual Rainfall

	CHIRPS data annual rainfall for Mihang'o (2006-2022)	KURS data annual rainfall (2006-2022)
Mean	841.6268333	888.5333333
Variance	69795.52206	70675.61067
Observations	6	6
Pooled Variance	70235.56636	
Hypothesized Mean Difference	0	
df	10	
t Stat	-0.306559735	
P(T<=t) one-tail	0.382733211	
t Critical one-tail	1.812461123	
P(T<=t) two-tail	0.765466423	
t Critical two-tail	2.228138852	

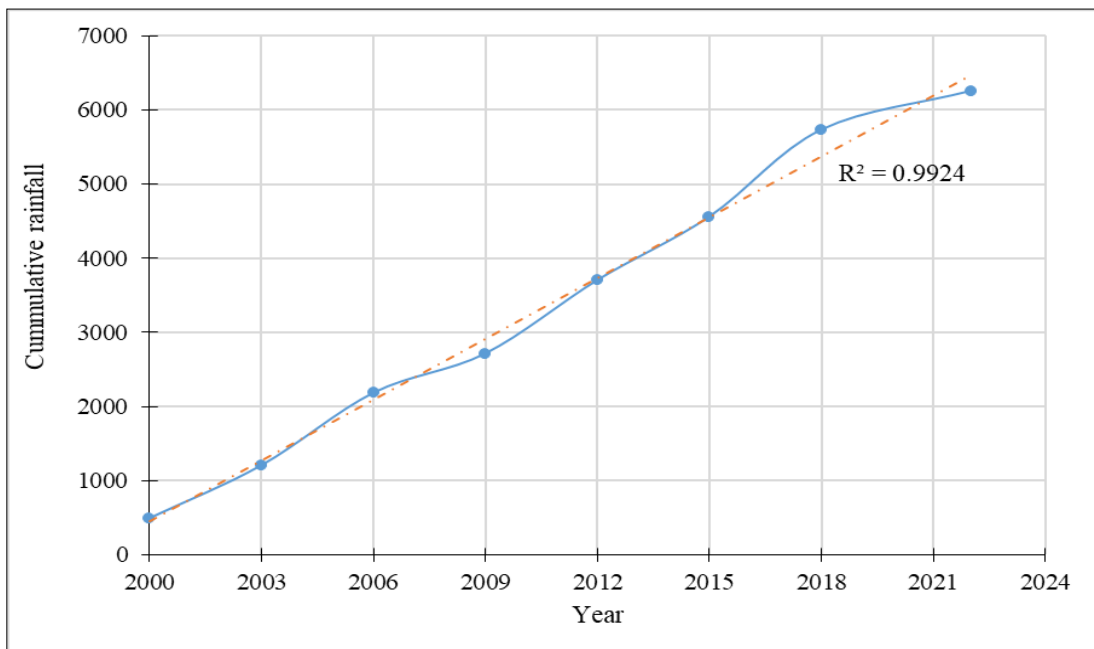


Figure 4.9: Mass Curve for Annual Rainfall (2000-2022)

Based on CHIRPS data, Mihang'o watershed received the highest rainfall amount in the year 2018, which totaled 1172.8 mm. The least rainfall was received in 2000, totalling 491.7 mm. The data indicates that Mihang'o's average annual rainfall is approximately 779 mm. Further, the data indicates two rainfall seasons: long rains (MAM) and short rains (ND). The watershed receives some rainfall in January and February and little rain between June and September.

The rainfall pattern in Mihang'o is consistent with the rainfall pattern of the larger Nairobi catchment. As shown in Figure 2.2, Nairobi has two rainy seasons and a single dry season. Nairobi's subtropical highlands climate is strongly influenced by its location at the eastern end of the East African Rift Valley and about 1700 meters MASL (Kilavi et al., 2018). The ITCZ migration north-south over the region influences rainfall seasonality in Nairobi. As the ITCZ moves southwards, Nairobi experiences short rains in ND (Kilavi et al., 2018; UCT, 2017). Little rainfall of about 80 mm is received between January and February when the ITCZ is in the region's south. As the ITCZ migrates northwards, Nairobi experiences long rains of about 310 mm in MAM. Little rain is received between June – October while the ITCZ remains in the north (Kilavi et al., 2018; UCT, 2017).

Inter-annual rainfall variability in Nairobi is significant because while the long-term average is 615 mm, some years may record below 370 mm or above 750 mm (UCT, 2017), which is comparable with rainfall data of Mihang'o watershed (Figure 4.6). This is because though November – December is a short rain season, outbreaks of cold air from the middle latitudes and an influx of Congo air mass may deliver rain in December (Kilavi et al., 2018). Also, after the long rains season and as the ITCZ migrates northwards, the Indian Monsoons' advection of moisture from the Indian Ocean may result in heavy orographically associated rainfall throughout May and June (Kilavi et al., 2018). Consistent with Mihang'o rainfall data (Figure 4.8), UCT (2017) stated that seasonal rainfall totals fluctuate independently, with the long rains varying by 260 mm from the long-term average (310 mm), and the short rains varying by 250 mm the long-term average (200 mm) (UCT, 2017).

Nairobi may display decadal rainfall variability, but even a 35-year record is insufficient to identify this variability (UCT, 2017). Only El Niño-Southern Oscillation (ENSO) may cause rainfall that is above-average, and La Niña may cause rainfall that is below-average on a multi-year timescale in Nairobi. Also, Nairobi does not portray a significant linear trend for total rainfall of the short and long rains (UCT, 2017).

Table 4.4 and Figure 4.10 display the results from Mann-Kendall trend tests for Mihang'o watershed rainfall. For the years of study, the average of Kendall's tau test (τ_b) results is 0.146, the average *p*-value (*p*) is 0.625, and the average Sen's slope test (β) is 0.832.

Table 4.4: Mann-Kendall Trend Test for Mihang'o Watershed Rainfall

Series\Test	Kendall's tau (τ_b)	<i>p</i> -value (<i>p</i>)	Sen's slope (β)
January	0.214	0.536	0.452
February	0.643	0.035	1.188
March	0.286	0.386	1.153
April	0.286	0.386	6.901
May	-0.071	0.902	-1.010
June	0.214	0.536	0.535
July	0.357	0.383	0.000
August	0.038	1.000	0.000
September	-0.214	0.536	-0.230
October	0.000	1.000	-0.099
November	-0.071	0.902	-0.640
December	0.071	0.902	1.734
Average	0.146	0.625	0.832

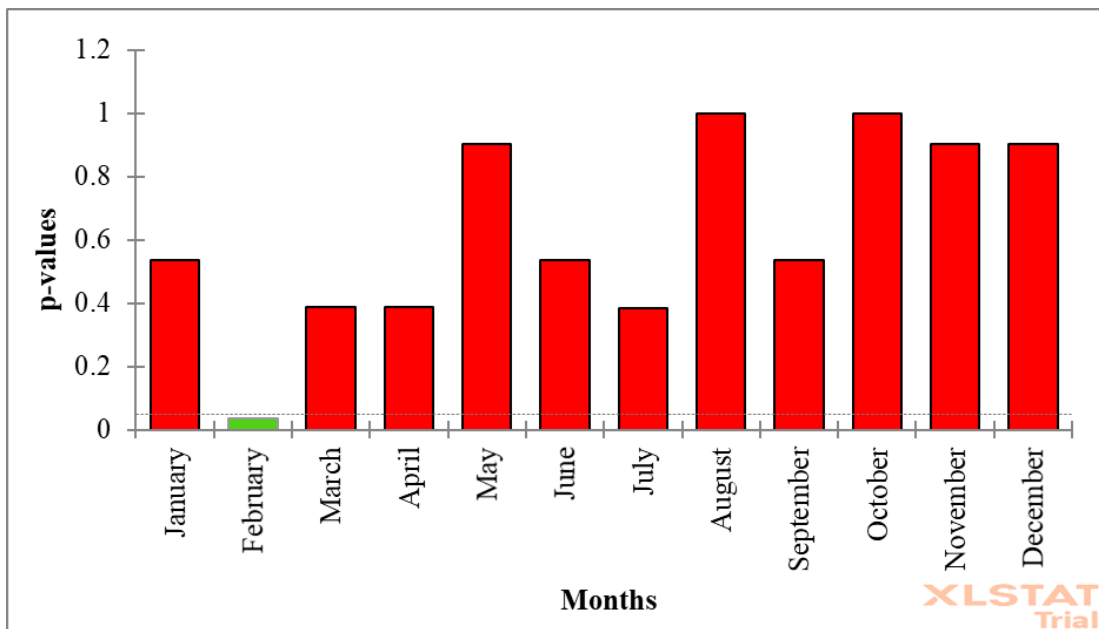


Figure 4.10: Mann-Kendall Test p -values

Though Sen's slope results ($\beta = .832$) show a positive rainfall trend and Kendall's tau results ($\tau b = .146$) show a slight correlation between rainfall amounts with time, the p -value (.625) strongly confirms that the null hypothesis is not statistically significant that there is no trend in the rainfall data time series of Mihang'o watershed. Except for the month of February, the p -value is $p > .05$ throughout, consequently, averaging $p = .625$. Additionally, the overall, or rather, established climate data of the region demonstrates no significant linear trend in rainfall (Kotikot et al., 2024; NCC, 2023; UCT, 2017). The p -value is the primary determinant of trend; the positive results for Sen's slope and Kendall's tau are due to annual rainfall fluctuations (Aswad et al., 2020; Serinaldi et al., 2020). Overall, the Mann-Kendall trend tests ($\tau b = .146$, $p = .625$, $\beta = .832$) show $p > .05$; therefore, based on the null hypothesis of this study (H_0), there is no trend in the rainfall data time series of Mihang'o watershed.

The Mann-Kendall trend tests results showing no linear trend in the rainfall data time series of Mihang'o watershed are aligned with established climate data of the region according to notable literature on this topic (Kotikot et al., 2024; NCC, 2023; UCT, 2017). Nonetheless, there are studies that had unique findings on Nairobi's rainfall trend. For instance, Mutua and Runguma (2020) who investigated the rainfall variability for Kenyan highlands from 1900 - 2012 found out a significant deterioration in the long rains, while the short rains trend continued significantly increasing over most of the highlands, particularly in Nairobi since the 1970s. Sindani et al. (2022) share the view that total long rains have been decreasing while total short rains have been increasing. However, their analysis, which focused on the Mount Elgon region examining 30 years of historical climate change trends and variability. Ayugi et al. (2016) too found a noticeable decrease in the long rains and slight increase in the short rains between 1971 and 2010 in Kenya in general. Therefore, the increase in short rains and decrease in long rains in the region is another reason for the discrepant findings in the Mihang'o rainfall data's Mann-Kendall trend tests ($\tau b = .146, p = .625, \beta = .832$) (Ayugi et al., 2016; Bonzemo et al.; Mutua & Runguma, 2020), besides the annual rainfall fluctuation (Aswad et al., 2020; Serinaldi et al., 2020).

Interestingly, Ayugi et al.'s (2016) analysis found significant decrease in rainfall over Kenya in general and according to them this was in line with trends of global warming. According to Mutua and Runguma (2020) between 1900 and 1940 Nairobi's annual rainfall showed a negative trend, and then thereafter a significant increase occurred, which was sustained until the end of the study period, except for the 1981 – 1990 decade, which indicated no change at all in annual records. Mutua and Runguma (2020) attribute the increase in total annual rainfall in Nairobi to the

rise in short rainfall amounts. More importantly, Nairobi was found to have an exceptionally high rainfall increase (18%) in between 2001-2012 in comparison to all other highlands investigated in their study. Mutua and Runguma's (2020) point of view is also supported by Ongoma et al. (2015), who investigated the possible effect of urbanization on rainfall variability over Nairobi using a 30-year dataset and found an increase in total rainfall from early 1990s, though the number of rainy days decreased.

According to Ongoma et al. (2015), one of the reasons for Nairobi's unique increase in rainfall compared to other places is due to Nairobi's Urban Heat Island (UHI) effect. The easterly winds that predominate Nairobi are associated with precipitation occasioned by moisture inflow into the country from the Indian Ocean are also another reason for Nairobi's continued increase in rainfall over time (Ongoma et al., 2015). The winds also transport pollutants from the eastern zone of the city; which is mainly the industrial area, to the western parts of the city. Consequently, the western part of the city contains a concentration of pollutants, primarily aerosols from anthropogenic emissions, which act as condensation nuclei that enhance cloud formation, leading to increased rainfall in this region. Furthermore, since the western side of the city is at a higher altitude, it likely serves as a lifting mechanism for air flowing from the east, facilitating cloud formation and increasing the likelihood of frequent and intense rainfall (Ongoma et al., 2015). However, Ongoma et al. (2015) observed no noticeable abrupt changes in annual total rainfall of Nairobi in general.

4.4 Runoff Amount Trend of Mihang'o Watershed

This subtopic is about the results for the third objective. The runoff amounts from Mihang'o watershed for each year of study were simulated using the HEC-HMS

model. Before presenting and discussing the runoff results, the HEC-HMS calibration results are presented and discussed.

4.4.1 HEC-HMS Calibration Results

Using ArcGIS, the basin model for Mihang'o watershed (Figure 4.11) was produced. The figure shows the watershed disintegrated into sub-basins based on the stream segments. The figure shows that Mihang'o watershed contains three sub-basins, labeled A, B, and C. Mihang'o watershed has one river junction, one river reach, and one sink at the outlet point. The ArcGIS also produced the sizes of each sub-basin. The sizes for sub-basins A, B, and C are 2.3 km^2 , 5.4 km^2 , and 9.9 km^2 , respectively. These parameters were replicated in a model of the watershed in the HEC HMS project. Figure 4.12 shows the modeled watershed in HEC-HMS based on the physical parameters.

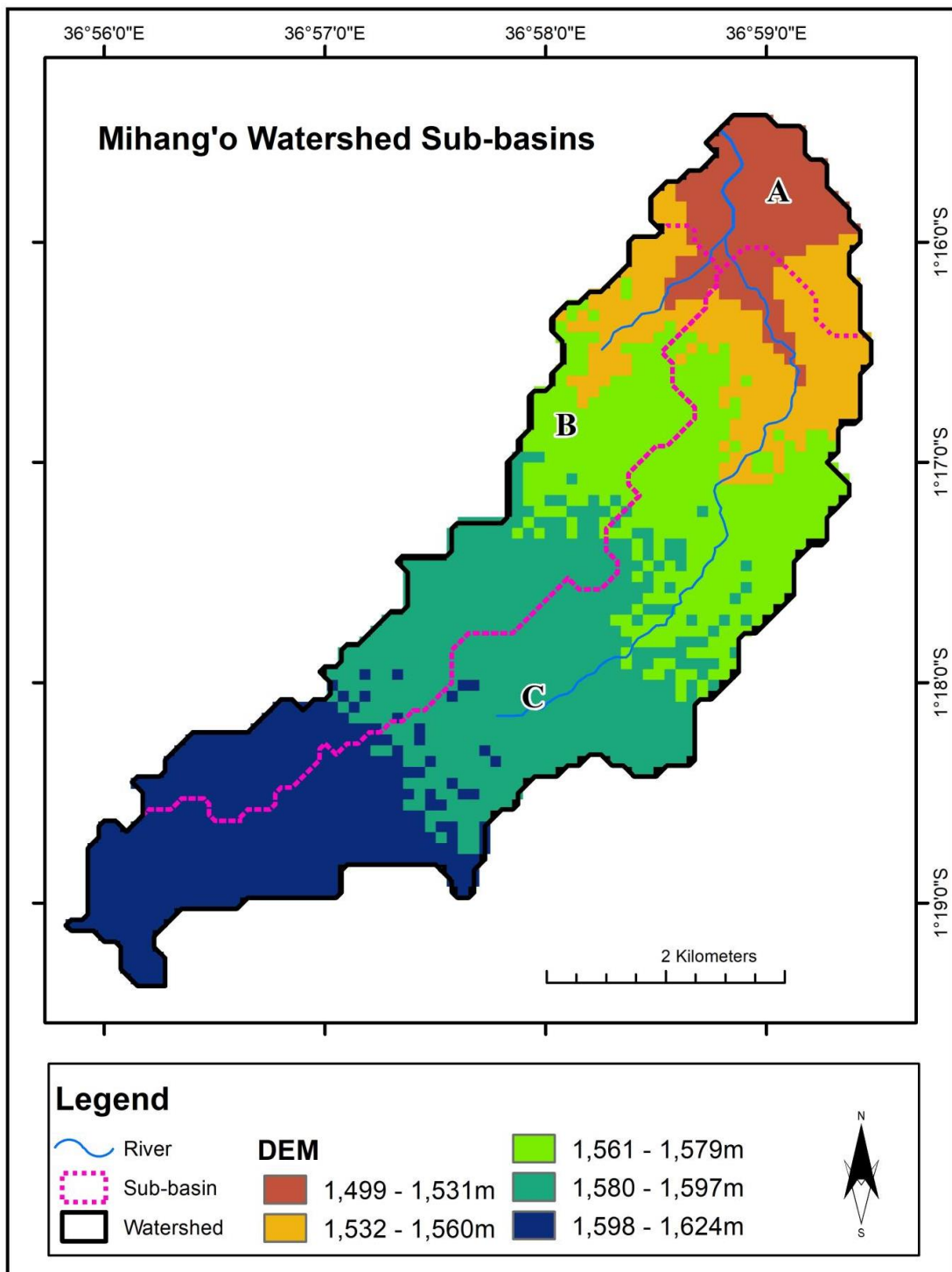


Figure 4.11: Mihang'o Watershed Basin Model

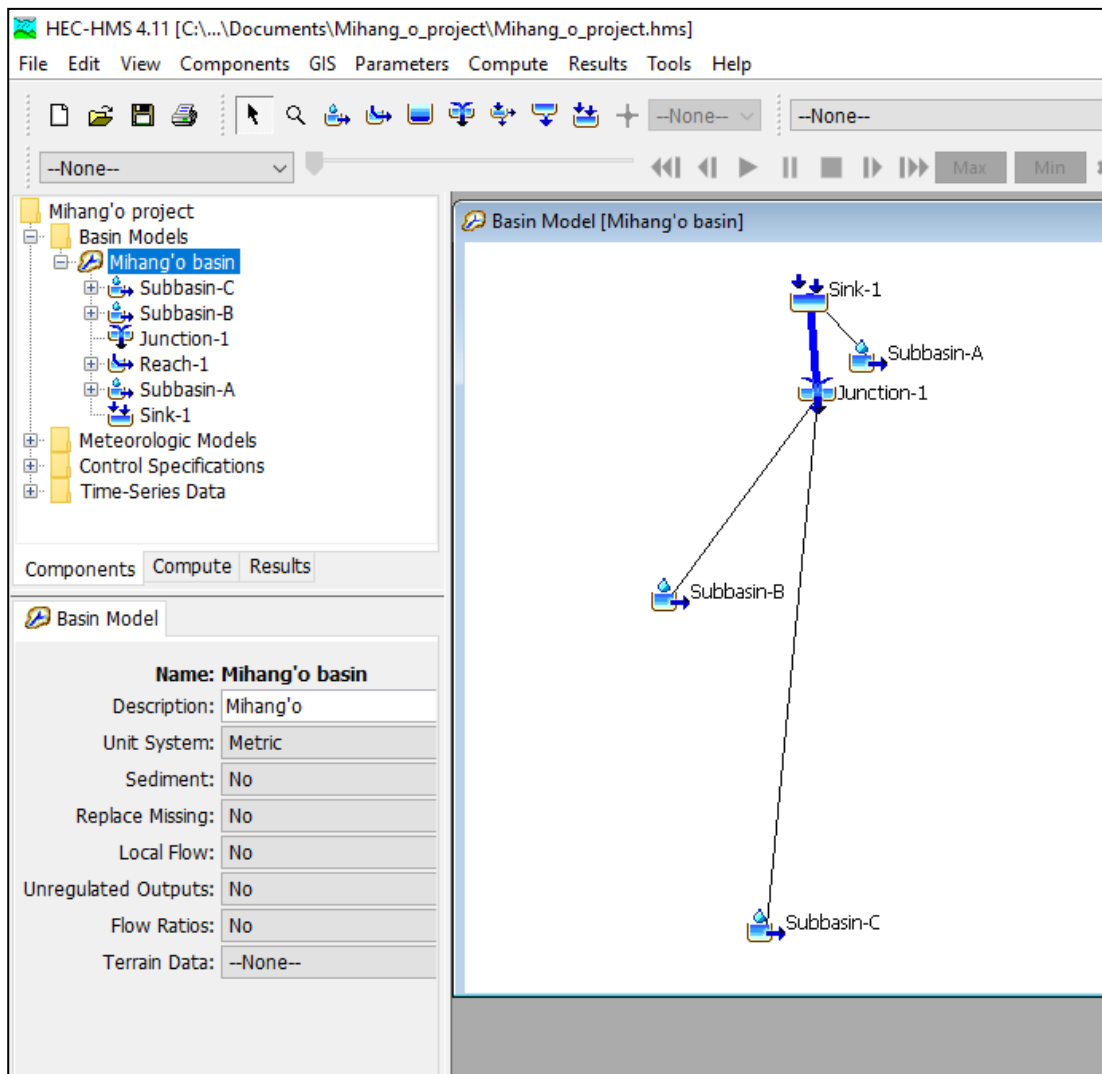


Figure 4.12: HEC HMS Schematic Network of Mihang'o Watershed

This schematic network of the watershed in Figure 4.12 is what is known as the basin model in HEC-HMS terms. The schematic network of the watershed shows that Sink I is the downstream of Sub-basin A and Reach I. Also, Reach I is the downstream of Junction I, which is the downstream of Sub-basin B and C. After creating a basin model, HEC HMS simulation also requires the loss, transform, and routing specifications (Tassew et al., 2019; USACE, 2009).

The Loss Model. The SCS-CN used is solely based on the curve number, a function of watershed's soil type and LU/LC. According to literature, soils in Mihang'o watershed are predominantly vertisols (Muli, 2008; Muthu & Santhi, 2015). To

countercheck literature evidence, soil analysis was conducted on the soil samples collected from five points of the watershed (Figure 4.13).

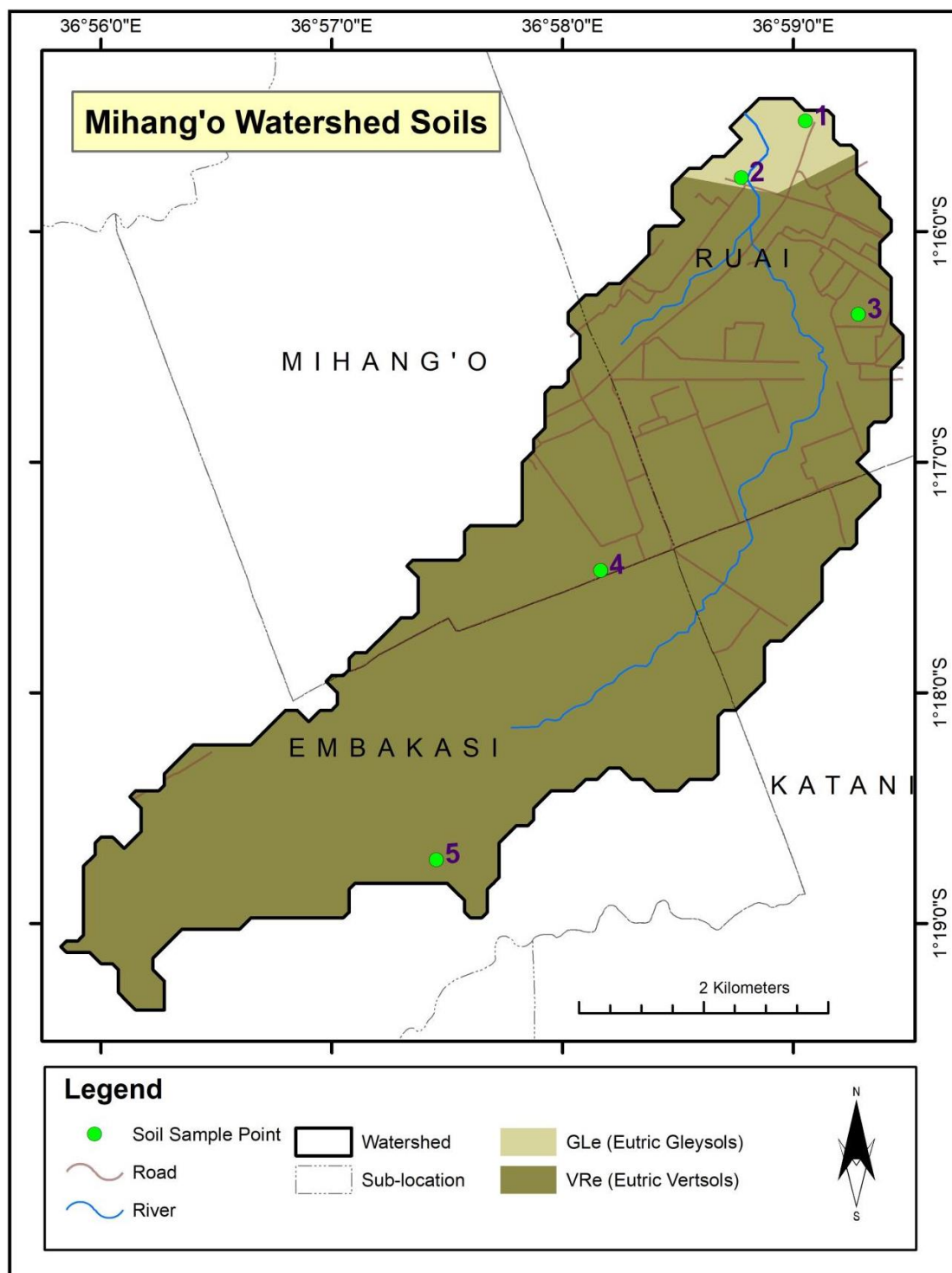


Figure 4.13: Soil Sample Points

Consistent with the Farm Management Handbook of Kenya and literature, only a small section of the watershed was found to contain gleysols and the rest of the

watershed contains vertisols (Onyancha et al., 2011). Soil samples at points 1 and 2 portrayed a wide range of unconsolidated materials, basically fluvial, with basic to acidic mineralogy, which are typical characteristics of eutric gleysols. Soils at sample points 3, 4, and 5 were a mixture of sediments from weathering rocks and gravelly clay material, which are typical features of eutric vertisols (Akech et al., 2013).

Based on the United States Department of Agriculture (USDA)-SCS soil classification, literature findings and soil analysis results show that the hydrological categorization of Mihang'o watershed's soil is mixture of Group C and Group D soils (Table 4.5) (Muthu & Santhi, 2015).

Table 4.5: USDA-SCS Soil Classification (Muthu & Santhi, 2015)

Hydrological Soil	Type of soil	Runoff Potential	Final Infiltration Rate (mm/hr)	Remarks
Group A	Deep, well-drained sands and gravels	Low	>7.5	High rate of water transmission
Group B	Moderately deep, well-drained with moderately fine to coarse textures	Moderate	3.8-7.5	Moderate rate of water transmission
Group C	Clay loams, shallow sandy loam, soils with moderately fine to fine textures	Moderately high	1.3-3.8	Moderate rate of water transmission
Group D	Clay soils that swell significantly when wet, heavy plastic and soils with a permanent high water table	High	<1.3	Low rate of water transmission

Group C soils are shallow sandy loam or clay loams with fine or moderately fine texture, and Group D soils are clay soils that swell when wet (Muthu & Santhi, 2015). According to the USDA, Group C soils' runoff potential is moderately high, and their infiltration rate ranges between 1.3 mm/hr and 3.8 mm/hr (Muthu & Santhi, 2015). Group D soils have high runoff potential and lowest permeability below 1.3 mm/hr. However, Muli (2008) suggested a wide permeability coefficient for soil in Mihang'o ranging between 0.13 mm/hr and 3.8 mm hr. Also, based on NASA's Distributed Active Archive Centers (DAACs) Global Hydrologic Soil Groups

(HYSOGs250m) for Curve Number, Mihang'o is dominated by Group D soils (Ross et al., 2018). Therefore, Mihang'o's predominant hydrological soil is Group D.

Regarding LU/LC, Mihang'o watershed transformed from an original shrubland to a developing urban area. Literature evidence showed that the watershed has a mixture of land uses representing a developing urban watershed. Further, Google Earth satellite image analysis and ground truthing (Figure 4.1) confirmed that Mihang'o encompasses residential units, commercial businesses, small scale businesses, churches, schools, hospitals, playgrounds, and administrative centres. Therefore, the impervious surfaces in the watershed include paved parking lots, driveways, and roofs. The tarmacked streets and roads, have paved curbs, storm sewers, and paved open ditches. There are also gravel and dirt roads in the watershed.

Therefore, because Mihang'o watershed has Group D soils but diverse land uses, several CNs for Group D soils were picked from the Table of Curve Number for Urban Areas (Table 4.6). Importantly, the CN for residential units was computed based on CivilGEO's theory that: To determine CN when all or part of the impervious area is not directly connected to the drainage system, then a supplement matrix (Figure 4.14) should be used if the total impervious area is equal to or greater than 30% because the absorptive capacity of the remaining pervious areas will not significantly affect runoff (CivilGEO, 2023). This approach was adopted because residential units in Mihang'o watershed are generally 1/8 of an acre and in most cases, buildings occupy the entire plot. This translated to a composite CN of 96 for residential units in the Mihang'o watershed. Consequently, the average CN was 92, which was used in this study. Table 4.7 presents the computation results of CN for Mihang'o Watershed.

Table 4.6: Curve Number for Urban Areas

Runoff curve numbers for urban areas				
Cover type and hydrologic condition	Cover description	Average percent impervious area	Curve numbers for hydrologic soil group	
			A	B
<i>Fully developed urban areas (vegetation established)</i>				
Open space (lawns, parks, golf courses, cemeteries, etc.) ^{3/} :				
Poor condition (grass cover < 50%)		68	79	86
Fair condition (grass cover 50% to 75%)		49	69	79
Good condition (grass cover > 75%)		39	61	74
Impervious areas:				
Paved parking lots, roofs, driveways, etc. (excluding right-of-way)		98	98	98
Streets and roads:				
Paved; curbs and storm sewers (excluding right-of-way)		98	98	98
Paved; open ditches (including right-of-way)		83	89	92
Gravel (including right-of-way)		76	85	89
Dirt (including right-of-way)		72	82	87
Western desert urban areas:				
Natural desert landscaping (pervious areas only) ^{4/}		63	77	85
Artificial desert landscaping (impervious weed barrier, desert shrub with 1- to 2-inch sand or gravel mulch and basin borders)		96	96	96
Urban districts:				
Commercial and business		85	89	92
Industrial		72	81	88
Residential districts by average lot size:				
1/8 acre or less (town houses)		65	77	85
1/4 acre		38	61	75
1/3 acre		30	57	72
1/2 acre		25	54	70
1 acre		20	51	68
2 acres		12	46	65
<i>Developing urban areas</i>				
Newly graded areas (pervious areas only, no vegetation) ^{5/}		77	86	91
				94

Source: CivilGeo (2023)

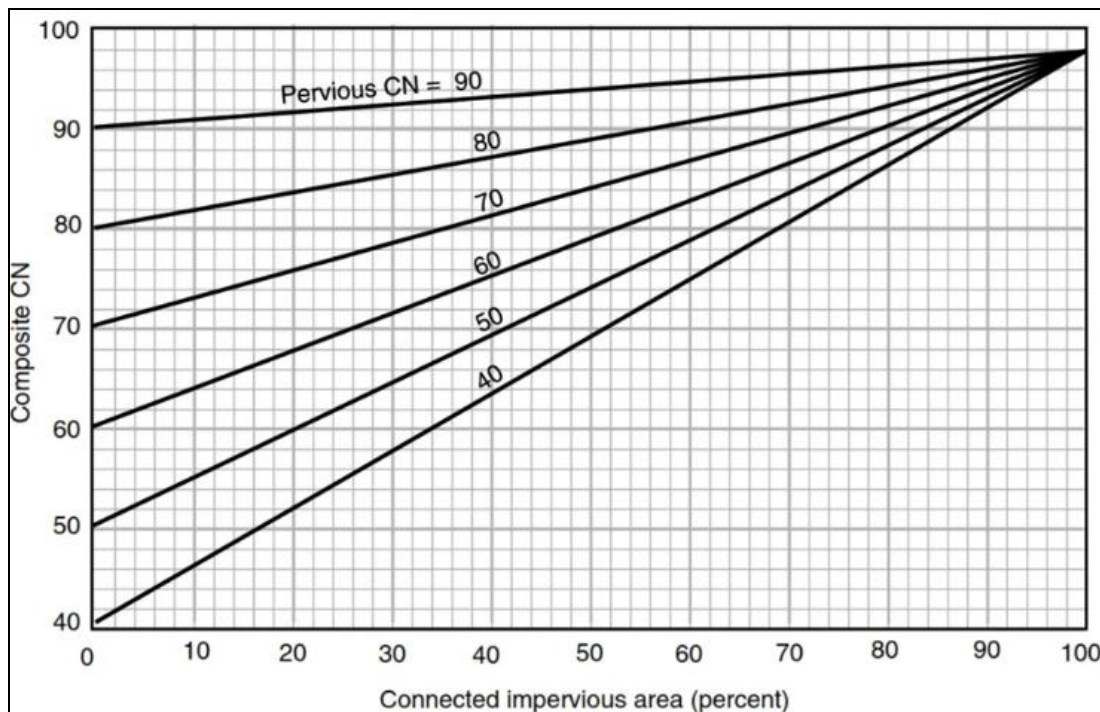


Figure 4.14: Supplement Matrix for Determining CN (CivilGeo, 2023)

Table 4.7: Curve Number for Mihang'o Watershed

Cover type and hydrologic condition	Places in the Mihang'o watershed	CN
Open space with poor condition (grass cover < 50%)	Airport, play fields,	89
Open space with poor condition (grass cover 50% to 75%)	Hotel compounds, hospital compound, recreation areas	84
Impervious areas: paved parking lots, roofs, driveways, paved streets and roads, paved curbs and storm sewers.	In residential area, in front of businesses and shopping complexes, along the roads and streets	98
Paved open ditches	Along the roads and streets	93
Gravel	Unpaved road, quarry	91
Dirt	Unpaved road, quarry	89
Commercial businesses and small industries	Closer to the Eastern bypass highway	95
Residential units	Throughout the watershed	96
Total CN		735
Average CN		91.88 or 92

Besides the CN value, the SCS-CN loss model also requires impervious surface coefficients as an input. The impervious surface percentage for each year of study served as the impervious surface coefficient. Table 4.8 shows the impervious surface coefficients used in this study.

Table 4.8: Impervious Surface Coefficients from 2000 - 2022

Year	2000	2003	2006	2009	2012	2015	2018	2022
Impervious surface coefficient (%)	2.78	5.63	9.32	10	11.53	12.73	15.11	22.21

Transform Model. The Soil Conservation Service Unit Hydrograph (SCS-UH) model used as the transform model requires lag time (T_{lag}) as the only input, but T_{lag} is a product of concentration time (T_c) (Equation 2.1 and Equation 2.2). The inputs for T_c are length of slope (S) and length of reach (L), which were derived from basin processing using ArcGIS. Table 4.9 is a summary of the slope and tributary reach, and the computed concentration time, and lag time for each sub-basin. Figure 4.11 showed the sub-basins of Mihang'o watershed and Figure 4.12 showed the schematic network of the watershed. The slope and reach length were derived from ArcGIS.

Table 4.9: Lag Time for Mihang'o Watershed Sub-basins

Sub-basin	Slope	Reach Length (ft)	T_c (min)	T_{lag} (min)
A	0.016	4101.05	23.19	13.914
B	0.015	20669.30	82.62	49.572
C	0.011	24770.34	107.0	64.200

Routing Model. Regarding the routing model, McCarthy stated that natural streams have X values ranging between 0 and 0.3, with a mean of 0.2. However, studies have shown that X 's value does not matter much on the output (Baláž et al., 2010; USACE, 2023). Therefore, $X = 0.2$ was picked for this study. Because the reach is short

(4101.05 ft) and joins a main tributary downstream, K was approximated as 0.5 based on the University of Colorado Boulder workings (Baláž et al., 2010).

Precipitation Data. The rainfall data needed in HEC-HMS is of a single rainfall event. The single rainfall event is tested against various impervious surface percentages to determine runoff trend. Importantly, the suitability of this approach was further enhanced by the fact that over the years, the Mihang'o watershed's impervious surface area statistically significantly increased ($p = .000$) and there was no trend in the rainfall data time series ($p = 0.697$). The single rainfall event used in this study was of 29th December, 2022 between 12 noon and 6 pm. Table 4.10 shows the data for the rainfall event on 29th December, 2022 between 12 noon and 6 pm.

Table 4.10: Measured Rainfall

Time (hours)	Precipitation (mm)
12 (noon)	0.5
13	0.8
14	1
15	1.1
16	1.2
17	0.6

Table 4.11 contains the summary of HEC-HMS calibration results. The table highlights the input parameters, selected models and their respective input data, and the input data values.

Table 4.11 Summary Table of HEC-HMS Model Calibration Results

Input parameters	Model	Specific Model Selected	Data Input	Data Input Values
Basin model (watershed physical parameters information)	Loss model	Soil Conservation Service Curve Number (SCS-CN)	CN	92
	Transform model	Soil Conservation Service Unit Hydrograph (SCS- UH)	T_{lag} (Lag time)	Sub-basin A (13.914), Sub-basin B (49.572), and Sub- basin (64.200)
	Routing model	Muskingum routing method	(i) Flood wave's travel duration (K) through the routing reach (ii) Dimensionless weight (X)	$X = 0.2$ $K = 0.5$
Precipitation data	Time-series data (precipitation model)	Specified hyetograph	Mihang'o watershed's rainfall data for 29 th December 2022 between 12 noon and 6 pm.	Data in Table 4.9
	Meteorologic models	-	Met 1(pre-defined specifications for Mihang'o watershed)	
	Control specifications	-	Start time: 29 Dec 2022, 12:00 End time: 29 Dec 2022, 23:00	

4.4.3 HEC-HMS Modeling

After putting together the supporting data required for the basin model, time-series data (precipitation model), meteorologic models, and control specifications, the HEC-HMS project was completed procedurally.

4.4.4 Runoff Amount Trend

Table 4.12 shows the runoff amount (mm) from the watershed for the years of study.

Table 4.12: Runoff Amount from Mihang'o Watershed

Year	2000	2003	2006	2009	2012	2015	2018	2022
Discharge/Runoff (mm)	0.18	0.32	0.51	0.54	0.62	0.69	0.81	1.18

The graph in Figure 4.15 represents the data in Table 4.11, and shows the runoff trend of Mihang'o watershed. The graph shows an increasing trend in the runoff amount over the years, with a drastic increase post 2015 to 2022. For instance, in 2015, the runoff was 0.69 mm, which sharply increased to 1.18 mm by 2022.

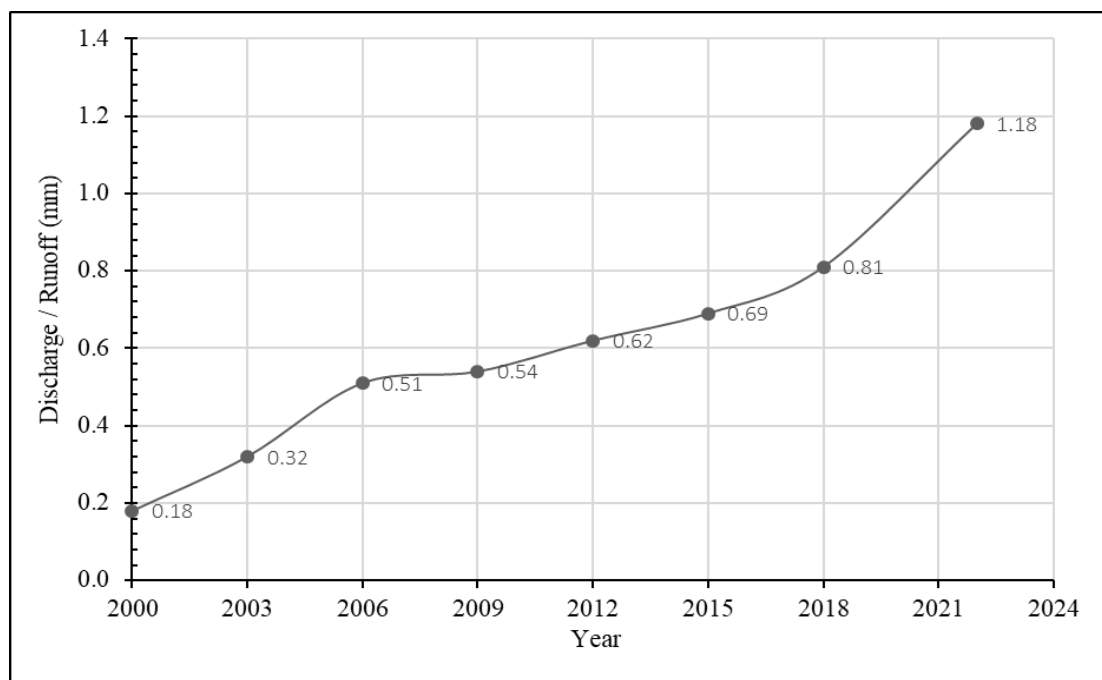


Figure 4.15: Runoff Trend of Mihang'o Watershed

Quality control through use of mass curve technique showed that data points for runoff are distributed on almost a straight line (Figure 4.16). This suggests that the data was homogenous and suitable for use in analysis and interpretation of runoff in Mihang'o watershed. The strong positive coefficient of determination ($0.9 < R^2 < 1$) reinforces the reliability of the data.

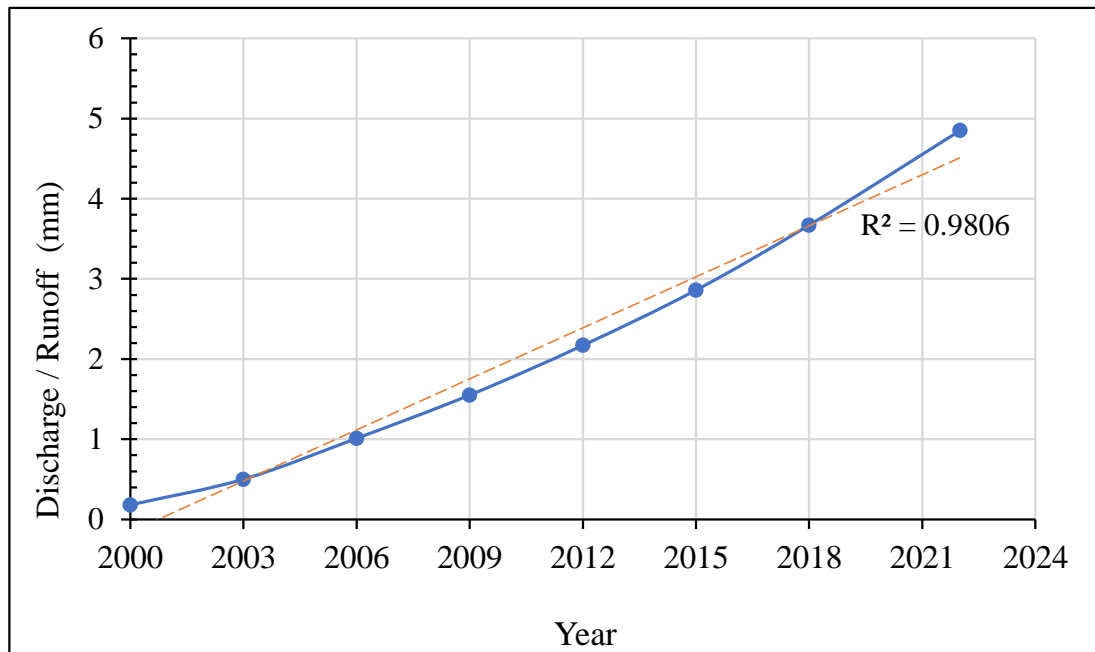


Figure 4.16: Mass Curve for Cumulative Discharge

The hypotheses for the third objective were:

H0 There is no trend in runoff time series of Mihang'o watershed.

H1 There is a positive trend in runoff time series of Mihang'o watershed.

A simple linear regression was calculated to predict runoff over the years. A significant regression equation was found ($F(1,6) = 91.215, p < .000$) with an R^2 of .938. The statistical results confirm that the trend in runoff increment is significant, with an approximate increment of 3.85% (0.045 mm) each year. Therefore, based on the alternative hypothesis (H1) of this study, there is a positive trend in runoff time series of Mihang'o watershed. The rainfall data input in the HEC-HMS model is a

control variable, as in a single rainfall event, the impervious surface area coefficient is the independent variable causing the increasing runoff trend, the dependent variable.

The runoff trend of Mihang'o watershed is consistent with the impervious surface area trend (Figure 4.5 and Figure 4.15). The figures show a gradual increase in the respective variables between 2000 and 2015, then a sharp increase between 2015 and 2022. A correlation analysis found a significant positive relationship between impervious surface area and runoff, $r(6) = .99, p < .000$. These results are consistent with findings from similar studies that support a positive correlation between impervious surface area and runoff amount from a watershed (Alsubeai & Burckhard, 2021; Poudel et al., 2020; Rahajeng, 2010; Xu & Zhao, 2016).

Notably, Poudel et al. (2020) concluded that results from their HEC-HMS project showed that an increase in impervious land cover significantly increases runoff volume. In Kenya, few studies have focused on runoff trend due to its relationship with impervious surface area in urban watershed, thus leaving a knowledge gap in this field and prompting this study. The studies reviewed focused on challenges resulting from flashfloods, inadequate drainage systems, management of urban drainage systems, and poor disposal of waste (Juma et al., 2022; Kibet et al., 2024; Kituyi, 2020; Musonye et al., 2022; Wanjiru, 2016). Nonetheless, the results from the studies conducted by Muthusi et al. (2020) and Barasa and Perera (2018) are consistent with this study. Muthusi et al. (2020) used the SCS-CN method integrated with remote sensing and GIS techniques to estimate urban runoff due to LULC changes in Mavoko Municipality, which borders Nairobi city, between 1989 and 2018. According to Muthusi et al. (2020), built-up areas that are largely impervious

increased from 24.6% in 1989 to 37.0% in 2018 while pervious land under grasslands, open spaces and barren land decreased from 65.5% to 44.5%, respectively. Also, 69% of the annual precipitation in 1989 was converted into runoff and this increased to 76% in 2018. Though Barasa and Perera (2018) conducted a similar study in a Sosiani River basin in the Rift Valley province, rather far from Nairobi, their observed discharge data showed that expansion of farmlands from 15.3% in 1970 to 75.2% in 2013 and urban areas from 0.4% to 10%, respectively triggered river peak discharge to increase from 167 m³/s (1970) to 233 m³/s (2013).

The reviewed literature and this study's findings collectively support the *Runoff Flow Changes resulting from Urbanization's Impervious Surface Area* conceptual framework adopted for this study (Figure 2.4). The general concept is that in a natural ground cover, runoff is 10%; as impervious surface cover increases to between 10% – 20%, runoff increases twice over forested catchments; in between 35% and 50% impervious surface cover, runoff increases threefold over forested catchments; and in between 75% and 100% impervious surface cover, runoff increases more than fivefold over forested catchments (Paul & Meyer, 2001).

Xu and Zhao (2016) explained that urbanization not only indicates a country's development level but also portrays human-environment interaction. The general trend is that runoff rises with an increase in human development. This starts with converting a forested area to agricultural land. The agricultural land may develop further into an urban area, thus increasing the imperviousness of surface cover and resultant runoff. According to Xu and Zhao (2016), over half of the rainfall in highly urbanized areas is converted to surface runoff because only a small fraction infiltrates the small patches of natural land.

Similarly, Mihang'o watershed initially contained large parcels of unoccupied scrubland and grassland, in which more precipitation infiltrated and runoff was minimal. For instance, Mihang'o watershed experienced low runoff in the early 2000s. Over the years, the gradual increase in development activities resulted in LULC changes. The watershed has experienced increasing construction of residential houses, roads, and commercial businesses. These developments have correspondingly increased the impervious surface area in the watershed. Consistently, the amount of runoff has been increasing in the watershed. The expansion of the eastern bypass highway starting in 2015 attracted speedy urbanization in the Mihang'o watershed, which has led to the observed drastic increase in runoff from the watershed from the year 2015.

CHAPTER FIVE: SUMMARY, CONCLUSIONS AND RECOMMENDATIONS

5.1 Introduction

This chapter provides a summary of the study's outcomes, presents the conclusions drawn from the results, and offers recommendations focused on policy formulation and areas for further research.

5.2 Objective One

The first objective was to evaluate change in impervious surface area of Mihang'o watershed from 2000 and 2022. The change in impervious surface area of Mihang'o watershed between the year 2000 and 2022 was assessed in this study. Impervious surface cover increased by 87.03% between 2000 and 2022. In the year 2000, the impervious surface area was 0.49 km^2 , representing 2.78% of the total surface area of Mihang'o watershed, which increased over the years to 3.91 km^2 in 2022, representing 22.21% of the watershed's total surface area. The linear regression results ($F(1,6) = 91.822, p < .001$) and R^2 of .939 confirmed that the trend in impervious surface increment is significant, thus supporting the alternative hypothesis (H1) of this study that there is a positive trend in the impervious surface area time series of Mihang'o watershed. The significant increase in impervious surface area in Mihang'o watershed by 87.03% in a span of 22 years underscores the importance of controlled urban development with the aim of upholding sustainable environmental practices such as maintaining green spaces despite the need for expanding the cities and towns.

5.3 Objective Two

The second objective was to assess trend of precipitation amount in Mihang'o watershed from 2000 and 2022. The precipitation trend of Mihang'o watershed

between the year 2000 and 2022 was analyzed in this study. The highest annual rainfall for Mihang'o watershed was 1172.8 in 2018 and the least was 491.7 in 2000 and the average annual rainfall is approximately 779 mm. The watershed has two rainfall seasons: long rains between March and May and short rains between November and December. The rainfall pattern in Mihang'o is consistent with the rainfall pattern and climate of the larger Nairobi catchment, which has no significant linear trend in rainfall. Further, the Mann-Kendall trend test ($p = .625$) show $p > .05$; therefore, based on the null hypothesis of this study (H_0), there is no trend in the rainfall data time series of Mihang'o watershed. Because rainfall data for Mihang'o watershed was found to have no trend, this study provides valuable insights that a trend in runoff from an urban watershed over a long period may not be directly influenced by rainfall pattern.

5.4 Objective Three

The third objective was to determine trend in runoff amount from Mihang'o watershed from 2000 and 2022. The trend of the amount of runoff from Mihang'o watershed between the year 2000 and 2022 was analyzed in this study. Runoff increased by approximately 84.75% from 0.18 mm in 2000 to 1.18 mm in 2022. The linear regression results ($F (1,6) = 91.215$, $p < .000$) and R^2 of .938 confirmed a significant increment in runoff, thus supporting the alternative hypothesis (H_1) of this study that there is a positive trend in the runoff time series of Mihang'o watershed. This study contributes to the growing body of knowledge on urban hydrology and emphasizes the direct impact of unmonitored increase in impervious surface area due to urbanization on the amount of flooding and runoff from an urban watershed.

5.5 Recommendations

- i. Regarding Objective 1, it is recommendable that proper urban planning efforts that aim at controlling increase of impervious surfaces and expanding green spaces to control runoff should be taken up by the government and individuals including green roofs, permeable pavements, urban forestry.
- ii. As for Objective 2, the seasonal and annual rainfall totals for Mihang'o watershed varies across the years, therefore, initiatives in increasing storage capacity of rainfall and runoff water should be encouraged to harvest excess rainwater that causes runoff and flooding during rainy seasons or years.
- iii. Pertaining to Objective 3, runoff from an urban watershed can be monitored effectively when runoff stations are installed in drainage channels. Otherwise, besides the above recommendations, runoff can be controlled through constructing on the streams retention basins and infiltration trenches.

Recommendations for Future Studies

- i. While this study provides valuable insights into the relationship between runoff and impervious surface area, it is limited by factors such as the specific geographic locations studied and the scope of the data collected. These limitations suggest that further research is needed to enhance our understanding of these dynamics in varied urban environments.
- ii. Also, future studies need to use higher resolution images to ensure more accurate supervised classification. Other models including WEAP or SWAT may be used to generate more findings for comparison.

REFERENCES

- Ahmad, I., Tang, D., Wang, T., Wang, M., & Wagan, B. (2015). Precipitation trends over time using Mann-Kendall and spearman's rho tests in swat river basin, Pakistan. *Advances in Meteorology*, 2015. <https://doi.org/10.1155/2015/431860>
- Akech, N. O., Omumbo, C. A., & Masibo, M. (2013). General geology of Kenya. In *Developments in Earth Surface Processes* (pp. 3-10). Elsevier.
- Alam, F., Salam, M., Khalil, N. A., khan, O., & Khan, M. (2021). Rainfall trend analysis and weather forecast accuracy in selected parts of Khyber Pakhtunkhwa, Pakistan. *SN Applied Sciences*, 3, 1-14. <https://link.springer.com/article/10.1007/s42452-021-04457-z>
- Aliye, M. A., Aga, A. O., Tadesse, T., & Yohannes, P. (2020). Evaluating the performance of HEC-HMS and SWAT hydrological models in simulating the rainfall-runoff process for data scarce region of Ethiopian Rift Valley Lake Basin. *Open Journal of Modern Hydrology*, 10(04), 105. DOI: 10.4236/ojmh.2020.104007
- Alsubeai, A. and Burckhard, S. (2021). Rainfall-runoff simulation and modelling using HEC-HMS and HEC-RAS models: Case study Tabuk, Saudi Arabia. *Natural Resources*, 12, 321-338. doi: 10.4236/nr.2021.1210022.
- Alves, M. d. C., Sanches, L. (2023). *Remote sensing and digital image processing with R - lab manual*. CRC Press.
- Aswad, F. K., Yousif, A. A., & Ibrahim, S. A. (2020). Trend analysis using Mann-Kendall and Sen's slope estimator test for annual and monthly rainfall for Sinjar district, Iraq. *Journal of Duhok University*, 23(2), 501-508. https://www.researchgate.net/publication/343787766_Trend_Analysis_Using_Mann-Kendall_and_Sen's_Slope_Estimator_Test_for_Annual_and_Monthly_Rainfall_for_Sinjar_District_Iraq
- Ayugi, B. O., Wen, W., & Chepkemoi, D. (2016). Analysis of spatial and temporal patterns of rainfall variations over Kenya. *Journal of Environment and Earth Science*, 6(11), 69-83. <https://core.ac.uk/download/pdf/234664768.pdf>
- Bajracharya, A. R., Rai, R. R., & Rana, S. (2015). Effects of urbanization on storm water run-off: A case study of Kathmandu Metropolitan City, Nepal. *Journal of the Institute of Engineering*, 11(1), 36-50. doi:10.3126/JIE.V11I1.14694
- Baláž, M., Danáčová, M., & Szolgay, J. (2010). On the use of the Muskingum method for the simulation of flood wave movements. *Slovak Journal of Civil Engineering*, 18(3), 14-20. doi: 10.2478/v10189-010-0012-6
- Barasa, B. N., & Perera, E. D. P. (2018). Analysis of land use change impacts on flash flood occurrences in the Sosiani River basin Kenya. *International Journal of River Basin Management*, 16(2), 179–188. <https://doi.org/10.1080/15715124.2017.1411922>
- Belay, Y. Y., Gouday, Y. A., & Alemnew, H. N. (2022). Comparison of HEC-HMS hydrologic model for estimation of runoff computation techniques as a design

- input: case of Middle Awash multi-purpose dam, Ethiopia. *Applied Water Science*, 12(10), 237. <https://link.springer.com/article/10.1007/s13201-022-01764-7>
- Bhat, V., Somanna, P., Harshith, V. (2019). Rainfall trend analysis: A parametric method. *International Journal of Engineering Research & Technology (IJERT)*. 06(15). <https://www.ijert.org/rainfall-trend-analysis-a-parametric-method>
- Bird. S.L. Harrison, J., Exum. L.R. Alberty, S.W. & Perkins, C. (2002). Screening to identify and prevent urban storm water problems: estimating impervious area accurately and inexpensively. *Proceedings of The National Water Quality Monitoring Conference, May 20-23, 2002.* https://www.researchgate.net/publication/265065287_Screening_to_Identify_and_Prevent_Urban_Storm_Water_Problems_Estimating_Impervious_Area_Accurately_and_Inexpensively
- Bosco, N. J., Geoffrey, M. M., & Kariuki, N. (2011). Assessment of landscape change and occurrence at watershed level in city of Nairobi. *African Journal of Environmental Science and Technology*, 5(10), 873-883. <http://www.academicjournals.org/AJEST>
- Brabec. E. Schulte. S. & Richards, P. (2002). Impervious surfaces and water quality: A Review of current literature and its implications for watershed planning. *Journal of Planning Literature*, 16(4). 499-514.
- Cambridge Dictionary. (2023). *Precipitation*. <https://dictionary.cambridge.org/dictionary/english/precipitation>
- Campbell, J. B. (2002). *Introduction to remote sensing*. Taylor & Francis.
- Chabaeva. A. Hurd. J., Civco. D. (2007). Quantitative assessment of the accuracy of spatial estimation of impervious cover. *ASPRS 2007 Annual Conference*. https://www.researchgate.net/publication/251869272_QUANTITATIVE_ASSESSMENT_OF_THE_ACCURACY_OF_SPATIAL_ESTIMATION_OF_IMPERVIOUS_COVER
- Chathuranika, I. M., Gunathilake, M. B., Badewela, P. K., Sachinthanie, E., Babel, M. S., Shrestha, S., & Rathnayake, U. S. (2022). Comparison of two hydrological models, HEC-HMS and SWAT in runoff estimation: application to Huai Bang Sai Tropical Watershed, Thailand. *Fluids*, 7(8), 267. <https://doi.org/10.3390/fluids7080267>
- Chiari, L., Della Croce, U., Leardini, A., & Cappozzo, A. (2005). Human movement analysis using stereophotogrammetry: Part 2: Instrumental errors. *Gait & Posture*, 21(2), 197-211. <https://doi.org/10.1016/j.gaitpost.2004.04.004>
- Civco. D., Chabaeva, A., & Hurd, J. (2006). A comparison of approaches to impervious surface characterization. *IEEE International Geoscience and Remote Sensing Symposium*. 1398-1402, doi: 10.1109/IGARSS.2006.361.
- CivilGeo. (2023). *Curve numbers for urban impervious areas*. <https://knowledge.civilgeo.com/knowledge-base/curve-numbers-for-urban-impervious-areas/>

- Climate Hazards Center. (2023). *CHIRPS: Rainfall Estimates from Rain Gauge and Satellite Observations*. <https://www.chc.ucsb.edu/data/chirps>
- Distancesto (2023). *Elevation from Nairobi to Utawala Bypass Stage*. <https://www.distancesto.com/route-elevation/ke/nairobi-to-utawala-bypass-stage/history/846274.html>
- Dougherty, M. Dymond. R., Goetz. S. J., Jantz. C. A., & Goulet, N. (2004). Evaluation of impervious surface estimates in a rapidly urbanizing watershed. *Photogrammetric Engineering and Remote Sensing* 70(11), 1275-1284. doi:10.14358/PERS.70.11.1275
- Draper, S. E., & Rao, S. G. (1986). Runoff prediction using remote sensing imagery. *Journal of the American Water Resources Association*, 22(6), 941-949. <https://doi.org/10.1111/j.1752-1688.1986.tb00766.x>
- Ebrahimian, A., Gulliver, J. S. Wilson, B. N. (2015). *Determination of effective impervious area in urban watersheds*. Center for Transportation Studies, University of Minnesota. <https://hdl.handle.net/11299/174667>.
- Ebrahimian, A., Gulliver, J. S., & Wilson, B. N. (2016a). Effective impervious area for runoff in urban watersheds. *Hydrological Processes*, 30(20), 3717-3729. <https://doi.org/10.1002/hyp.10839>
- Ebrahimian, A., Wilson, B. N., & Gulliver, J. S. (2016b). Improved methods to estimate the effective impervious area in urban catchments using rainfall-runoff data. *Journal of Hydrology*, 536, 109-118. <https://doi.org/10.1016/j.jhydrol.2016.02.023>
- Exum. L. R. Bird, S. L. Harrison. J. & Perkins. C. A. (2005). *Estimating and projecting impervious cover in the Southeastern United States*. Environmental Protection Agency. https://www.edwardsaquifer.org/wp-content/uploads/2019/02/2005_Exum-etal_ImperviousCover.pdf
- Ferreira, R. G., Dias, R/ L. S., Castro, J. S., Santos, V. J., Calijuri, M. L., Silva, D. D. (2021). Performance of hydrological models in fluvial flow simulation. *Ecological Informatics*, 66(101453). <https://doi.org/10.1016/j.ecoinf.2021.101453>
- Gachanja, J., Karanja, J., Nato, J., Ngugi, R., Njogu, H., Nyaware, B., Mbaka, C., Mwatu, S. & Sitati, M. (2023). *Urban economic growth in Africa: A case study of Nairobi City County, Kenya*. Kenya Institute for Public Policy Research and Analysis (KIPPRA) and Africa Growth Initiative (AGI). https://www.brookings.edu/wp-content/uploads/2023/02/2023_AGI_Nairobi-Case-Study_Final_23.02.16.pdf
- Gebre, S. L. (2015). Application of the HEC-HMS model for runoff simulation of Upper Blue Nile River Basin. *Hydrology: Current Research*, 6(2), 1-8. doi:10.4172/2157-7587.1000199
- Granato, G. E. (2010). *Methods for development of planning-level estimates of stormflow at unmonitored sites in the conterminous United States*. U.S. Department of Transportation, Federal Highway Administration.

- Güneralp, B., Reba, M., Hales, B. U., Wentz, E. A., & Seto, K. C. (2020). Trends in urban land expansion, density, and land transitions from 1970 to 2010: A global synthesis. *Environmental Research Letters*, 15(4), 044015. doi 10.1088/1748-9326/ab6669.
- Guo, Y., Zhang, Y., Zhang, T., Wang, K., Ding, J., Gao, H. (2019). Surface Runoff. In: Li, X., Vereecken, H. (eds). *Observation and measurement of ecohydrological processes* (pp. 241–306). Springer Berlin Heidelberg. https://doi.org/10.1007/978-3-662-48297-1_8
- Hamilton, B., Coops, N. C., & Lokman, K. (2021). Time series monitoring of impervious surfaces and runoff impacts in Metro Vancouver. *Science of the Total Environment*, 760, 143873. <https://doi.org/10.1016/j.scitotenv.2020.143873>
- Jenifer, M. A., & Jha, M. K. (2021). Assessment of precipitation trends and its implications in the semi-arid region of Southern India. *Environmental Challenges*, 5, 100269. <https://doi.org/10.1016/j.envc.2021.100269>
- Juma, B., Olang, L. O., Hassan, M. A., Mulligan, J., & Shiundu, P. M. (2022). Simulation of flood peak discharges and volumes for flood risk management in the ungauged urban informal settlement of Kibera, Kenya. *Physics and Chemistry of the Earth, Parts A/B/C*, 128, 103236. <https://doi.org/10.1016/j.pce.2022.103236>
- Kalra, A., Paudel, S., Wang, Y., Acharya, A., Joshi, N., & Gupta, R. (2022). Application of the HEC-HMS Model for runoff simulation of Big Muddy River, Illinois. *World Environmental and Water Resources Congress 2022*. 481-491. <https://doi.org/10.1061/9780784484258.044>
- Kandane-Rathnayake, J. C. & Enticott, L.E. (2013). Data distribution: normal or abnormal? Data distribution: normal or abnormal? *Phillips*, 53(2), 257-259. <https://doi.org/10.1111/j.1537-2995.2012.03814.x>
- Kibet, I. Mutungi, R., Murangiri, G., Mawio, P. M., & Kiptum, C. (2024). Hydrological analysis and storm water drainage design for Westlands, Nairobi. *International Research Journal of Modernization in Engineering Technology and Science*, 6(5) 8278- 8283. https://www.irjmets.com/uploadedfiles/paper//issue_5_may_2024/57556/final/fin_irjmets1716903974.pdf
- Kilavi, M., MacLeod, D., Ambani, M., Robbins, J., Dankers, R., Graham, R., Titley, H., Salih, A. A. M., & Todd, M. C. (2018). Extreme rainfall and flooding over central Kenya including Nairobi city during the long-rains season 2018: Causes, predictability, and potential for early warning and actions. *Atmosphere*, 9(12), 472. <https://doi.org/10.3390/atmos9120472>
- Kituyi, M. N. (2020). *Influence of monitoring and evaluation process on performance of urban drainage systems: A case of Nairobi county* [Unpublished Postgraduate Diploma]. Africa Nazarene University.
- Kotikot, S. M., Smithwick, E. A. H. & Greatrex, H. (2024). Observations of enhanced rainfall variability in Kenya, East Africa. *Scientific Reports*, 14, 12915. <https://doi.org/10.1038/s41598-024-63786-2>

- Lastra, J., Fernández, E., Díez-Herrero, A., & Marquinez, J. (2008). Flood hazard delineation combining geomorphological and hydrological methods: an example in the Northern Iberian Peninsula. *Natural Hazards*, 45, 277-293. <https://doi.org/10.1007/s11069-007-9164-8>
- Lee, J. G., & Heaney, J. P. (2003). Estimation of urban imperviousness and its impacts on storm water systems. *Journal of Water Resources Planning and Management*, 129(5), 419-426. [https://doi.org/10.1061/\(ASCE\)0733-9496\(2003\)129:5\(419](https://doi.org/10.1061/(ASCE)0733-9496(2003)129:5(419)
- Li, Y., & Wang, C. (2009). Impacts of urbanization on surface runoff of the Dardenne Creek watershed, St. Charles County, Missouri. *Physical Geography*, 30(6), 556-573. doi:10.2747/0272-3646.30.6.556
- Ligtenberg, J. (2017). *Runoff changes due to urbanization: A review*. <https://www.diva-portal.org/smash/get/diva2:1067287/FULLTEXT01.pdf>
- Mbuthia, M., Kiroro, F., Malik, A. & Goldblatt, R. (2022, March 30). *Mapping the impact of urbanization on vegetation in Nairobi, the 'green city in the sun'*. International Initiative for Impact Evaluation. <https://www.3ieimpact.org/blogs/mapping-impact-urbanization-vegetation-nairobi-green-city-sun>
- Mikelsons, K., & Wang, M. (2021). Global clear sky near-surface imagery from multiple satellite daily imagery time series. *ISPRS Journal of Photogrammetry and Remote Sensing*, 180, 238–254. <https://doi.org/10.1016/j.isprsjprs.2021.08.013>
- Miller, J., Kim, H., Kjeldsen, T. R., Packman, J., Grebby, S., & Dearden, R. (2014). Assessing the impact of urbanization on storm runoff in a peri-urban catchment using historical change in impervious cover. *Journal of Hydrology*, 515, 59-70. doi.org/10.1016/j.jhydrol.2014.04.011
- Muli, N. M. (2008). Rainfall-runoff flood modelling in Nairobi urban watershed, Kenya. Thesis [Unpublished master's thesis]. Kenyatta University.
- Mundia, C. N., & Aniya, M. (2005). Analysis of land use/cover changes and urban expansion of Nairobi city using remote sensing and GIS. *International journal of Remote sensing*, 26(13), 2831-2849. doi:10.1080/01431160500117865
- Mundia, C. N., & James, M. M. (2014). Dynamism of land use changes on surface temperature in Kenya: A case study of Nairobi City. *International Journal of Science and Research (IJSR)*, 3(4), 38-41. <https://www.ijsr.net/archive/v3i4/MDIwMTMxMzg5.pdf>
- Munyoki, F., Makokha, M., & Obiero, K. (2024). Assessment of land use and land cover change dynamics and drivers in Mbagathi River Catchment in Kajiado County, Kenya. *Open Access Library Journal*, 11(2), 1-12. doi: 10.4236/oalib.1111019
- Musonye, P. K., Ucakuwun, E. K., & Munyao, T. M. (2022). On-site runoff management, challenges and prospects in Amalemba, an urban informal settlement in Kakamega municipality, Kakamega County, Kenya. *Africa Environmental Review Journal*, 5(1), Pg 130–140. <https://doi.org/10.2200/aerj.v5i1.45>

- Muthu, A. L., & Santhi, M. H. (2015). Estimation of surface runoff potential using SCS-CN method integrated with GIS. *Indian Journal of Science and Technology*, 8(28), 1-5. doi:10.17485/ijst/2015/v8i28/83324
- Muthusi, N. N., Dulo, S. O., & Ndiba, P. K. (2020). Runoff estimation for an urban area using SCS-CN method, remote sensing and geographic information systems approach: A Case Study of Mavoko Municipality, Kenya. *International Journal of Engineering Research & Technology (IJERT)*, 9, 4. 854 – 860. doi:10.13140/RG.2.2.16265.26729
- Mutua, M., & Runguma, S. N. (2020). Annual and seasonal rainfall variability for the Kenyan highlands from 1900-2012. *Journal of Climatology & Weather Forecasting*, 8(3), 260. doi: 10.35248/2332-2594.2020.8.260
- Mwathi, P. M. (2016). *Effects of land use and land cover dynamics on environmental quality of Nairobi city and its environs* [Unpublished doctoral dissertation]. University of Nairobi.
- Nairobi City County (2023). *County annual development plan (CADP) 2024/2025*. <https://nairobiassembly.go.ke/ncca/wp-content/uploads/paperlaid/2023/NAIROBI-CITY-COUNTY-ANNUAL-DEVELOPMENT-PLAN-FY-2024-2025.pdf>
- O'Driscoll, M., Clinton, M., Jefferson, A., Manda, A., & McMillan, S. (2010). Urbanization effects on watershed hydrology and in-stream processes in the Southern United States. *Water*, 2(3), 605-648; doi:10.3390/w2030605
- Okwiri, W. (2021). Heavy winds, floods leave trail of destruction in Ruai- Photos. *Standard Media*. <https://www.standardmedia.co.ke/counties/article/2001402630/heavy-winds-floods-leave-trail-of-destruction-in-ruai-photos>
- Ongoma, V., Otieno, S. A., & Onyango, A. O. (2015). Investigation of the possible influence of urbanization on rainfall variability over Nairobi City, Kenya. *Momona Ethiopian Journal of Science*, 7(2), 222-239. <http://repository.seku.ac.ke/handle/123456789/1838>
- Onyancha, C., Mathu, E., Mwea, S., & Ngeci, W. (2011). A study on the engineering behaviour of Nairobi subsoil. *ARPJ Journal of Engineering and Applied Sciences*, 6(7), 85-96. <http://erepository.uonbi.ac.ke>.
- Owuor, M. O., & Mwiturubani, D. A. (2022). Correlation between flooding and settlement planning in Nairobi. *Journal of Water and Climate Change*, 13(4), 1790-1805. <https://doi.org/10.2166/wcc.2022.335>
- Paul, M. J. & Meyer, J. L. (2001). Streams in the Urban Landscape. *Annual Review of Ecology and Systematics*, 32.333–365. <https://doi.org/10.1146/annurev.ecolsys.32.081501.114040>
- Poudel, U., Ahmad, S., & Stephen, H. (2020, May). Impact of urbanization on runoff and infiltration in Walnut Gulch Experimental Watershed. *Watershed Management Conference 2020*. 219-232. <https://ascelibrary.org/doi/abs/10.1061/9780784483060.020#:~:text=The%20simulation%20results%20of%20HEC,a%20deficit%20of%20groundwater%20supply>.

- Rahajeng, E. (2010). *Application HEC-HMS to predict hydrograph (Case Study in Lebak Petal Sub Basin)*. AFITA 2010 International Conference: The Quality Information for Competitive Agricultural Based Production System and Commerce. <https://repository.ipb.ac.id/jspui/bitstream/123456789/41722/1/Application%20HEC-HMS%20to%20Predict%20Hydrograph.pdf>
- Rezaei, A. R., Ismail, Z. B., Niksokhan, M. H., Ramli, A. H., Sidek, L. M., & Dayarian, M. A. (2019). Investigating the effective factors influencing surface runoff generation in urban catchments—A review. *Desalination Water Treat*, 164, 276-292. doi:10.5004/dwt.2019.24359
- Ross, C. W., Prihodko, L., Anchang, J., Kumar, S., Ji, W., & Hanan, N. P. (2018). HYSGOs250m, global gridded hydrologic soil groups for curve-number-based runoff modeling. *Scientific Data*, 5(1), 1-9. <https://doi.org/10.1038/sdata.2018.91>
- Sahu, S. A. L. I. L., Pyasi, S. K., & Galkate, R. V. (2020). A review on the HEC-HMS rainfall-runoff simulation model. *International Journal of Agricultural Science and Research*, 10(4), 183-190. https://www.researchgate.net/publication/344779598_A REVIEW ON THE HEC-HMS RAINFALL-RUNOFF SIMULATION MODEL
- Science Education Resource Center. (June 16, 2020). *What is Google Earth?* https://serc.carleton.edu/introgeo/google_earth/what.html#:~:text=Google%20Earth%20is%20a%20geobrowser,as%20a%20three%2Ddimensional%20globe.
- Şen, Z. (2017). Innovative trend significance test and applications. *Theoretical and Applied Climatology*, 127, 939-947. doi 10.1007/s00704-015-1681-x
- Serinaldi, F., Chebana, F., & Kilsby, C. G. (2020). Dissecting innovative trend analysis. *Stochastic Environmental Research and Risk Assessment*, 34, 733-754. https://eprints.ncl.ac.uk/file_store/production/265850/59D0F880-FD1B-4DE0-A4B1-F831E7D909E3.pdf
- Seto, K.C. and Shepherd, J.M. (2009) Global urban land-use trends and climate impacts. *Current Opinion in Environmental Sustainability*, 1, 89-95. <http://dx.doi.org/10.1016/j.cosust.2009.07.012>.
- Shuster, W. D., Bonta, J., Thurston, H., Warnemuende, E., & Smith, D. R. (2005). Impacts of impervious surface on watershed hydrology: A review, *Urban Water Journal*, 2(4), 263-275, doi:10.1080/15730620500386529
- Sindani, B. B. W., Ochieng'Olago, D., Olaka, L. A., & Amwata, D. A. (2022). Analysis of 30 years' historical climate change trends and variability in Mt. Elgon, Kenya, Africa. *Journal of Sustainability, Environment and Peace*, 5(1). <https://uonjournals.uonbi.ac.ke/ojs/index.php/jsep/article/view/1239>
- Stanuikynas, T. J., Van, D. J., Newcomb, D. J. (2000). *Impervious surface methodology: A methodology for defining and assessing impervious surfaces in the Raritan River basin*. Jersey Water Supply Authority. <https://doi.org/doi:10.7282/T3MP537V>
- Sultan, D., Tsunekawa, A., Tsubo, M., Haregewyn, N., Adgo, E., Meshesha, D. T., Fenta, A. A., Ebabu, K., Berihun, M. L. & Setargie, T. A. (2022). Evaluation of lag time and time of concentration estimation methods in small tropical

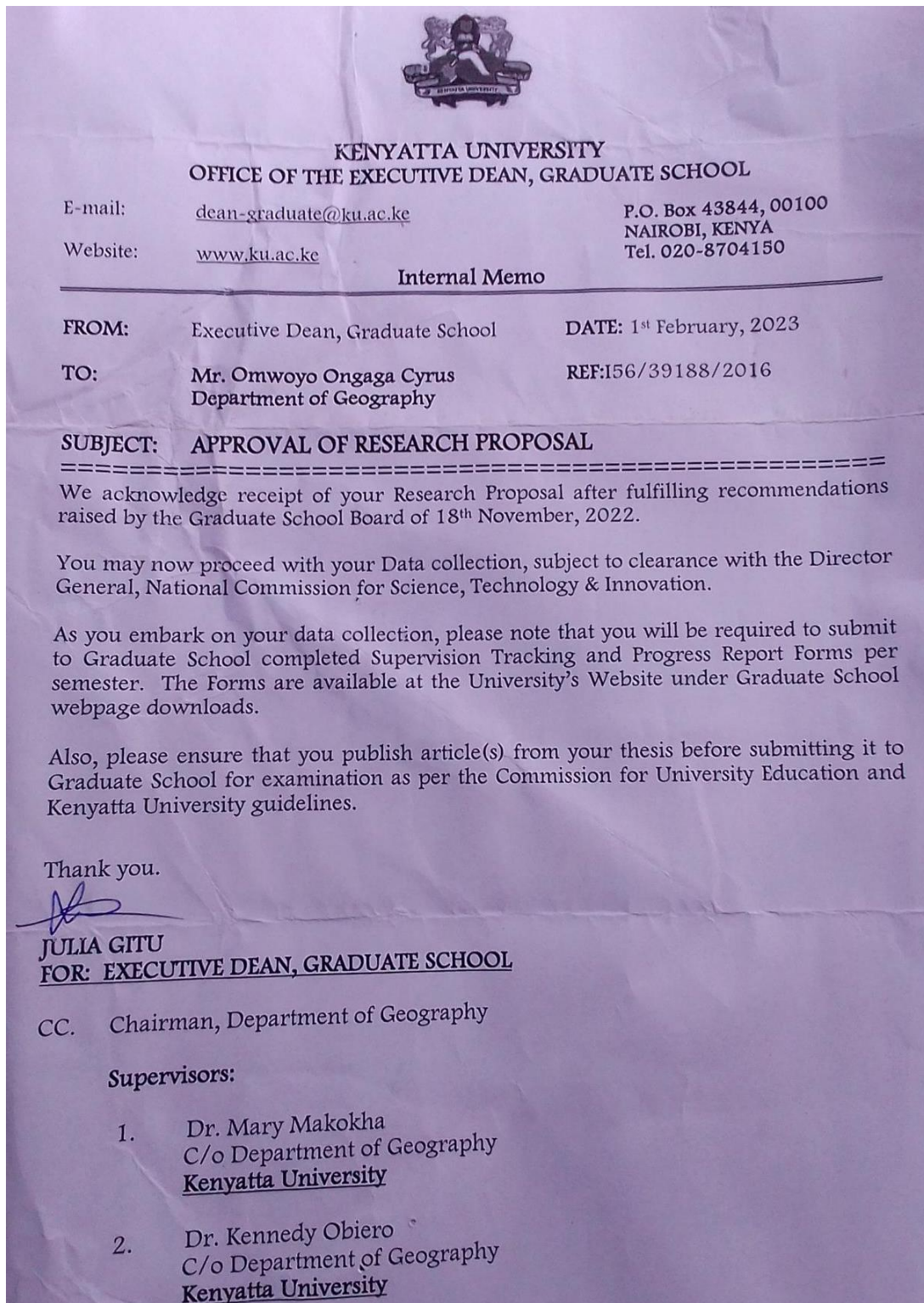
- watersheds in Ethiopia. *Journal of Hydrology: Regional Studies*, 40, 101025. <https://doi.org/10.1016/j.ejrh.2022.101025>
- Tang, W., Feng, W., Zheg, M., & Shi, J. (2018). Land cover classification of fine-resolution remote sensing data. In S. Liang (Ed.), *Comprehensive remote sensing* (pp. 17 – 28). Elsevier.
- Tassew, B. G., Belete, M. A., & Miegel, K. (2019). Application of HEC-HMS model for flow simulation in the Lake Tana Basin: The case of Gilgel Abay Catchment, Upper Blue Nile Basin, Ethiopia. *Hydrology*, 6(1), 21. doi:10.3390/hydrology6010021
- Tom, R. O., George, K. O., Joanes, A. O., & Haron, A. (2022). Review of flood modelling and models in developing cities and informal settlements: A case of Nairobi city. *Journal of Hydrology: Regional Studies*, 43, 101188. <https://doi.org/10.1016/j.ejrh.2022.101188>
- Treppiedi, D., Cipolla, G., Francipane, A., & Noto, L. V. (2021). Detecting precipitation trend using a multiscale approach based on quantile regression over a Mediterranean area. *International Journal of Climatology*, 41(13), 5938-5955. <https://doi.org/10.1002/joc.7161>
- United Nations (2018). *68% of the world population projected to live in urban areas by 2050, says UN*. Retrieved from <https://www.un.org/development/desa/en/news/population/2018-revision-of-world-urbanization-prospects.html>
- University of Cape Town. (2017). *Nairobi climate profile: Full technical version*. https://www.urbanark.org/sites/default/files/resources/Nairobi_climate_profile_full_technical_v2_0.pdf
- US Army Corps of Engineers. (2009). *Hydrologic Modeling System HEC-HMS: Quick Start Guide*. Hydrologic Engineering Center.
- US Army Corps of Engineers. (2023). Muskingum Model. Basic Concepts and Equations. In *HEC-HMS Technical Reference Manual*. Hydrologic Engineering Center.
- Verma, A. K., Jha, M. K., & Mahana, R. K. (2010). Evaluation of HEC-HMS and WEPP for simulating watershed runoff using remote sensing and geographical information system. *Paddy and Water Environment*, 8, 131-144. <https://doi.org/10.1007/s10333-009-0192-8>
- Wanjiru, W. S. (2016). Assessment of flash floods in the streets of Nairobi city, their relationship with rainfall and surface runoff drainage and their impacts to its residents. [Unpublished undergraduate thesis]. University of Nairobi. <https://meteorology.uonbi.ac.ke/sites/default/files/cbps/sps/meteorology/Silvia.pdf>
- Water Resources Authority. (2014). *Water resources allocation thresholds for classification of permits*. Second edition. Nairobi.
- Willems, P., Olsson, J., Arnbjerg-Nielsen, K., Beecham, S., Pathirana, A., Gregersen, I. B., Henrik Madsen, Van-Thanh-Van Nguyen (2012). *Impacts of climate change on rainfall extremes and urban drainage systems*. IWA Publishing.

- Xu, Z., & Zhao, G. (2016). Impact of urbanization on rainfall-runoff processes: case study in the Liangshui River Basin in Beijing, China. *Proceedings of the International Association of Hydrological Sciences*, 373, 7-12. <https://doi.org/10.5194/piahs-373-7-2016>
- Yu, X., & Zhang, J. (2023). The Application and Applicability of HEC-HMS Model in Flood Simulation under the Condition of River Basin Urbanization. *Water*, 15(12), 2249. <https://doi.org/10.3390/w15122249>

APPENDICES

Appendix A: Research Approval Documents

(a) Approval of Research Proposal by Kenyatta University's Graduate School Research



(b) NACOSTI's Research Permit



Appendix B: Screenshots Collected During HEC-HMS Procedures

The figure consists of four separate windows of the HEC-HMS 4.11 software, arranged in a 2x2 grid.

- Top Left Window:** Shows the Basin Model [Mihang'o basin] Current Run [Run 1_2000]. It displays a network diagram with nodes: Sink-1, Subbasin-A, Junction-1, Subbasin-B, and Subbasin-C. The Subbasin-C node has a blue water icon. Below the diagram is a detailed configuration panel for Subbasin-C.
- Top Right Window:** Shows the same Basin Model [Mihang'o basin] Current Run [Run 1_2000]. This window shows a simplified configuration panel for Subbasin-C, focusing on Initial Abstraction (MM) settings.
- Bottom Left Window:** Shows the same Basin Model [Mihang'o basin] Current Run [Run 1_2000]. This window shows a simplified configuration panel for Subbasin-C, focusing on Graph Type (Standard (PRF 484)) and Lag Time (MIN) (64.2).
- Bottom Right Window:** Shows the Control Specifications panel. It lists Control 1, which is defined as a Control specification for Mihang'o peo. The panel includes fields for Start Date (ddMMYYYY), Start Time (HH:mm), End Date (ddMMYYYY), End Time (HH:mm), and Time Interval (15 Minutes). A Gage 1 entry is also visible under Time-Series Data.

HEC-HMS 4.11 [C:\...\Documents\Mihang_o_project\Mihang_o_project.hms]

File Edit View Components GIS Parameters Compute Results Tools

-None-

Subbasin-C
Subbasin-B
Junction-1
Reach-1
Subbasin-A
Sink-1
Meteorologic Models
Met 1
Control Specifications
Control 1
Time-Series Data
Precipitation Gages
Gage 1
29Dec2023, 12:00 - 29Dec2023, 18:00

Components Compute Results

Time-Series Gage Time Window Table Graph

Gage Name: Gage 1

*Start Date (ddMMYYYY) 29Dec2023
 *Start Time (HH:mm) 12:00
 *End Date (ddMMYYYY) 29Dec2023
 *End Time (HH:mm) 18:00

Time-Series Gage Time Window Table Graph

Time (ddMMYYYY, HH:mm)	Precipitation (MM)
29Dec2023, 12:00	
29Dec2023, 13:00	0.5
29Dec2023, 14:00	0.8
29Dec2023, 15:00	1.0
29Dec2023, 16:00	1.1
29Dec2023, 17:00	1.2
29Dec2023, 18:00	0.6

HEC-HMS 4.11 [C:\...\Documents\Mihang_o_project\Mihang_o_project.hms]

File Edit View Components GIS Parameters Compute Results Tools

-None-

Subbasin-C
Subbasin-B
Junction-1
Reach-1
Subbasin-A
Sink-1
Meteorologic Models
Met 1
Control Specifications
Control 1
Time-Series Data
Precipitation Gages
Gage 1
29Dec2023, 12:00 - 29Dec2023, 18:00

Components Compute Results

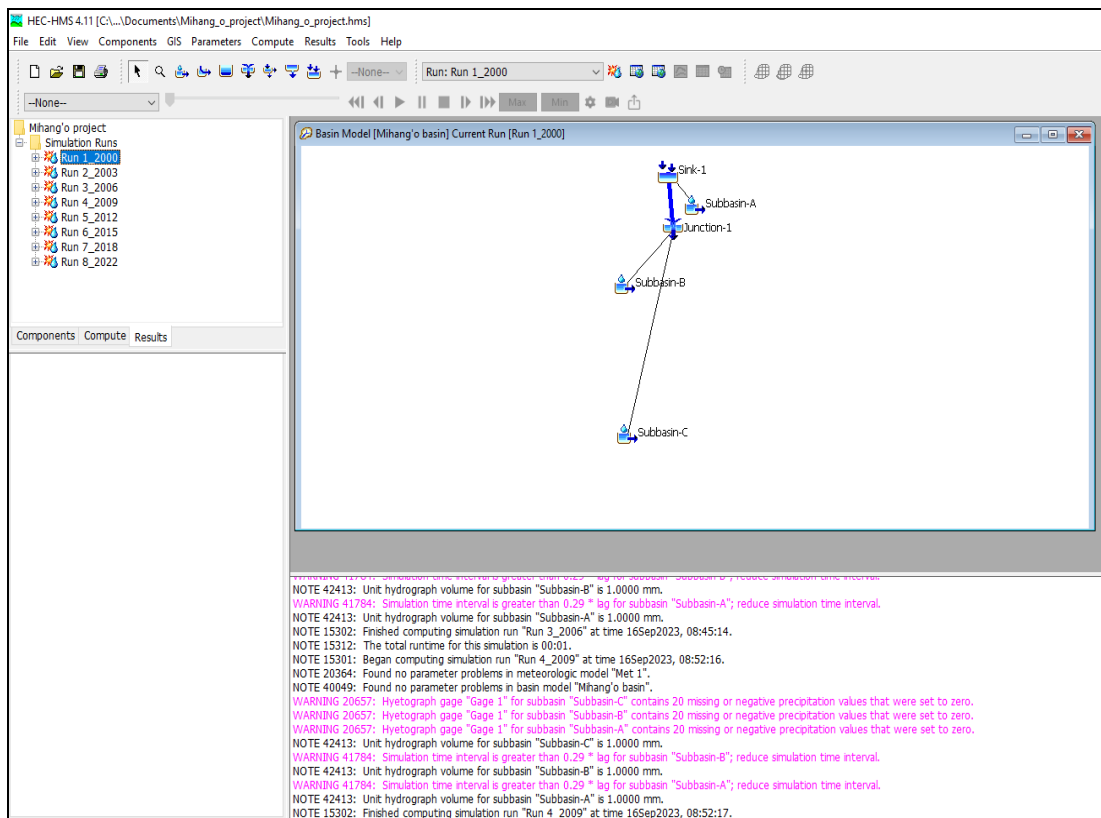
Time-Series Gage Time Window Table Graph

Precipitation (MM)

1.3
1.2
1.1
1.0
0.9
0.8
0.7
0.6
0.5
0.4

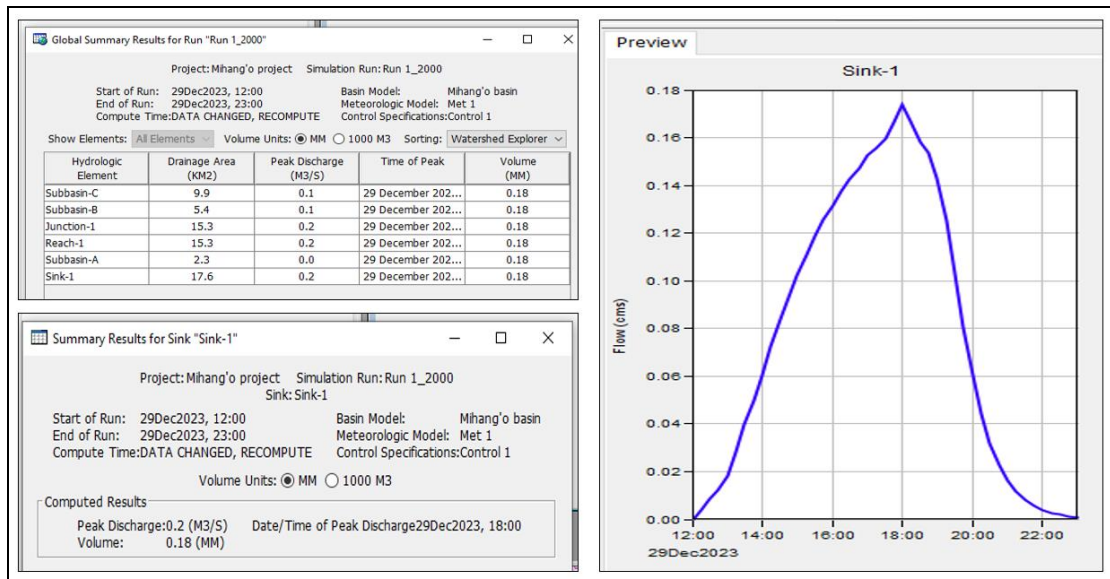
12:00 13:00 14:00 15:00 16:00 17:00 18:00

29Dec2023

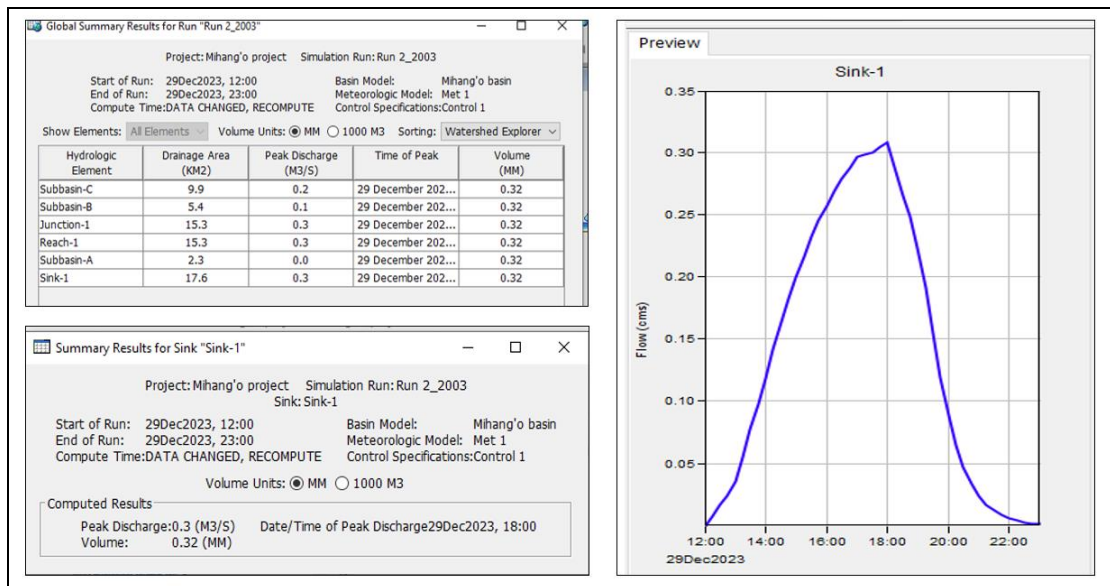


Appendix C: HEC-HMS Results Windows for the Years of Study

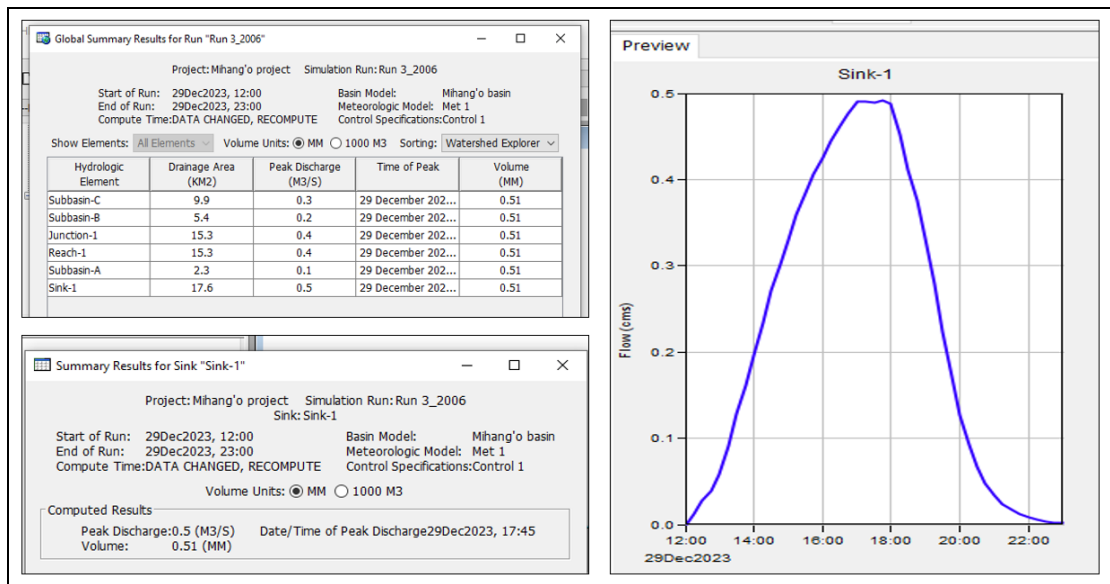
Run 1_2000



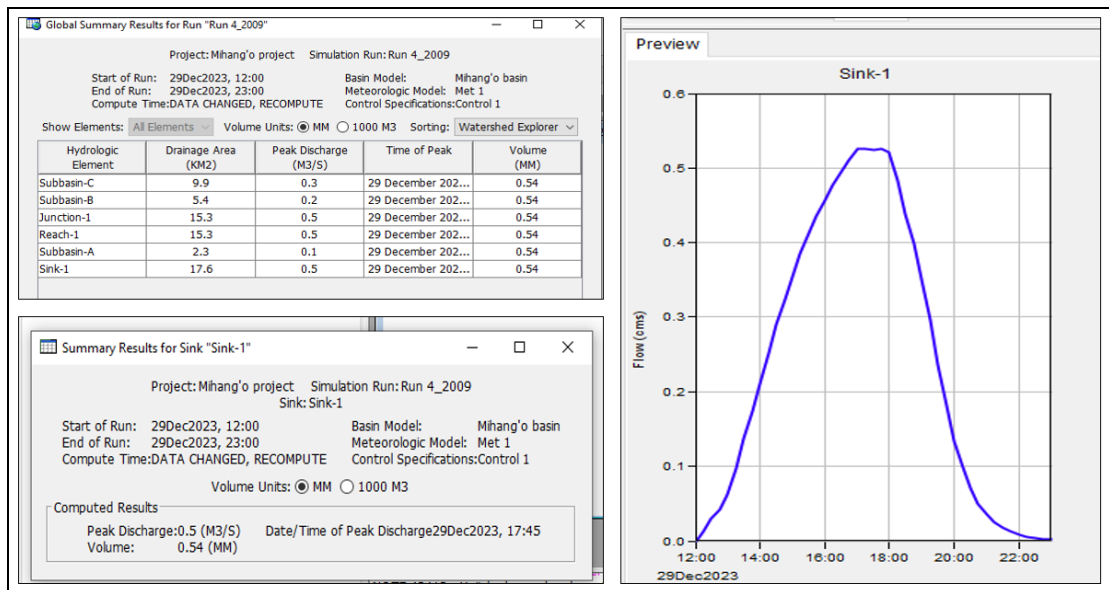
Run 2_2003



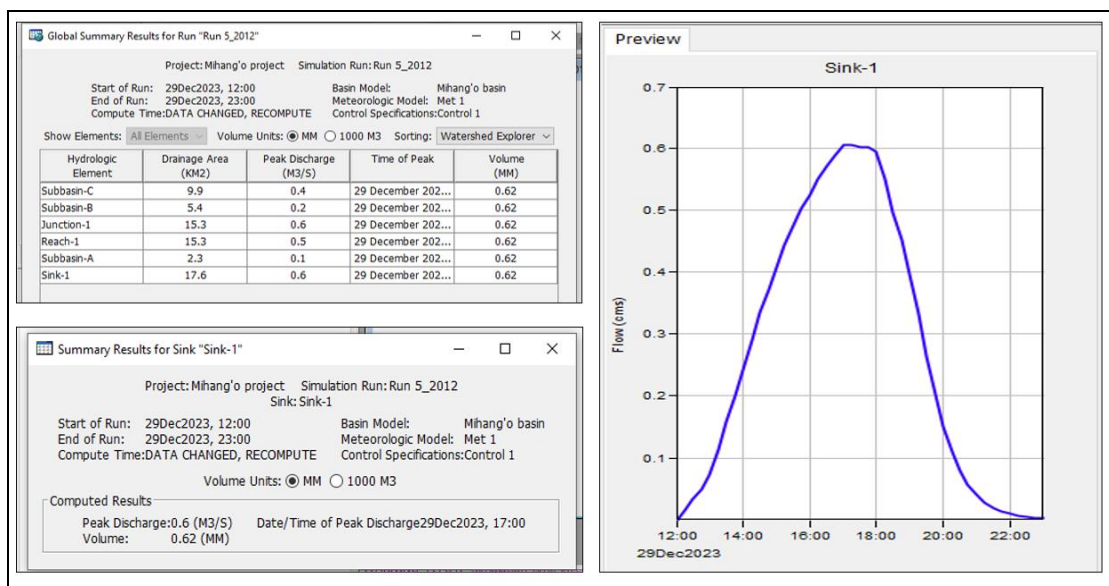
Run 3_2006



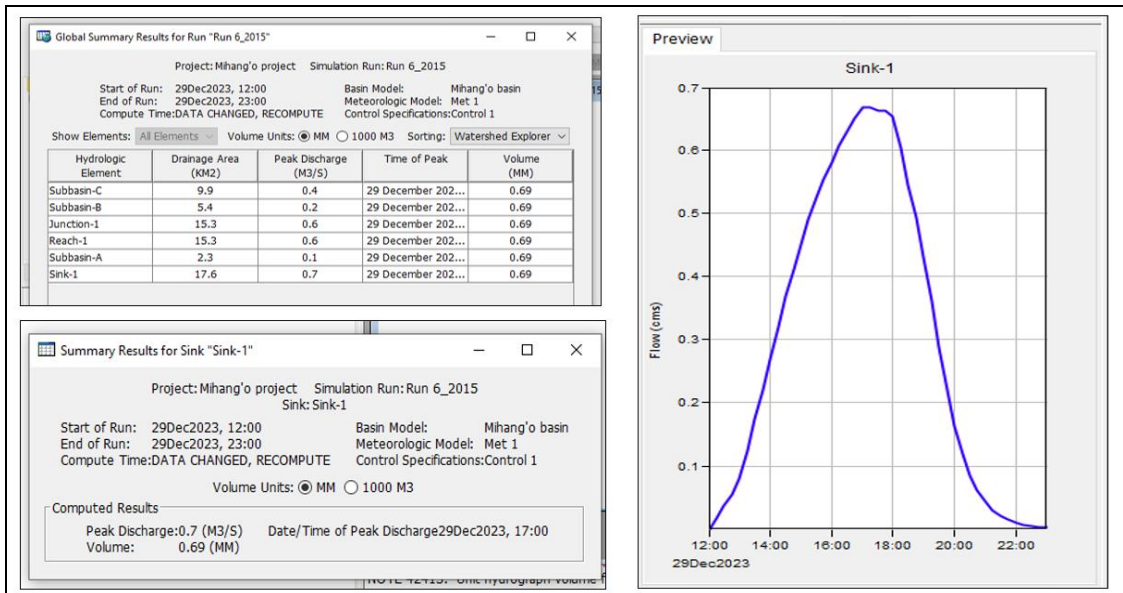
Run 4_2009



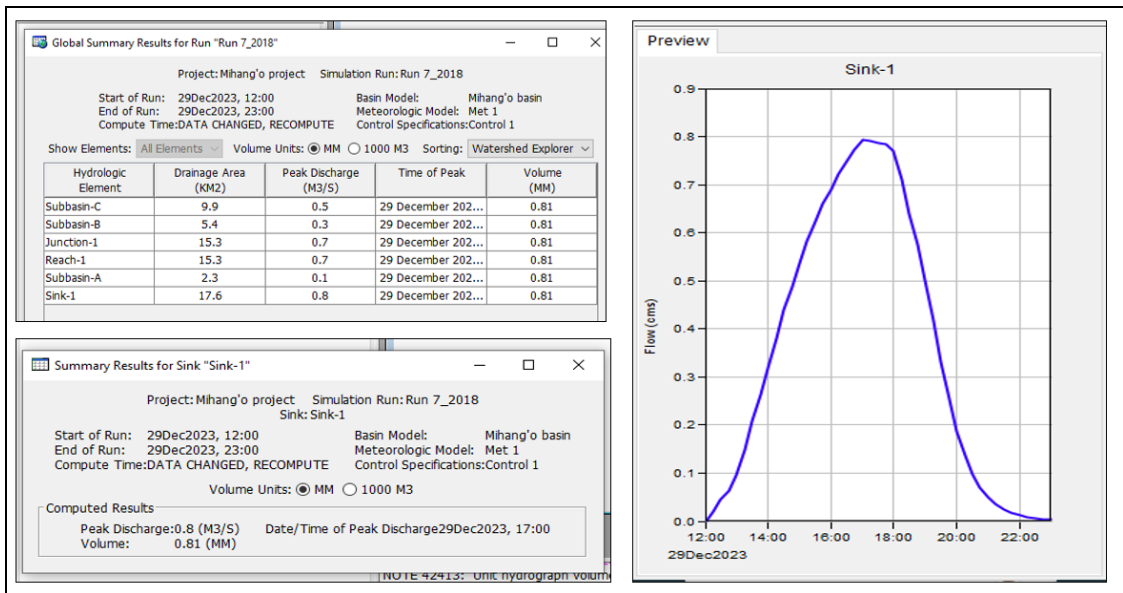
Run 5_2012



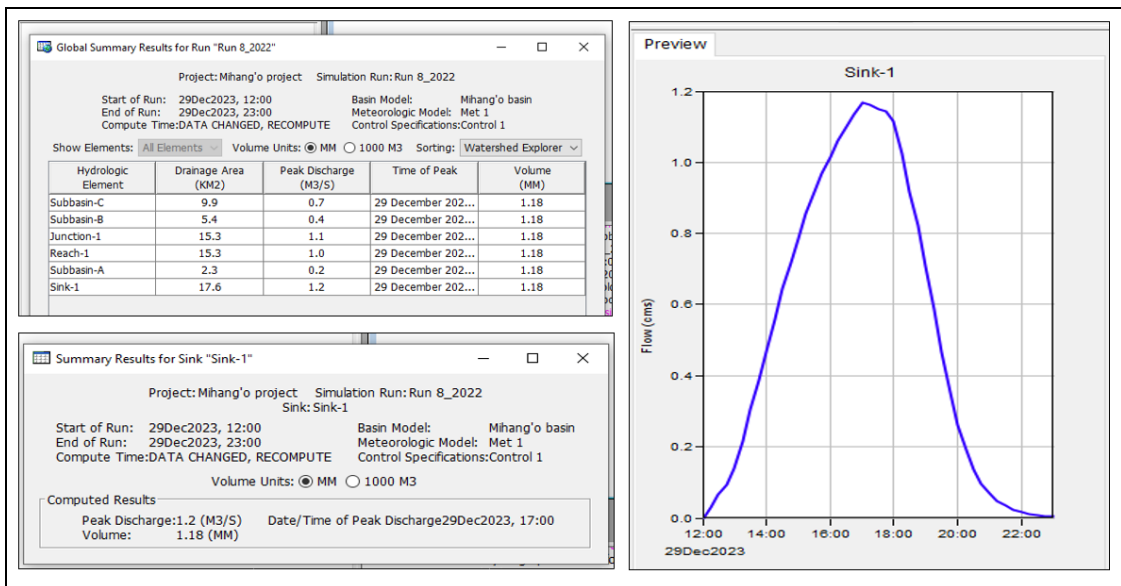
Run 6_2015



Run 7_2018



Run 8_2022



Appendix D: Matrix Results from Supervised Classification

Year	Accuracy	Matrix
2000	0.808777	[[20, 0, 1, 2, 1, 0], [0, 38, 2, 1, 2, 1], [1, 4, 67, 8, 2, 1], [0, 3, 5, 80, 1, 1], [3, 3, 1, 4, 39, 3], [1, 6, 1, 2, 1, 14]]]
2003	0.789969	[[14, 2, 2, 2, 3, 1], [0, 34, 6, 2, 2, 0], [1, 4, 66, 8, 3, 1], [0, 1, 8, 79, 2, 0], [2, 2, 2, 4, 42, 1], [1, 2, 2, 2, 1, 17]]]
2006	0.755486	[[13, 0, 4, 5, 2, 0], [0, 29, 8, 5, 1, 1], [0, 3, 73, 5, 1, 1], [1, 1, 10, 78, 0, 0], [4, 3, 4, 8, 32, 2], [0, 2, 4, 2, 1, 16]]]
2009	0.786834	[[16, 1, 2, 4, 1, 0], [0, 31, 5, 6, 2, 0], [0, 4, 70, 7, 1, 1], [1, 1, 6, 81, 1, 0], [3, 4, 3, 6, 37, 0], [0, 2, 4, 3, 0, 16]]]
2012	0.711765	[[21, 1, 7, 1, 1, 0], [4, 26, 3, 4, 4, 0], [1, 1, 24, 3, 1, 0], [2, 0, 2, 24, 0, 0], [6, 2, 1, 5, 23, 0], [0, 0, 0, 0, 0, 3]]]
2015	0.723529	[[22, 2, 2, 1, 4, 0], [5, 30, 1, 2, 3, 0], [4, 3, 20, 2, 1, 0], [3, 5, 2, 16, 2, 0], [0, 4, 0, 0, 33, 0], [1, 0, 0, 0, 0, 2]]]
2018	0.717647	[[23, 4, 2, 1, 1, 0], [4, 28, 4, 4, 1, 0], [1, 5, 19, 4, 1, 0], [1, 1, 2, 22, 2, 0], [2, 4, 1, 3, 27, 0], [0, 0, 0, 0, 0, 3]]]
2022	0.694118	[[22, 5, 0, 2, 2, 0], [3, 30, 2, 5, 1, 0], [1, 6, 19, 0, 4, 0], [1, 3, 2, 21, 1, 0], [4, 5, 3, 2, 23, 0], [0, 0, 0, 0, 0, 3]]]

Appendix E: Javascript Code used to Retrieve CHIRPS Data from Google Earth

```

//Load land cover from copenicus
//var dataset = ee.Image("COPERNICUS/Landcover/100m/Proba-V-C3/Global/2017")
var dataset = ee.Image("COPERNICUS/Landcover/100m/Proba-V-C3/Global/2017")

///.select('discrete_classification');
//Map.addLayer(dataset, {}, "Land Cover");
//end of
//load asset geometry. With land cover
//var AOI = ee.FeatureCollection('users/AOI_New');
var AOI = ee.FeatureCollection('users/Omwoyo_AOI');

//load feature collection into map canvas
Map.addLayer(AOI, {}, 'Omwoyo_AOI');
//Map.addLayer(AOI, {}, 'AOI_New');
// classification band
var BandSelc = dataset.select('discrete_classification');

// reduce image to vector
var vector = dataset.addBands(BandSelc).reduceToVectors({
  reducer: ee.Reducer.median(),
  geometry: AOI,
  scale: 100,
  tileScale: 2,
  bestEffort: true,})

// list of class value
var classVal = vector.aggregate_array('discrete_classification_1').distinct()
print('List of Values:',classVal)

// classifiacation value
var sClass = 100

// filtering vector dataset by value
var ClassSelected = vector.filterMetadata('discrete_classification_1','equals',sClass)

// Load collection
//var CHIRPS= ee.ImageCollection('UCSB-CHG/CHIRPS/DAILY');
var CHIRPS =ee.ImageCollection("ECMWF/ERA5_LAND/HOURLY")
//Define date range of interest
var precip = CHIRPS.filterDate('2021-11-28','2021-11-30');
var TS5 = ui.Chart.image.series(precip, AOI, ee.Reducer.mean(),1000,
'system:time_start').setOptions({
title: 'Precipitation Full Time Series',
vAxis: {title: 'mm/pentad'}, });
print(TS5);
var precip1year=CHIRPS.filterDate('2022-04-01','2022-04-30');
var TS1 = ui.Chart.image.series(precip1year, AOI, ee.Reducer.mean(),1000,
'system:time_start').setOptions({
title: 'Precipitaon 1-Year Time Series',
vAxis: {title: 'mm/DAY'}, });
print(TS1);
var yearPrecip = precip1year.mean().clip(AOI);

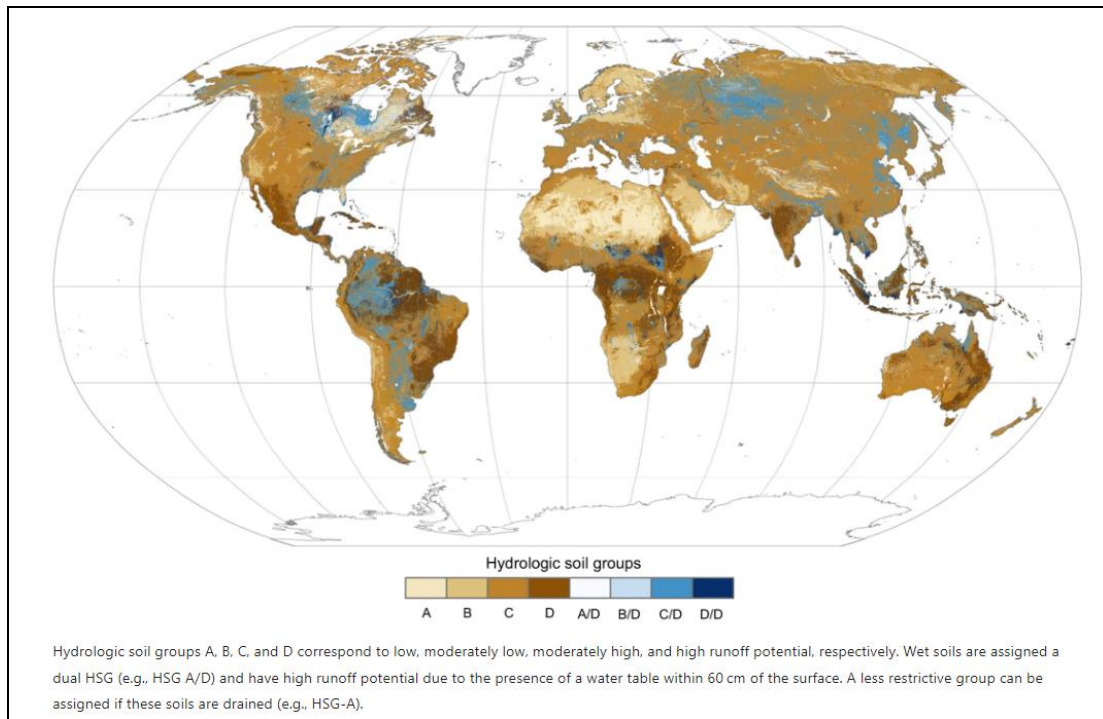
```

```
var meanPrecip = precip.mean().clip(AOI);
Map.addLayer(yearPrecip, {min: 0, max: 40,
  palette:['lightblue','blue','darkblue']}, 'Year Precipitation');
Map.addLayer(meanPrecip, {min: 0, max: 40,
  palette:['lightblue','blue','darkblue']}, 'Mean Precipitation');
var yearPrecip = precip1year.mean().clip(AOI);
```

Appendix F: Precipitation on December 29th, 2022

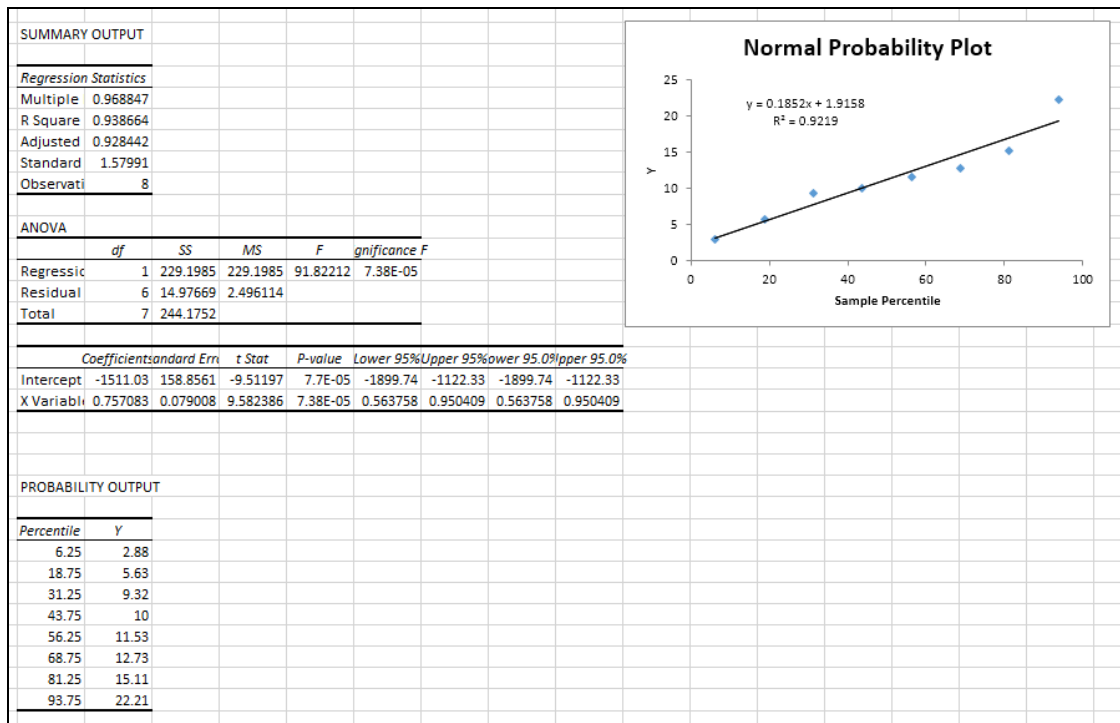
The screenshot shows a Microsoft Excel spreadsheet titled "Appendix F: Precipitation on December 29th, 2022". The data is organized into two main sections: December 29, 2022, and December 30, 2022. Each section has a header row with "Time" and "precipitation" columns. The data is recorded in hourly intervals from 0 to 23. The precipitation values are as follows:

12/29/2022	
Time	precipitation
0	0
1	0
2	0.13
3	0.11
4	0.9
5	0.7
6	0
7	0
8	0
9	0
10	0
11	0
12	0.5
13	0.8
14	1
15	1.1
16	1.2
17	0.6
18	0
19	0
20	0
21	0
22	0.2
23	0.1
12/30/2022	
0	0
1	0
2	0

Appendix G: Global Hydrologic Soil Groups (HYSOGs250m) for Curve Number

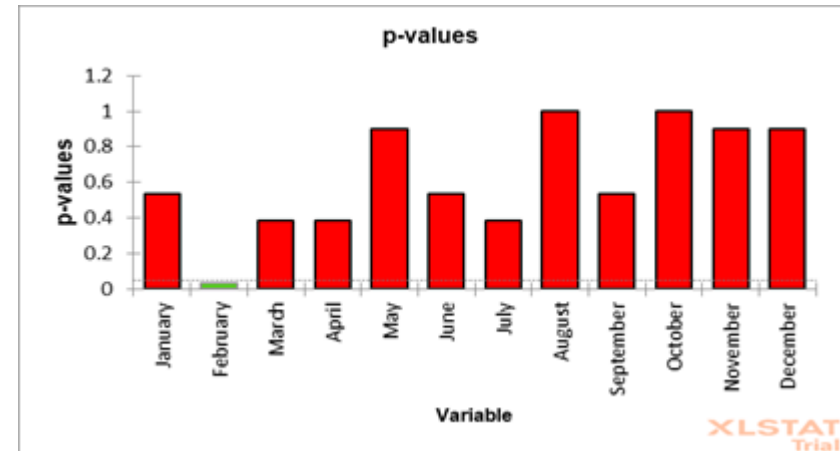
Source: Ross et al. (2018)

Appendix H: Linear Regression Analysis for Impervious Surface Area Trend



Appendix I: Mann-Kendall Trend Test Summary Results

Series\Test	Kendall's tau	p-value	Sen's slope
January	0.214	0.536	0.452
February	0.643	0.035	1.188
March	0.286	0.386	1.153
April	0.286	0.386	6.901
May	-0.071	0.902	-1.010
June	0.214	0.536	0.535
July	0.357	0.383	0.000
August	0.038	1.000	0.000
September	-0.214	0.536	-0.230
October	0.000	1.000	-0.099
November	-0.071	0.902	-0.640
December	0.071	0.902	1.734
Average	0.146	0.625	0.832



An approximation has been used to compute the p-value.

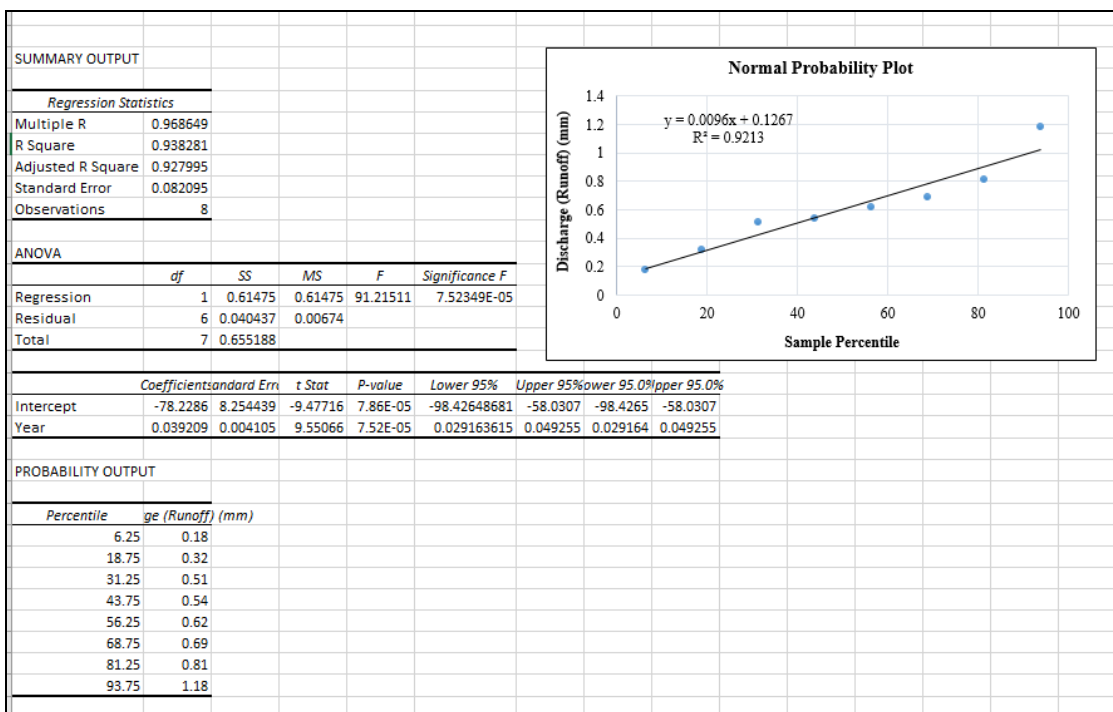
Test interpretation:

H0: There is no trend in the series

Ha: There is a trend in the series

As the computed p-value is greater than the significance level alpha=0.05, one cannot reject the null hypothesis H0.

Appendix J: Linear Regression Analysis for Runoff Trend



Appendix K: Correlation Analysis for Impervious Surface Area and Runoff

